Dissertation ETH No. 21640

SODIUM PHOSPHAETHYNOLATE AS A BUILDING BLOCK

A dissertation submitted to the
ETH Zurich
For the degree of
Doctor of Sciences

Presented by
Dominikus Heift
Dipl.-Chem., Universität zu Köln
Born May 8th, 1984
Citizen of Germany

Accepted on the recommendation of
Prof. Dr. H. Grützmacher, examiner
Prof. Dr. M. Kovalenko, co-examiner

2013

Publications

The present work is based on the following publications:
D. Heift, Z. Benkő and H. Grützmacher, *Dalton Trans.* **2014**, 43, 831-840. Coulomb repulsion versus cycloaddition: Formation of anionic four-membered rings from sodium phosphacyanate, Na(OCP).

D. Heift, Z. Benkő and H. Grützmacher, Is the phosphaethynolate anion, $(OCP)^-$, an ambident nucleophile? A spectroscopic and computational study, *Dalton Trans.* **2014**, DOI: 10.1039/c3dt53569j

D. Heift, Z. Benkő and H. Grützmacher, Synthesis of heterocycles from phosphaketenes: Interplay between aromaticity and bond strengths, *to be submitted.*

D. Heift, Z. Benkő, R. Suter, R. Verel and H. Grützmacher, A simple access to 1,2,4-oxadiphospholes from sodium phosphaethynolate, Na(OCP), *to be submitted.*

D. Heift, Z. Benkő and H. Grützmacher, Redox induced interconversion of a monocyclic phosphide anion and an annulated diazaphospholenium cation, *to be submitted.*

D. Heift, Z. Benkő and H. Grützmacher, Tetramerization of Isocyanates around a P^- anion, *to be submitted.*

Further Publications:
F. F. Puschmann, D. Stein, D. Heift, C. Hendriksen, Z. A. Gál, H.-F. Grützmacher and H. Grützmacher, *Angew. Chem. Int. Ed.*, **2011**, 50, 8420-8423.
A. Klein, K. Butsch, S. Elmas, C. Biewer, D. Heift, S. Nitsche, I. Schlipf and H. Bertagnolli, *Polyhedron*, **2012**, 31, 649-656.
S. Alidori, D. Heift, G. Santiso-Quinones, Z. Benkő, H. Grützmacher, M. Caporali, L. Gonsalvi, A. Rossin and M. Peruzzini, *Chem. Eur. J.*, **2012**, 18, 14805-14811.

Public Presentations

8th European Workshop on Phosphorous Chemistry, Münster, **2011**, Poster

9th European Workshop on Phosphorous Chemistry, Rennes, **2012**, Talk

19th International Conference on Phosphorous Chemistry, Rotterdam, **2012**, Poster

10th European Workshop on Phosphorous Chemistry, Regensburg, **2013**, Talk

Acknowledgement

The present work would not have been possible without the help and support of various people, to whom I would like to express deep gratitude.

I would like to thank Prof. Dr. Hansjörg Grützmacher for the opportunity to work on a very interesting topic in his research group and for his continuous inspiration.
I am thankful to my co-referee Prof. Dr. Maksym Kovalenko.

In particular I would like to thank Dr. Zoltán Benkő for the fruitful collaboration during the last years. Zoli, I learned so much from you and it was a pleasure to discover with you the basics of OCP chemistry! The combination of my experiments with your calculations was the key for understanding the reactivity of this little anion! Thank you very much for all your help as well as for the great times we spent together outside of ETH!

I would like to thank Dr. Hartmut Schönberg for his general assistance and support and Dr. René Verel for his support in NMR related problems.
A big thank-you goes to all my PhD and Post-doc colleagues in the working group for the pleasant work atmosphere. Thank you for all the support in in the daily lab work as well as nice moments outside of lab. Vito, thank you for the good time in lab H 114! (by the time you got used to my chaos in the lab…). Georgina, I thank you for all your help in chemical and non-chemical issues, especially for proofreading my thesis. Amos, thank you for helping me with several X-ray structures.
Furthermore I would like to thank all former group members, especially Florian, who helped me in many ways in the beginning of my PhD.

Finally, I would like to thank my parents, who always supported me and made it possible for me to study chemistry.

General remark

All the calculations in this thesis were performed by Dr. Zoltán Benkő.

Abstract

In the present work the reactivity of the phosphaethynolate anion, $(OCP)^-$, towards various electrophiles has been explored. Furthermore, the $(OCP)^-$ anion has been employed as a reactant in cycloaddition chemistry.

Carbon dioxide and two equivalents of Na(OCP) form in an equilibrium reaction an adduct of the composition $Na_2(P_2C_3O_4)$. The anion of this salt, $[O_2C{-}P(CO)_2P]^{2-}$, is built up by a four-membered 1,3-diphosphetane-2,4-dione ring and a carboxylate unit attached to one of the phosphorus atoms. A remarkable π-delocalization was observed within the OCPCO moiety.

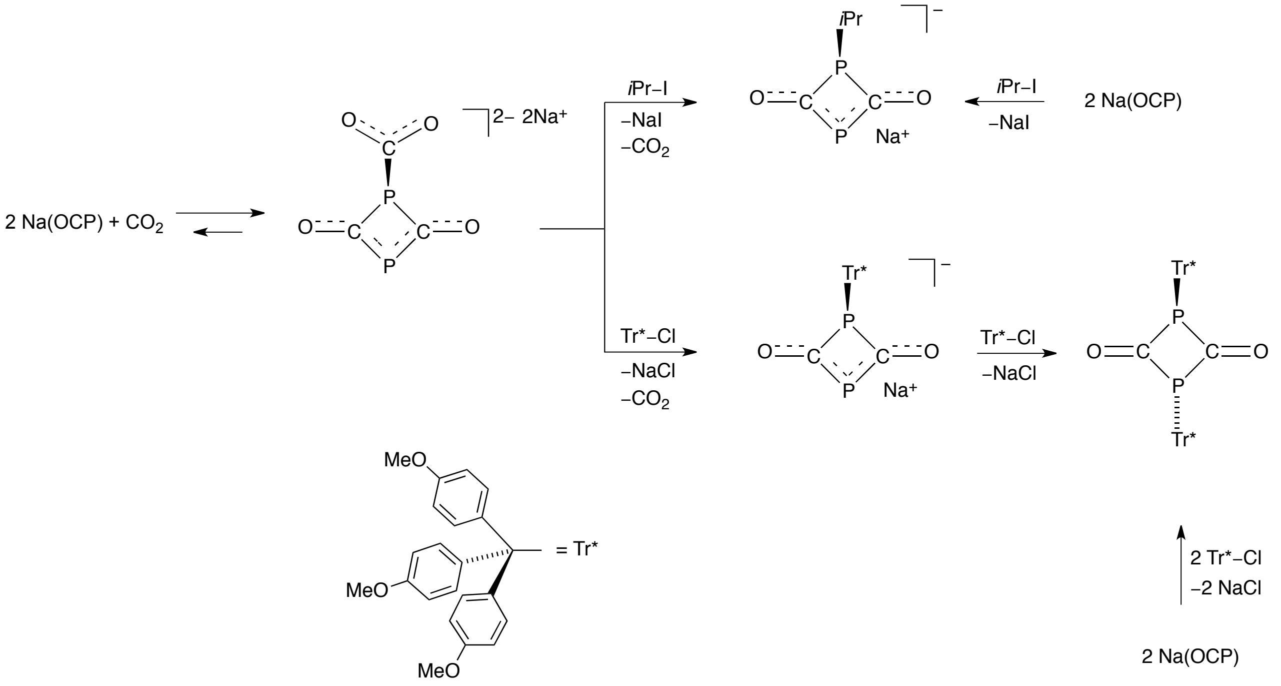

Scheme A1

The stepwise reaction mechanism leading to $Na_2(P_2C_3O_4)$ was investigated with quantum chemical calculations. Accompanied by the release of CO_2, $Na_2(P_2C_3O_4)$ reacts with both 2-iodopropane and 4,4',4"-trimethoxytriphenylmethyl chloride to form four-membered cyclic anions (Scheme A1). For comparison the analogous reactions were performed with Na(OCP) instead of $Na_2(P_2C_3O_4)$ and the results are discussed in detail.

The reactivity of Na(OCP) towards triorganyl compounds of the heavier group 14 elements (R_3EX R = Ph or ^{i}Pr; E = Si, Ge, Sn, Pb; X = Cl, OTf) (Scheme A2) was investigated. In the case of E = Si two constitutional isomers were formed and characterized *in situ*: R_3SiOCP is the kinetic and R_3SiPCO the thermodynamic product, representing the first experimental evidence of the ambident character of the $(OCP)^-$ anion. Applying theoretical calculations and spectroscopic methods, the compound previously reported incorrectly as $^iPr_3SiOCP$ was unambiguously identified as $^iPr_3SiPCO$. The heavier analogues form exclusively the phosphaketene isomer R_3EPCO (E = Ge, Sn, Pb). DFT calculations were performed to gain deeper insight into the bonding and thermodynamic stability of these compounds.

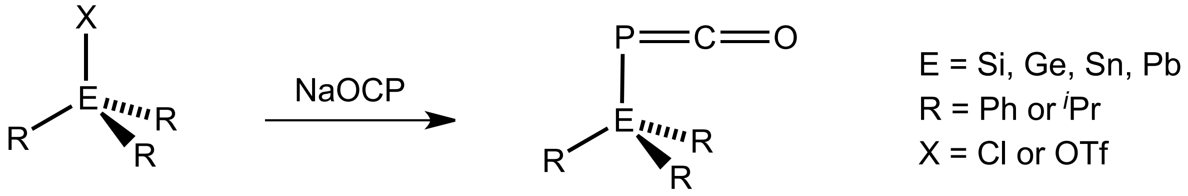

Scheme A2

Na(OCP) provides easy access to silyl and stannyl substituted five-membered heterocycles containing three phosphorous atoms (Scheme A3). The structure of the heterocyclic anion depends on the nature of the tetrel atom involved. While the silyl analogue $[P_3(COSiR_3)_2]^-$ is an aromatic triphospholide, the stannyl compound $[P(CO)_2(PSnR_3)_2]^-$ exhibits a delocalized OCPCO fragment. The hydrolysis of both anions delivers the same cyclic species $[P(CO)_2(PH)_2]^-$. A silyl functionalized 1,2,4,1’,2’,4’- hexaphosphaferrocene was obtained from $[P_3(COSiR_3)_2]^-$ in a simple and effective procedure (Scheme A3). Computations and NMR spectroscopic

investigations were performed to elucidate the formation mechanism of the anionic species.

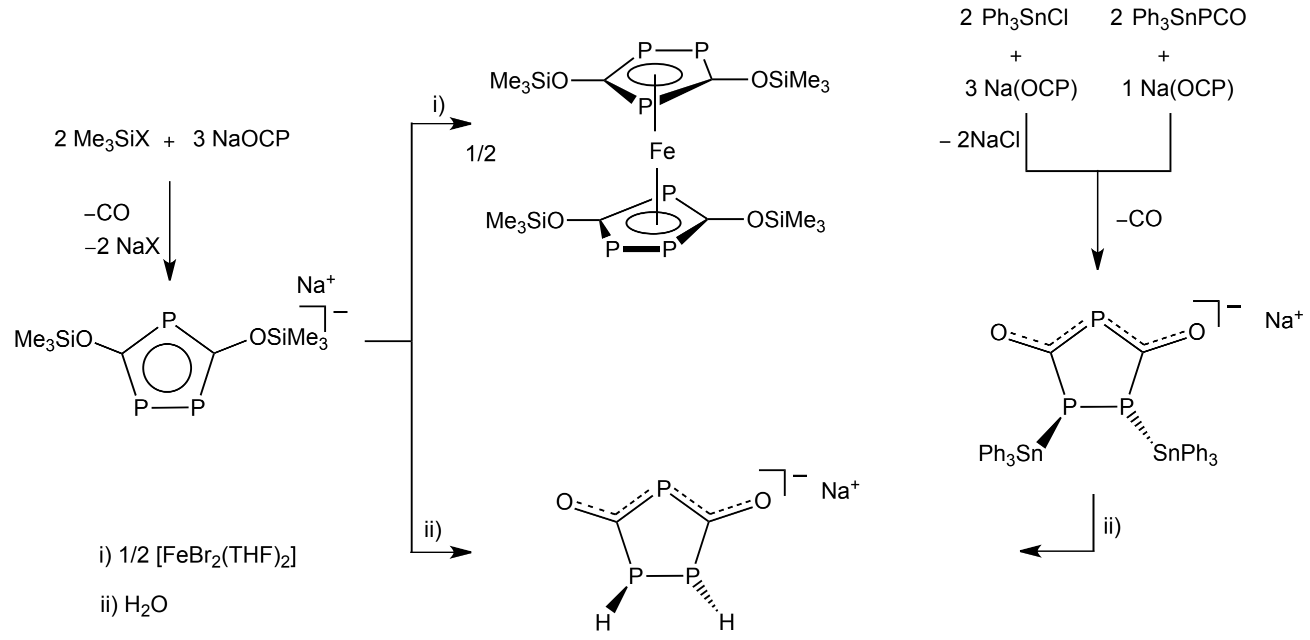

Scheme A3

The reaction of Na(OCP) with aromatic acyl chlorides delivers ester functionalized 1,2,4-oxadiphospholes in a clean and P-atom economic way (Scheme A4). The reaction mechanism has been elucidated by means of detailed NMR-spectroscopic, kinetic and computational studies. The initially formed acyl phosphaketene undergoes a pseudocoarctate cyclization with an $(OCP)^-$ anion under the loss of carbon monoxide yielding a five-membered ring anion. The nucleophilic attack of the formed heterocyclic anion on an acyl chloride molecule results in the 1,2,4-oxadiphosphole. The transient acyl phosphaketene is conserved during the reaction in the form of four-membered ring adducts, which act as a reservoir. The phosphaethynolate anion was proven to have three different roles: as a nucleophile, an en-component in [2+2] cycloadditions and a formal P^- transfer reagent.

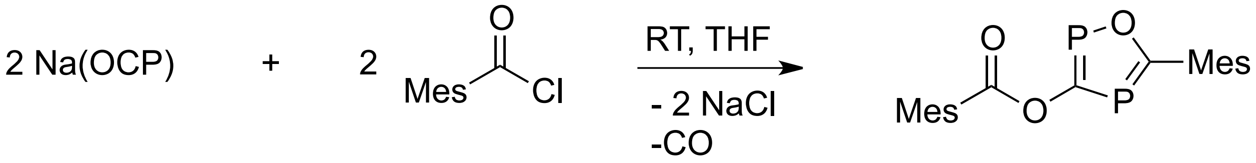

Scheme A4

An imino-functionalized, anionic 1,3,5-diazaphosphinane was obtained from the reaction of Na(OCP) with two equivalents of dicyclohexylcarbodiimide (DCC). One electron oxidation of this anion results in the formation of a diphosphane, which is the dimer of the initially generated radical species. The oxidation of this anion with elemental iodine leads to an annulation reaction (Scheme A5). The formed 1,3,2-diazaphospholenium cation was successfully reduced with elemental magnesium to give back the 1,3,5-diazaphosphinanide anion. These structural changes can be rationalized with the Umpolung resulting from the oxidation or reduction. Theoretical calculations propose that phosphinidene species are involved in the rearrangement processes.

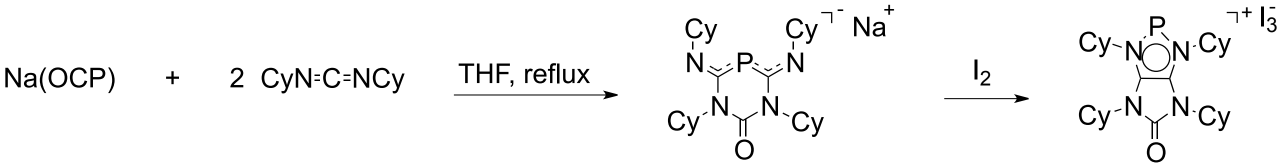

Scheme A5

Na(OCP) has been found to act as a simple and effective catalyst for the trimerization of isocyanates. Some anionic species involved in this process can be described as adducts of isocyanates and a P^- anion, having a general composition of $[P(OCNR)_n]^-$ (n = 2–5). The structures of two of these adducts (n = 2 and 4) were also characterized by single crystal X-ray diffraction analysis. The spiro phosphoranide (n = 4), which is the latent form of a catalytic species, exhibits two five-membered PC_2N_2 rings (n = 2) connected by a 10-P-4 phosphorus spiro atom. The isocyanate units of this spiro anion can be completely replaced by a more reactive isocyanate (Scheme A6). This P^{-} transfer reaction was successfully applied in the synthesis of polyurethane networks having embedded phosphoranide functions, which preserved their activity in isocyanate trimerization.

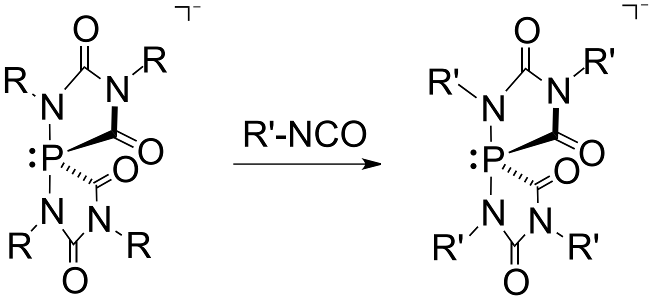

Scheme A6

In summary, the phosphaethynolate anion $(OCP)^{-}$ has a high potential as building block in phospha-organic chemistry. Three different types of reactivity have been observed for this anion: Firstly, to take part in cycloadditions, providing synthetic access to four-, five- and six-membered heterocyclic ring anions. Secondly, $(OCP)^{-}$ is an ambident nucleophile. Preferably it reacts on the P atom with an electrophile. As a result, various monomeric heterophosphaketenes as well as their [2+2] cycloaddition products with $(OCP)^{-}$ could be obtained. Thirdly, $(OCP)^{-}$ can react as a P^{-} transfer reagent, being accompanied by the loss of carbon monoxide. This reactivity was demonstrated in the formation of new heterocycles.

Zusammenfassung

In Rahmen der vorliegenden Arbeit wurde die Reaktivität des Phosphaethynolate Anions, $(OCP)^{-}$, gegenüber verschiedenen Elektrophilen erforscht. Weiterhin wurde das $(OCP)^{-}$ Anion als Reaktionspartner in Cycloadditionen eingesetzt und untersucht. Kohlenstoffdioxid und zwei Äquivalente Na(OCP) bilden in einer Gleichgewichtsreaktion ein CO_2 Addukt der Zusammensetzung $Na_2(P_2C_3O_4)$. Das Anion dieses Salzes, $[O_2C\text{-}P(CO)_2P]^{2-}$, ist wie ein viergliedriger 1,3-Diphosphetan-2,4-dionring aufgebaut, wobei eine Carboxylateinheit an eines der Phosphoratome gebunden ist (Abbildung A1). Innerhalb der OCPCO Einheit liegt eine außergewöhnliche π-Delokalisierung vor.

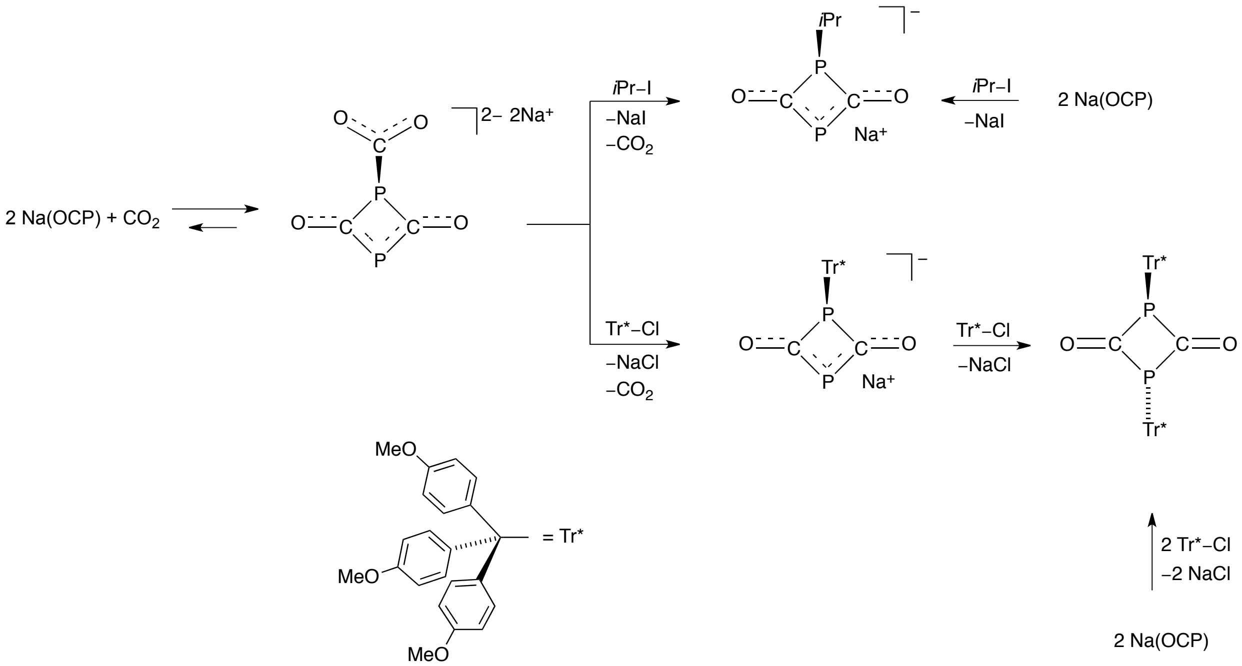

Abbildung A1

Der stufenweise Bildungs-Mechanismus von $Na_2(P_2C_3O_4)$ wurde untersucht. Sowohl mit 2-Iodopropan, als auch mit 4,4‘,4‘‘-Trimethoxytriphenylmethylchlorid reagiert $Na_2(P_2C_3O_4)$, unter CO_2-Gasentwicklung, zu viergliedrigen, cyclischen Anionen. Zum

Vergleich wurden die analogen Umsetzungen ausgehend von Na(OCP) durchgeführt und die Resultate ausführlich beschrieben.

Die Reaktivität von Na(OCP) gegenüber Triorganylhalogenidverbindungen der schwereren Elemente der 14. Gruppe (R_3EX R = Ph oder ^{i}Pr; E = Si, Ge, Sn, Pb; X = Cl, OTf) wurde untersucht (Abbildung A2). Für E = Si wurden *in situ* zwei konstitutionelle Isomere gefunden und charakterisiert: R_3SiOCP ist das kinetische Produkt und bei R_3SiPCO handelt es sich um das thermodynamische Produkt, womit der experimentelle Beweis für den ambidenten Charakter des $(OCP)^-$ Anions erbracht ist. Mittels spektroskopischer Methoden und quantenchemischer Rechnungen konnte die Verbindung $^i Pr_3SiPCO$ eindeutig identifiziert werden, welche zuvor in der Literatur fälschlicherweise als $^i Pr_3SiOCP$ beschrieben wurde. Die schwereren Analogen bilden ausschließlich das entsprechenden Phosphaketen-Isomer R_3EPCO (E = Ge, Sn, Pb).

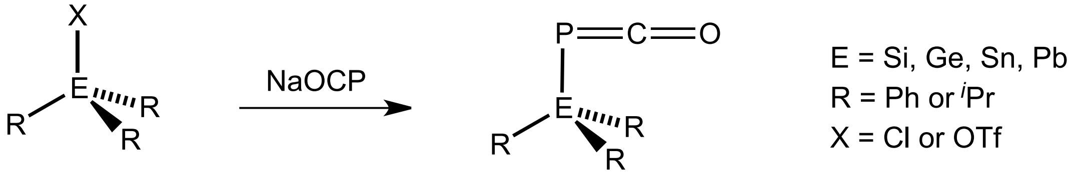

Abbildung A2

Na(OCP) bietet einen einfachen Zugang zu silylierten und stannylierten fünfgliedrigen Heterocylen, welche drei Phosphoratome enthalten. Die Struktur des heterocyclischen Anions hängt von der Natur des involvierten tetrel Atoms ab. Während es sich bei dem Silyl-Analogon $[P_3(COSiR_3)_2]^-$ um ein aromatisches Triphospholid handelt, weist die Stannylverbindung $[P(CO)_2(PSnR_3)_2]^-$ eine delokalisierte OCPCO Einheit auf. Die Hydrolyse dieser beiden Anionen führt zu der gleichen cyclischen Spezies $[P(CO)_2(PH)_2]^-$. Ein silyliertes 1,2,4,1',2',4'-Hexaphosphaferrocen wurde aus $[P_3(COSiR_3)_2]^-$ in einer einfachen, effektiven Synthese dargestellt (Abbildung A3).

NMR-spektroskopische und theoretische Methoden wurden angewandt, um den Bildungsmechnismus der anionischen Spezies aufzuklären

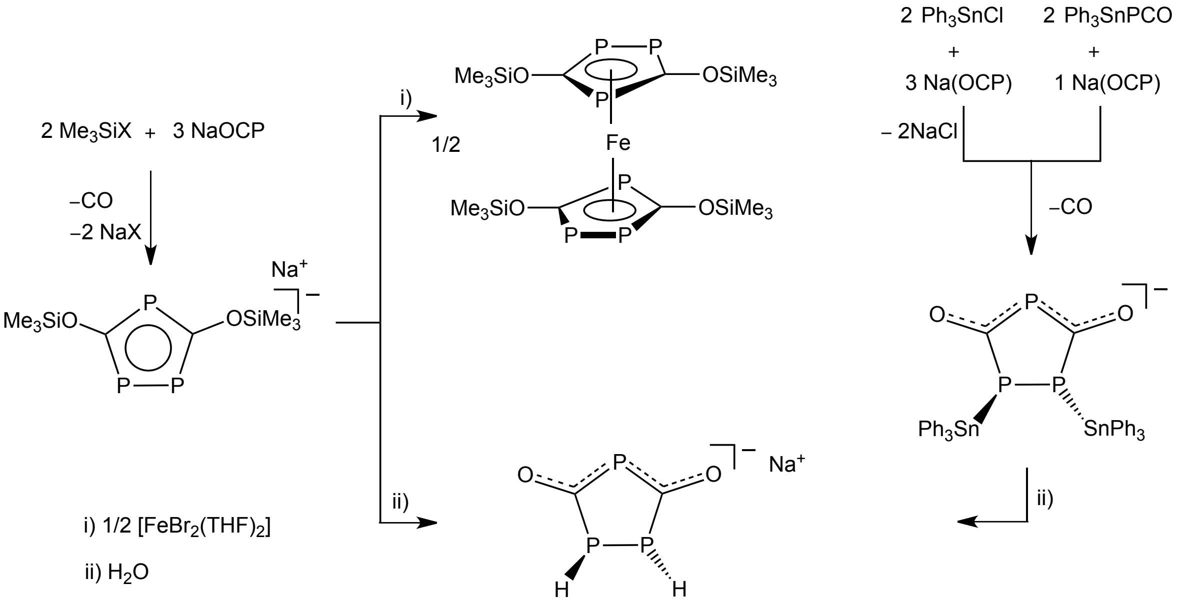

Abbildung A3

Funktionalisierte 1,2,4-Oxadiphosphole können in einer sauberen, bezüglich Phosphor Atom-ökonomischen Reaktion, aus Na(OCP) und aromatischen Säurechloriden dargestellt werden (Abbildung A4). Der Reaktionsmechanismus wurde mittels eingehender NMR-spektroskopischer, kinetischer und theoretischer Untersuchungen aufgeklärt. Das Phosphaketen, welches gleich zu Anfang der Reaktion gebildet wird, reagiert in einer pseudo-coarctierten Cyclisierung mit einem $(OCP)^-$ Anion unter Abspaltung von Kohlenstoffmonoxid zu einem fünfgliedrigen anionischen Heterozyklus. Dieses Anion greift ein Säurechloridmolekül nukleophil an, wobei das 1,2,4-Oxadiphosphol gebildet wird. Das anfänglich gebildete Acylphosphaketen wird während der Reaktion in Form von viergliedrigen Ringaddukten konserviert, welche als Reservoir fungieren. Es konnte gezeigt werden, dass das Phosphaethinolatanion auf drei verschiedene Art und Weisen reagiert: als Nukleophil, als En-Komponente in [2+2] Cycloadditionen und als formales P^- Transferreagenz.

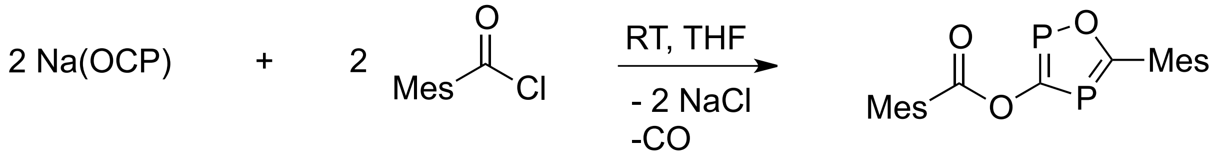

Abbildung A4

Ein imino-funktionalisiertes 1,3,5-Diazaphosphinan wurde aus der Umsetzung von Na(OCP) mit zwei Äquivalenten Dicyclohexyldiisocyanat (DCC) erhalten (Abbildung A5). Die Einelektron-Oxidation dieses Anions führt zur Bildung eines Diphosphans, wobei es sich um das Dimer der anfänglich gebildeten Radikalspezies handelt. Wird dieses Anion mit elementarem Iod oxidiert, findet eine Anellierungsreaktion statt. Das hierbei erhaltene 1,3,2-Diazaphospholeniumkation wurde erfolgreich mit elementarem Magnesium reduziert; dabei konnte das 1,3,5-Diazaphosphinanidanion zurückgewonnen werden. Die beobachteten strukturellen Veränderungen lassen sich durch die Umpolung erklären, die aus der Oxidation beziehungsweise Reduktion resultiert.

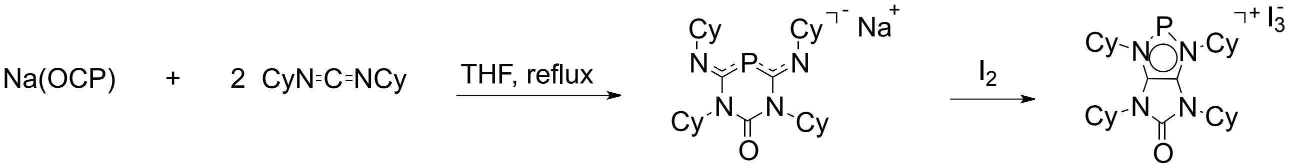

Abbildung A5

Natriumphosphaethynolat, Na(OCP), konnte als einfacher und effektiver Katalysator für die Trimerisierung von Isocyanaten identifiziert werden. Einige der anionischen Spezies, welche an diesem Prozess beteiligt sind, können als Addukte von Isocyanaten und einem P^{-}Anion mit der allgemeinen Komposition $[P(OCNR)_{n}]^{-}$ (n = 2-5) beschrieben werden. Die Struktur zweier dieser Addukte (n = 2 und 4) wurden mittels

Einkristallröntgendiffraktometrie untersucht. Bei dem Spiro-Phosphoranid ($n = 4$) handelt es sich um die latente Form einer katalytischen Spezies. Diese enthält zwei fünfgliedrige PC_2N_2-Ringe ($n = 2$), welche durch ein 10-P-4 Spiro-Phosphoratom verbunden sind. Die Isocyanateinheiten dieses Spiro-Anions lassen sich vollständig durch diejenige eines reaktiveren Isocyanats austauschen (Abbildung A6). Diese P^- Übertragungsreaktion wurde erfolgreich in der Synthese von Polyurethannetzwerken angewendet. Die erhaltenen Netzwerke weisen eingebettete Phosphoranidfunktionen auf, welche ihre Aktivität in der Trimerisierung von Isocyanaten bewahren.

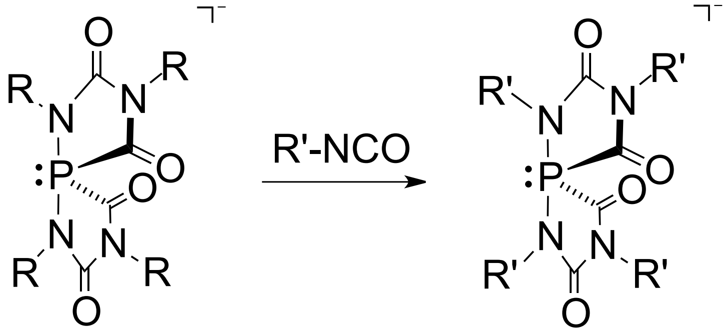

Abbildung A6

Zusammenfassend kann festgestellt werden, dass das Phosphaethynolate Anion $(OCP)^-$ ein großes Potential als Baustein in der Phospha-Organischen Chemie aufweist. Drei verschiedene Arten von Reaktivität wurden für dieses Anion beobachtet: Erstens, es kann in Cycloadditionen reagieren. Dies bietet den synthetischen Zugang zu vier-, fünf- und sechs-gliedrigen heterocyclischen Anionen. Zweitens, das $(OCP)^-$ Anion ist ein ambidentes Nukleophil, reagiert jedoch bevorzugt über das P Atom. Folglich konnten eine Reihe verschiedener monomerer Heterophosphaketene und deren [2+2] Cycloadditionsprodukte dargestellt werden. Drittens, $(OCP)^-$ kann als P^- Transferreagenz fungieren, dies geschieht unter der Freisetzung von Kohlenmonoxid. Neue Heterocyclen konnten auf Grund dieser Reaktivität erhalten werden.

1. Introduction

For over a century, organophosphorous chemistry was confined to the investigation of trivalent, tricoordinate ($\lambda^3\sigma^3$) and pentavalent, tetracoordinate ($\lambda^5\sigma^4$) phosphorous compounds.[1] The "double bond rule"[2] was at that time widely accepted. It stated that stable (p-p) π multiple bonds between, for example, phosphorus and elements of the second period would not be stable.[1, 3, 4] This assertion was refuted in the 1960s by the syntheses of the first unsaturated phosphorous compounds, in particular phosphacyanines ($\lambda^3\sigma^2$ phosphenium cations)[5] and as an aromatic representative 2,4,6-triphenylphosphabenzene.[6] Around the same time Gier reported the generation of the extremely reactive phosphaacetylene, H−C≡P, from phosphine in a rotating arc struck between graphite electrodes[7] (Scheme 1.1).

$$PH_3 \xrightarrow{\substack{\text{arc struck between}\\ \text{graphite electrodes}}} H{-}C{\equiv}P \quad + \quad HC{\equiv}CH \quad + \quad H_2C{=}CH_2$$

Scheme 1.1 Generation of phosphaacetylene from phosphane.

The discovery of these molecules containing PC multiple bonds paved the way for the comprehensive chemistry of a new class of compounds, namely low-coordinate phosphorous compounds.[4] After the discovery of H−C≡P, many derivatives of phosphaalkynes (alkylidynephosphanes) R−C≡P were reported.[3, 4] Relatively bulky substituents are needed to suppress the oligo/polymerization of these unsaturated phosphorous compounds.[8] A landmark in the history of phosphaalkynes was the synthesis of ^{t}Bu−C≡P from trisilylphosphane $P(TMS)_3$ and pivaloyl chloride, ^{t}BuCOCl, published by Becker *et al.* in 1981 (Scheme 1.2). Variation of this synthetic route gave access to a large number of phosphaalkynes.[4]

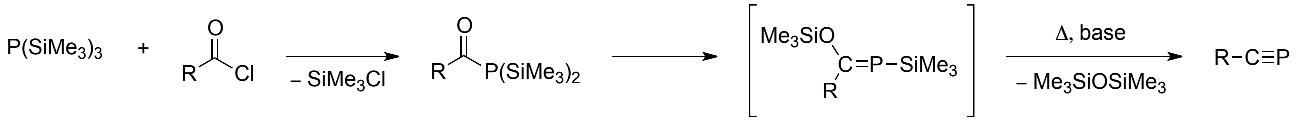

Scheme 1.2 Synthesis of *t*Bu−C≡P from P(TMS)$_3$ and pivaloyl chloride.

In contrast to H−C≡P, which oligomerizes at −130°C,[7] ^{t}Bu−C≡P is a thermally stable colorless liquid, which boils at 60°C.[9] ^{t}Bu−C≡P has a remarkable kinetic stability, but the CP triple bond can undergo various reactions. The relatively easy synthetic access to this compound explains the plethora of reactions, which involve ^{t}Bu−C≡P as building block. Employing phosphaalkynes, specifically ^{t}Bu−C≡P, in cycloaddition reactions allowed the preparation of many phosphorous heterocycles and cage structures,[10] of which a few milestones are shown in Figure 1.1. For example, the reaction of ^{t}Bu−C≡P with Na/K alloy delivers a mixture of 1,2-diphospholide and 1,2,4-triphospholide.[11] These cyclopentadienyl analogue five-membered ring anions can bind in a η^5 fashion to a transition metal center and many sandwich complexes with such ligands (ferrocene-analogues) have been reported[12-14].

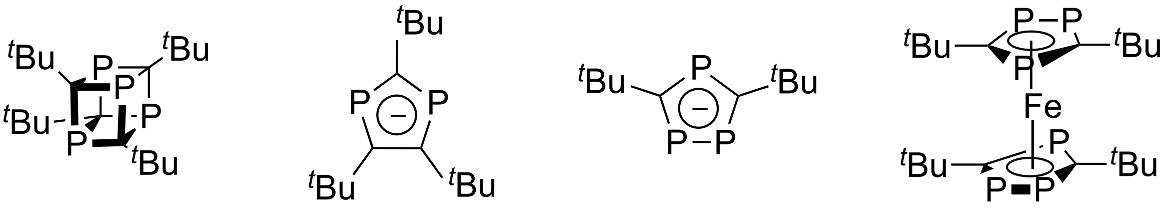

Figure 1.1 Oligomerization products of ^{t}Bu−C≡P.

As an alternative to sterically demanding groups, a PC triple bond may be protected from oligomerization by the introduction of a charge into the moiety, since the Coulomb repulsion between the species of the same charge hinders their aggregation. Formal introduction of the substituent R = O$^-$ on a phosphaalkyne moiety delivers the phosphaethynolate anion ($^-$O−C≡P).

The $(OCP)^-$ anion (**1**), which is the phosphorous analogue of the cyanate anion $(OCN)^-$, was first synthesized by Becker *et al.* more than two decades ago as a lithium salt from lithium bis(trimethylsilyl)phosphide and dimethyl carbonate[15] (Scheme 1.3a). The phosphacyanate salts $[M(OCP)_2]$ (M = Ca−Ba) can analogously be prepared from the corresponding bis(trimethylsilyl)phosphides and dimethyl carbonate[16]. Interestingly, the stability of these alkali earth metal phosphaethynolate salts depends strongly on the nature of the cation M^{2+} and the solvent. Only $[Ca(OCP)_2(DME)_3]$ could be isolated as a crystalline solid, while a dianion containing two $(OCP)^-$ units was obtained with M = Sr^{2+}.[16]

Meanwhile, several routes to obtain $(OCP)^-$ have been published. All are based on the initial nucleophilic attack of a phosphide precursor on the carbon atom of a CO source (Scheme 1.3 b-f). The reaction of sodium phosphide with carbon monoxide gas under pressure, at ambient temperature gives Na(OCP) and hydrogen (b).[17] Similarly, in a recently published procedure CO gas was reacted with the potassium salt of the P_7^{3-} cluster in presence of [18]-crown-6 (c).[18] Furthermore, the decarbonylation of iron pentacarbonyl by sodium phosphide yields Na(OCP) accompanied by Colman's reagent (d).[17] In a remarkably different approach, the reaction of a borane-capped niobium phosphide anion with carbon dioxide at room-temperature delivers $(OCP)^-$ (e). Recently, a simple and effective synthesis for the sodium salt $[NaOCP(dioxane)_x]$ ($x \approx 2.5$) from basic chemicals (sodium, red phosphorous, ethylene carbonate) has been developed, allowing the preparation of pure material in a good yield (ca. 70% based on P) (f). This sodium salt can be briefly handled on air and was reported to be surprisingly stable in water.[17] The benefits of this method – inexpensive starting materials, one-pot procedure and good yield – were the decisive factors in the choice of this procedure for the synthesis of Na(OCP) used in the present work.

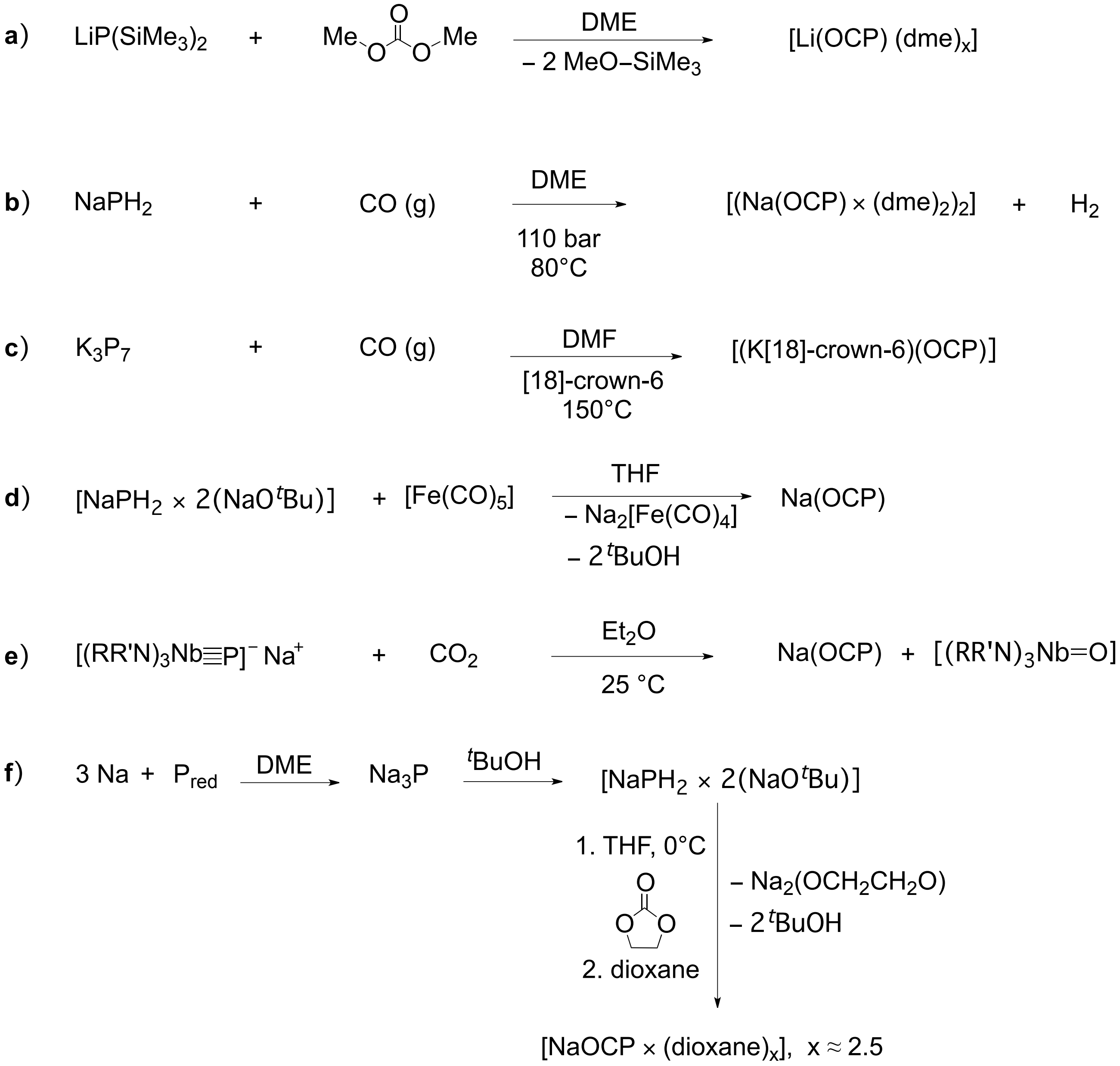

Scheme 1.3 Synthetic approaches to the $(OCP)^-$ anion.

So far, the reactivity of the phosphaethynolate anion has been little investigated. The reaction of Li(OCP) with carbon disulfide at −78°C delivers the sulfur analogue, Li(SCP). When treated with iodine or sulfur dioxide $(OCP)^-$ undergoes oxidative tetramerization to give $(P_4C_4O_4)^{2-}$ (Scheme 1.4).[19]

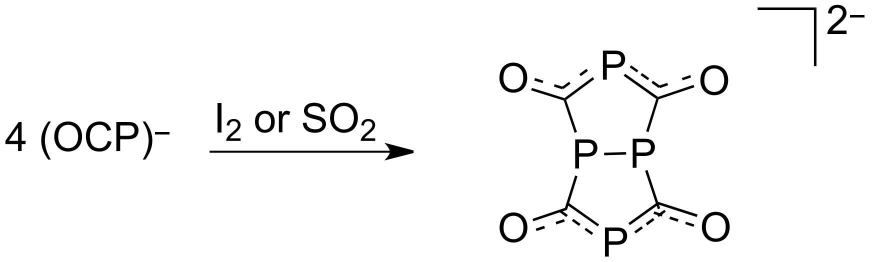

Scheme 1.4 Oxidative tetramerization of $(OCP)^{-}$.

The reaction products of Li(OCP) with sulfur or selenium, the four-membered anionic cycles (**A**) were described (Figure 1.2),[19] which shows the potential of the $(OCP)^{-}$ ion in [2+2] cycloaddition chemistry. Likewise, very recently Jupp and Goicoechea described the formation of four-membered ring anions **B** and **C** in the reaction of K(OCP) with a ketene or bulky carbodiimide, respectively.[18]

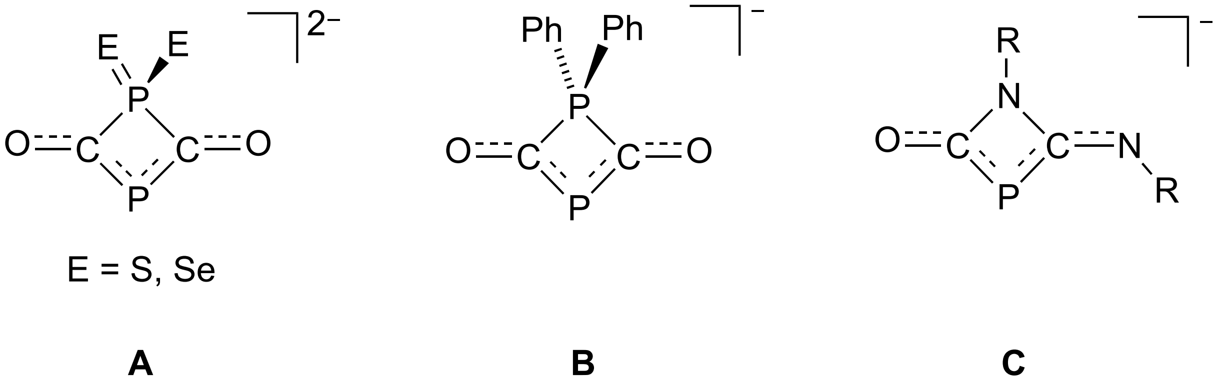

Figure 1.2 Four-membered ring adducts of $(OCP)^{-}$.

Transition metal complexes bearing the pseudo-halogen $(NCO)^{-}$ as ligand, cyanato and isocyanato complexes, are known in the literature.[20-23] The reactivity of the phosphacyanate anion $(OCP)^{-}$ towards a transition metal center, however, has previously been hardly studied. In a simple salt metathesis reaction the first metallaphosphaketene $[Re(PCO)(CO)_2(triphos)]$ was prepared from Na(OCP) and $[Re(OTf)(CO)_2(triphos)]$ (Scheme 1.5). In this complex, the PCO moiety binds via the

P atom to the rhenium center. While the Re-P bond in this metallaphosphaketene exhibits a high covalent character, the P-N bond in the analogous isocyanato complex [Re(NCO)(CO)$_2$(triphos)], is more ionic and the compound is best described as a classical Werner-type complex (M←N$^+$≡C−O$^-$).[24]

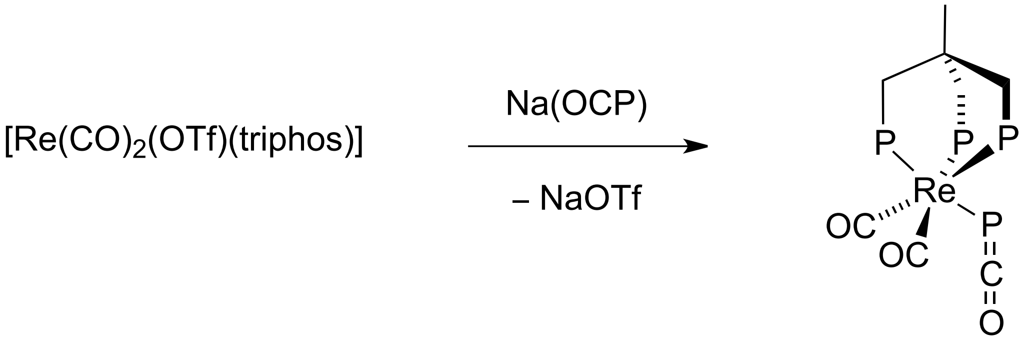

Scheme 1.5 Synthesis of the metallaphosphaketene [Re(PCO)(CO)$_2$(triphos)].

The accessibility of this metallaphosphaketene from (OCP)$^-$ highlights the nucleophilic character of this anion. The present work provides a systematic investigation concerning the reactivity of sodium phosphacyanate towards numerous electrophiles, such as alkyl halides, acid chlorides and organotetrel halides (Figure 1.3).

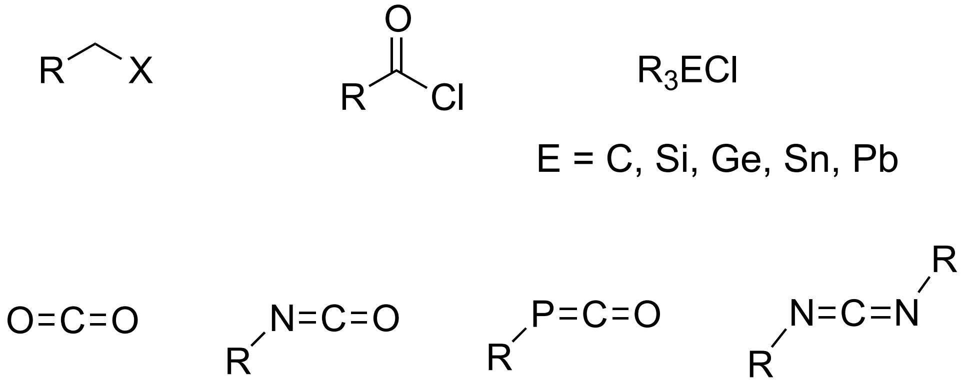

Figure 1.3: Reactants investigated in the present work.

Inspired by the broad scope of cycloaddition chemistry involving CP triple bond species, a number of isoelectronic heteroallenes, in particular carbon dioxide, isocyanates, phosphaketenes and carbodiimides were reacted with Na(OCP).

2. The reaction of Na(OCP) with carbon dioxide: Formation of anionic four-membered rings

2.1 Introduction

The chemistry of phosphorus compounds with multiple bonds, specifically with phosphaalkenes and phosphaalkynes, has grown into a mature field of main group element chemistry over the last decades.[1] These compounds comprise activated π-bonds, which can be employed in various types of cycloaddition reactions. As an example, the *tert*-butylphosphaethyne (^{t}Bu−C≡P) proved to be a highly useful building block for the synthesis of a plethora of ring and cage structures.[1, 3]

Phosphaketenes (R−P=C=O) are likewise unsaturated compounds, which show an enhanced reactivity. Most likely, this is the reason for the fact that only a few examples of phosphaketenes have been reported so far. Among the phosphaketenes with organic substituents R, the supermesityl (Mes* = 2,4,6-tri-*tert*-butylphenyl) analogue is the only stable derivative.[25] When cooled to −15 °C in solution, it partly dimerizes to form 1,3-diphosphetane-2,4-dione (**2**$^{\text{Mes*}}$) (Scheme 2.1), whose structure was also confirmed by an X-ray diffraction study with single crystals.[26]

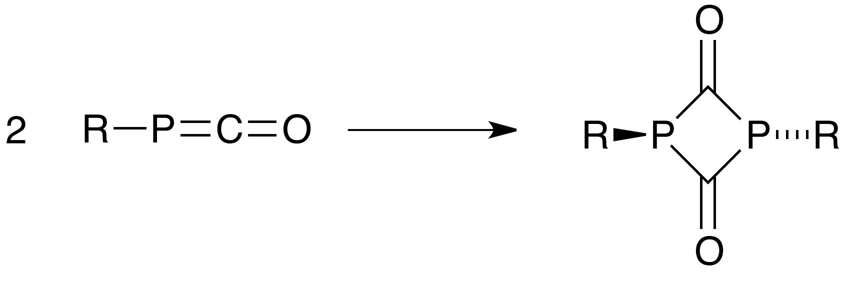

2

R = Mes* (**2**$^{\text{Mes*}}$), ^{t}Bu (**2**$^{t\text{Bu}}$), Tr (**2**$^{\text{Tr}}$)

Scheme 2.1 Dimerization of phosphaketenes.

With sterically less demanding substituents, as in the case of *tert*-butylphosphaketene (generated at −90 °C) dimerization to $\mathbf{2}^{t\mathbf{Bu}}$ occurs already at −60 °C.[27] Furthermore, 1,3-diphosphetane-2,4-dione bearing triphenylmethyl (trityl) groups ($\mathbf{2}^{\mathbf{Tr}}$) has been reported.[28]

Weber and co-workers attempted to synthesize metallaphosphaketenes of the type $(C_5R_5)(CO)_2Fe{-}P{=}C{=}O$ (R = H, ^{t}Bu) by reacting the corresponding bromo iron(II) complexes with [Li(OCP) × 2 DME] in a simple ion-exchange reaction.[29] However, exclusively the metalla-1,3-diphosphetane-2,4-dione ($\mathbf{2}^{[\mathbf{Fe}]}$) was formed (see Scheme 2.2), and the monomeric metallaphosphaketene could not be detected by *in situ* ^{31}P-NMR spectroscopy. The chromium-pentacarbonyl complex of the iron compound $\mathbf{2}^{[\mathbf{Fe}]}$ was characterized by single crystal X-ray diffraction:

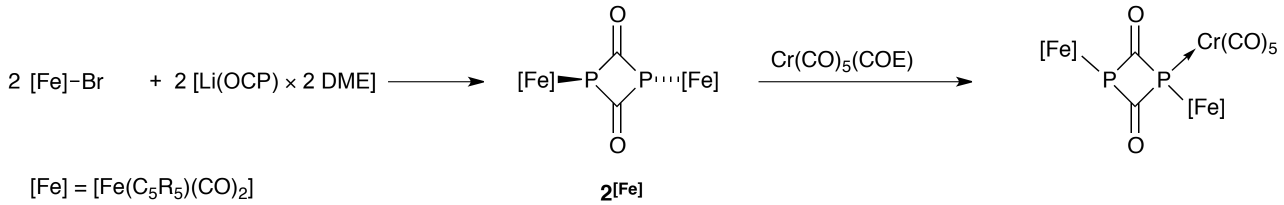

Scheme 2.2 Formation of the metalla-1,3-diphosphetane-2,4-dione $\mathbf{2}^{[\mathbf{Fe}]}$, COE: cyclooctene.

The formation of this type of dimer is characteristic for phosphaketenes and this Woodward-Hoffmann allowed $[2\pi_s + 2\pi_a]$ dimerization has been shown to follow a synchronous concerted mechanism.[30] As a stable monomeric phosphaketene $[(\text{triphos})(CO)_2Re{-}P{=}C{=}O]$, has been reported.[24] Sterically unprotected phosphaketenes can be “stabilized” in the coordination sphere of transition metal complexes as was shown in the case of a methylphosphaketene tungsten complex.[31]

The phosphaethynolate anion can be described as a superposition of the phosphaketenide (**1a**) (Figure 2.1), phosphaethynolate (**1b**) and resonance structure **1c**, which is a donor-acceptor complex of a P^- ion and carbon monoxide. Similarly to the description of a transition metal carbonyl complex, the CO unit acts as a σ-donor and a π-acceptor.

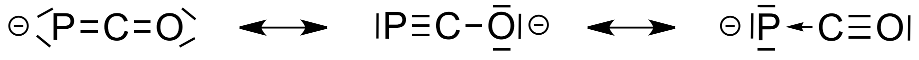

1a **1b** **1c**

40.2 % 51.7% 7.1%

Figure 2.1 Resonance structures of the phosphaethynolate anion.

Natural resonance theory (NRT) calculations showed that the weights of the structures is slightly in favor of **1b** (51.7%) compared to 40.2% for **1a**.[24] Resonance structure **1c** contributes with 7.1%.

Both mesomeric structures **1a** and **1b** have a phosphorus atom engaged in a multiple bond, and consequently the (P≡C−O$^-$)/(O=C=P$^-$) ion can be expected to undergo various types of cycloadditions. Due to Coulomb repulsion, however, the phosphaketene-like spontaneous dimerization of two anions is very unlikely (Figure 2.2).

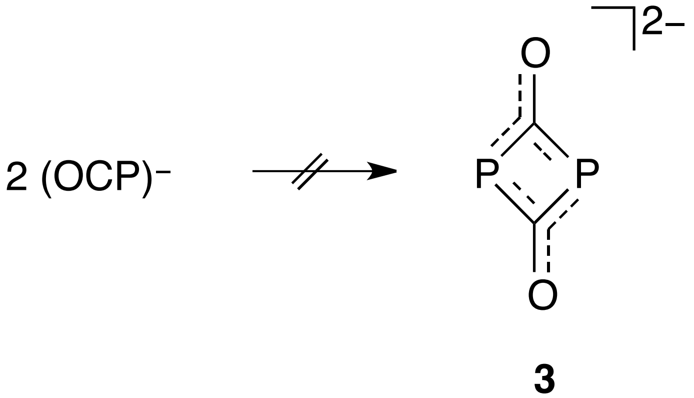

3

Figure 2.2 Hypothetical dimer of the (OCP)$^-$ anion.

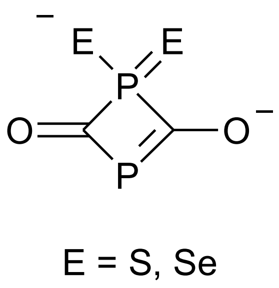

Figure 2.3 Product from the oxidation of the $(OCP)^{-}$ anion with elemental sulphur or selenium.

The only reported dianions related to **3** are the oxidation products of Li(OCP) with sulphur and selenium (Figure 2.3). Except for the ^{13}C-NMR chemical shifts no further analytical information is accessible for these compounds.[32]

In this chapter the synthesis, characterization and computational investigation of the carbon dioxide adduct of the (hypothetical) dimer $(P_2C_2O_2)^{2-}$ (**3**) is discussed. To a certain extent it can be regarded as a phosphorus analogue of the squarate anion $(C_4O_4)^{2-}$.

2.2 Synthesis and structure

A continuous stream of carbon dioxide was passed through a solution of Na(OCP)(dioxane)$_x$ ($x = 2.5 - 2.7$) in THF at room temperature, and quickly a color change from colorless to yellow was observed. After an hour two broad resonances at $\delta = 105$ and 270 ppm ($\nu_{1/2} \approx 4500$ Hz) of similar intensity in the ^{31}P-NMR spectrum indicate the formation of a product with two inequivalent phosphorus atoms. Alongside the reaction product the ^{31}P-NMR spectrum indicates a small remaining amount (ca. 15%) of the starting material Na(OCP) at δ (^{31}P) = −394 ppm. Removal of the solvent under reduced pressure delivered the yellow sodium salt of **4**, which is insoluble in apolar solvents (Scheme 2.3).

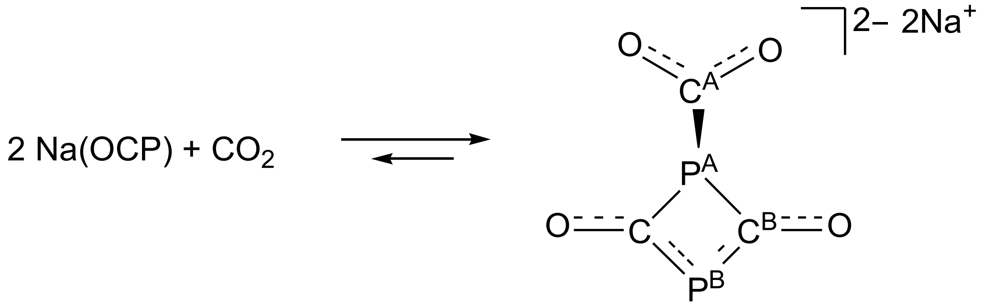

Scheme 2.3 Synthesis and structure of the dianion **4**. The suffixes A and B label the different carbon and phosphorus nuclei (see text).

To account for the very broad resonances in the ^{31}P-NMR spectrum at room temperature, low temperature NMR studies of the solution containing the reaction product were performed. But even at −100 °C the system shows the same broad resonances. To exclude the possible presence of a paramagnetic species, the solution was examined by EPR-spectroscopy and found to be EPR silent.

To obtain a properly characterizable product, simple cation exchange reactions with various salts (e.g. alkali, earth alkali halides and triflates and lanthanide halides) were tried. None of these had a measurable impact on the features of the NMR spectra with the exception of barium triflate. The ^{31}P-NMR spectrum of this reaction mixture shows – besides the remaining minor signal of Na(OCP) – two much sharper, but still broadened ($\nu_{½}$ = 50 Hz) singlets of the same intensity at δ = 102 and 279 ppm (representing the phosphorus atoms P^A and P^B, respectively) which show no detectable coupling between the two P atoms. The remarkable decrease of the line width of the ^{31}P-resonances suggests the hindrance of a dynamic exchange phenomenon, in which somehow the coordination modes of the counter cations are involved. However, based on the negligible change in the chemical shifts, it can be assumed that the identity of the phosphorus containing anion **4** remains unchanged. The ^{13}C-NMR spectrum contains a doublet at δ = 183 ppm ($^1J_{PC}$ = 45 Hz) and a doublet of doublets at δ = 233 ppm ($^1J_{PC}$ = 60 Hz, $^1J_{PC}$ = 25 Hz) besides the solvent peaks, the signal arising from the triflate anion and the doublet originating from unreacted Na(OCP) (δ = 166 ppm, $^1J_{PC}$

= 46 Hz). Both ^{13}C resonances of **4** are typical for carbonyl compounds: the one at δ = 183 ppm (C^A) is characteristic for carboxylate salts (and carboxylic acids)[33] and shows coupling to one phosphorus atom only. The coupling constant ($^1J_{PC}$ = 45 Hz) indicates a direct P-C linkage ($P{-}C^AO_2^-$). Similar values have been reported for free and complexed phosphinoformates (e.g. δ = 183.7 ppm, $^1J_{PC}$ = 18 Hz for Ph_2PCO_2Na).[34] The other resonance (for C^B) shows coupling to two different phosphorus atoms, and its chemical shift fits to that of 1,3-diphosphetane-2,4-diones (Table 2.1). A comparable ^{13}C-NMR chemical shift of $\delta = 243$ ppm has been reported for the low coordinated phosphorus nucleus in the sulphur/selenium oxidation product of Li(OCP) (see Figure 2.3). Although proper integration is not possible, the intensities of the doublet (C^A) and the doublet of doublet (C^B) suggest a ratio of 1 : 2 for the C^A and C^B carbon atoms. Based on these NMR investigations the structure shown in Scheme 2.3 is proposed for the reaction product **4**. The phosphorus atom (P^A) of this unsymmetrical 1,3-diphosphetane-2,4-dione structure is connected to a carboxylate (CO_2^-) unit (*vide supra*) and the ^{31}P resonance at lower frequency is assigned to this λ^3,σ^3 phosphorus atom. The other ^{31}P chemical shift at higher frequency (δ = 279 ppm) is attributed to the dicoordinated P^B atom of the four-membered ring. Both, the disodium and barium salt of **4** can be obtained as pale-yellow amorphous powders, which in case of the barium salt is contaminated with $Na(O_3SCF_3)$ as by-product.

The infrared (IR) absorptions and NMR chemical shifts of the sodium salt of anion **4** were computed in order to bolster our structure assignment. (The use of sodium as counter cations in the calculations is preferred, since no inclusion of relativistic effects is needed.) Relevant experimental and computed data are listed in Table 2.1.

Table 2.1 Experimental ^{31}P-, ^{13}C-NMR chemical shifts (δ, ppm; s: singlet, d: doublet, dd: doublet of doublet), coupling constants (*J*, Hz) and characteristic IR frequencies (*ν*, cm^{-1}) for $\mathbf{2}^{\mathbf{Mes*}}$, $\mathbf{2}^{\mathbf{[Fe]}}$, the barium salt of **4** and the calculated values for the anion **4** with sodium counter ions (B3LYP/aug-cc-pVDZ level of theory).

	$\mathbf{2}^{\mathbf{Mes*}[a]}$	$\mathbf{2}^{\mathbf{[Fe]}\,[b]}$	Ba^{2+} salt of **4**	Calculated anion $\mathbf{4}^{[c]}$
$\delta(P^A)$	23.6 (s)	110.9 (s)	102	124
$\delta(P^B)$	-	-	279 (s)	275
$\delta(C^A)$	-	-	183 (d)	180
$\delta(C^B)$	216.2 (d)	253.1 (d)	233 (dd)	243
$^1J(P^A,C^A)$	-	-	45	49.6
$^1J(P^A,C^B)$	53.8	50.2	60	31.2
$^1J(P^B,C^B)$	-	-	25	36.2
$\nu(C^AO_2)_{sym}$	-	-	1235	1263
$\nu(C^AO_2)_{asym}$	-	-	1532	1575
$\nu(C^BO)_{asym}$	1645	1600	1464	1499

[a] see ref.[26]
[b] see ref.[29]
[c] calculated with Na^+ counter ions.

The experimental IR frequencies of **4** agree nicely with the calculated ones and support the molecular structure of the compound (see Table 2.1). In the solid state, the disodium and barium salt of **4** show similar IR absorptions, but the solution IR spectrum of the disodium salt contains numerous absorptions in the CO stretching region indicating the presence of different $Na_2(P_2C_3O_4)$ species. The symmetric and asymmetric vibrations of the carboxylate fragment (at ν = 1235 and 1532 cm^{-1}, respectively) are similar to the values of phosphinoformates (ν = 1320 and 1536 cm^{-1} for Ph_2PCO_2Na).[34] The strong and characteristic asymmetric vibration band of the $P_2(CO)_2$ unit is observed at ν = 1464 cm^{-1}. Compared to the neutral compounds $\mathbf{2}^{\mathbf{Mes*}}$ and $\mathbf{2}^{\mathbf{[Fe]}}$, this band is shifted by about 150 cm^{-1} to lower wave numbers indicating a substantially decreased bond order of the C=O bond of the $P_2(CO)_2$ ring in **4**. This suggests that as expected a substantial part of the negative charge is localized on the oxygen atoms as shown in the resonance structures **4** and **4'** below (Figure 2.4).

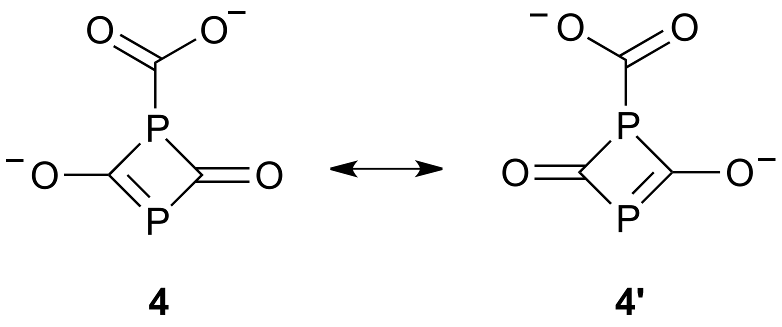

Figure 2.4 Resonance structures describing the electronic structure of dianion **4**.

It was not possible to obtain single crystals of $Na_2(P_2C_3O_4)$ **4**, therefore the computed structure of **4** with two sodium cations is discussed in comparison with that of model compound $\mathbf{2^{Me}}$ (R = Me, *trans* isomer), $Na_2(P_2C_2O_2)$ **3** – the dimeric form of Na(OCP) – and $\mathbf{5^{Me}}$, the monoanion $(MeP_2C_2O_2)^-$ with a methyl group bound to one phosphorus atom. The most important bond lengths, Wiberg bond indices (WBI) and natural population analysis (NPA) charges are collected in Table 2.2.

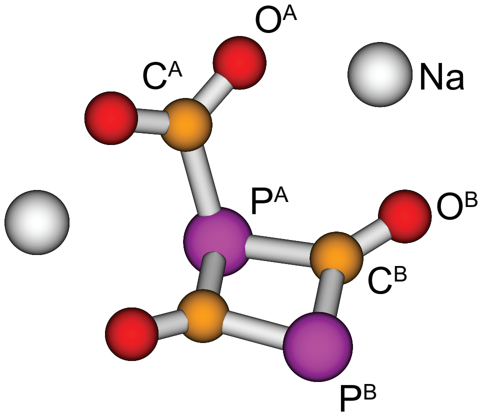

Figure 2.5 Optimized structure of dianion **4** with sodium counter ions.

Table 2.2 Calculated P-C and C-O bond lengths (*d*, Å), Wiberg bond indices (WBI, −) in parentheses, sum of bond angles around the trivalent P atoms [Σ°(P)] and NPA charges (*q*, e) of $\mathbf{2}^{\mathbf{Me}}$, **3**, **4** and $\mathbf{5}^{\mathbf{Me}}$ at the B3LYP/aug-cc-pVDZ level of theory. Anions **3** and **4** were calculated with Na^+ as counter ions.

	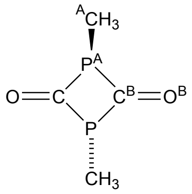 $\mathbf{2}^{\mathrm{Me}}$	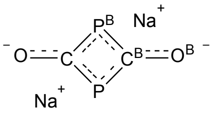 3	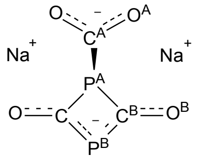 4	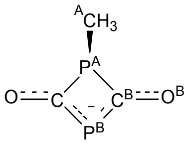 $\mathbf{5}^{\mathbf{Me[a]}}$
$d(P^A–C^A)$	1.871 (0.94)	-	1.926 (0.87)	1.888 (0.92)
$d(P^A–C^B)$	1.898 (0.93)	-	1.912 (0.89)	1.927 (0.88)
$d(P^B–C^B)$	-	1.865 (1.08)	1.817 (1.17)	1.835 (1.15)
$d(C^A–O^A)$	-	-	1.259 (1.42)	-
$d(C^B–O^B)$	1.204 (1.81)	1.249 (1.52)	1.243 (1.52)	1.126 (1.64)
Σ°(P)	299.7	-	283.0	280.7
$q(P)$	P^A: +0.67	P^B: −0.04	P^A: +0.48, P^B: +0.32	P^A: +0.53, P^B: +0.11
$q(C)$	C^B: +0.04	C^B: −0.05	C^A: +0.62, C^B: −0.05	C^B: −0.02
$q(O)$	O^B: −0.54	O^B: −0.74	O^A: −0.83, O^B: −0.74	O^B: −0.66

[a] Calculated without any counter ion.

As expected, the simple 1,3-dimethyl-1,3-diphosphetane-2,4-dione ($\mathbf{2}^{\mathbf{Me}}$) is best described with two normal-valent λ^3,σ^3 phosphorus centers [Σ°(P) = 299.7] forming P-C single bonds, while the carbon centers are involved in C=O double bonding. There is little delocalization in this heterocycle. In the hypothetical dianion $(P_2C_2O_2)^{2-}$ **3**, the P-C bonds shorten slightly but remain in the usual range of P-C single bonds again indicating little π-electron delocalization (see also the WBI). The C-O bonds lengthen significantly from 1.20 Å to 1.25 Å indicating a bond order of 1.5. The structure of **3** is significantly altered in its CO_2 adduct **4**. The three-coordinated phosphorus center

P^A [$\Sigma°(P) = 283.0$] forms three long P-C single bonds to its carbon neighbors with WBIs somewhat below one. The second, two-coordinated phosphorus atom P^B has much shorter bonds to the adjacent carbon centers C^B and the WBI increases to about 1.2. The C-O lengths are again typical for bonds of the order 1.5. Consequently, **4** can be described as a charge transfer complex between the dianion $(P_2C_2O_2)^{2-}$ **3** and a carbon dioxide molecule. In this formal charge transfer process (for a more likely route leading to **4** see below), a mono-anionic π-delocalized $(O\text{-}C^B\text{-}P^B\text{-}C^B\text{-}O)^-$ unit is formed to which another anionic $(P\text{-}CO_2)^-$ "phosphinoformate" fragment is attached.

$\mathbf{5^{Me}}$ is obtained formally from **4** by replacement of the carboxylate unit with a methyl group. On the basis of the "averaged" bond lengths, there is a π-delocalization within the $(O\text{-}C^B\text{-}P^B\text{-}C^B\text{-}O)^-$ unit in $\mathbf{5^{Me}}$, however, slightly less pronounced compared to **4**. The CO bonds in $\mathbf{5^{Me}}$ possess a slightly higher double bond character and the P^B phosphorus atom is less positively charged than in **4**.

With the exception of **3**, the computed partial charges show the expected pattern, that is the negative charges are mainly carried by the electronegative oxygen centers, while the phosphorus atoms in $\mathbf{2^{Me}}$ and **4** are positively charged. In all 1,3-diphosphetane-2,4-dione rings the carbon centers C^B are almost neutral; the C^A in the carboxylate group in **4** is expectedly positively charged. Interestingly, in **3** all atoms carry a negative partial charge, which may explain why this hypothetical dianion will suffer from a Coulomb-explosion under spontaneous decay into two monomeric $(OCP)^-$ monoanions.

2.3 VT-NMR experiments

Phosphinoformates as well as complexes between neutral phosphanes and CO_2 are thermally unstable and in the latter case require additional stabilization by a Lewis acid (see CO_2 activation by frustrated Lewis acid-base pairs).[35, 36] Even after prolonged reaction times under slight CO_2 pressure, reaction mixtures with the disodium salt of **4** contain about 15% of Na(OCP) suggesting the equilibrium shown in Scheme 2.3.

To demonstrate this, a sample of the sodium salt of **4** and an internal standard (PPh_3) was prepared and sealed in a NMR tube. ^{31}P-NMR-spectra were recorded at three different temperatures (for details see the experimental section). Although it was not possible to quantitatively evaluate this equilibrium because of the uncertainty in the CO_2 concentration and side-reactions (*vide infra*), qualitatively an increase of the Na(OCP) concentration with increasing temperature was clearly observed (by 10% at 40 °C and 34% at 55 °C). This process is reversible (if heating for longer time periods is prevented) and cooling of the mixtures to room temperature almost reinstalls the initial relative concentrations of **4** and Na(OCP).

Longer warming of the sodium salt of **4** in THF leads to the slow formation of the previously reported tetrameric dianion $(P_4C_4O_4)^{2-}$ as the product of an oxidation reaction[19] (detected by ^{31}P-NMR- and IR-spectroscopy). The reaction mixture contains − besides some unreacted **4** − indeed carbon monoxide (detected by ^{13}C-NMR) and oxalate (detected by IR spectroscopy) as reduction products and also carbonate ions. This remarkable reaction underscores the high reducing power of Na(OCP).[24] When Na(OCP) is reacted with CS_2, which has a higher adiabatic electron affinity (+0.30 eV) than CO_2 (−0.66 eV)[37] only the tetrameric $(P_4C_4O_4)^{2-}$ dianion is observed in marked contrast to the reaction of Li(OCP) with CS_2 at low temperature, which was reported to give Li(SCP). (A similar reaction has been observed when Li(OCP) was treated with sulfur dioxide at low temperature, in this case the primarily forming $SO_2^{-\bullet}$ radical forms the disulfite $(S_2O_4)^{2-}$ anion).[32, 38]

2.4 Mechanistic investigations

Two plausible routes may lead to the formation of the dianion **4**. (a) Two $(OCP)^-$ anions dimerise to the cyclic dimer **3**, which is then trapped by a CO_2 molecule or, (b)

CO_2 undergoes a nucleophilic attack by $(OCP)^-$ at the carbon center and to this adduct a second equivalent of Na(OCP) is added in a (formal) cycloaddition process. To gain deeper insight into the formation of **4** computations have been performed at the B3LYP/6-31+G*(THF) level.

As mentioned above, Coulomb repulsion will favor the spontaneous decomposition of the dianion **3** and consequently hinder the agglomeration of two Na(OCP) species. Hence, route (a) is not very likely and furthermore there is no indication for the formation of the dimeric dianion **3** when a solution of Na(OCP) is kept at low temperatures. Based on computations, the dimerization of Na(OCP) is indeed slightly endothermic ($\Delta_r E = 5.7$ kcal mol^{-1}) and when the entropy factor is taken into account the Gibbs free energy rises to $\Delta_r G^{298\,K} = 19.9$ kcal mol^{-1}. It is thus very unlikely that **4** is formed *via* route (a).

On route (b) two possible adducts of Na(OCP) and CO_2 can be considered: $[O_2C{-}O{-}C{\equiv}P]^-$ and $[O_2C{-}P{=}C{=}O]^-$. The former one, which results from the nucleophilic attack of the oxygen center of the ambiphilic $(OCP)^-$ anion, is significantly less stable by 19.2 kcal mol^{-1} than the other isomer, $[O_2C{-}P{=}C{=}O]^-$. Consequently, only this latter isomer was considered in the computation of the minimum energy reaction pathway (MERP) shown in Figure 2.6.

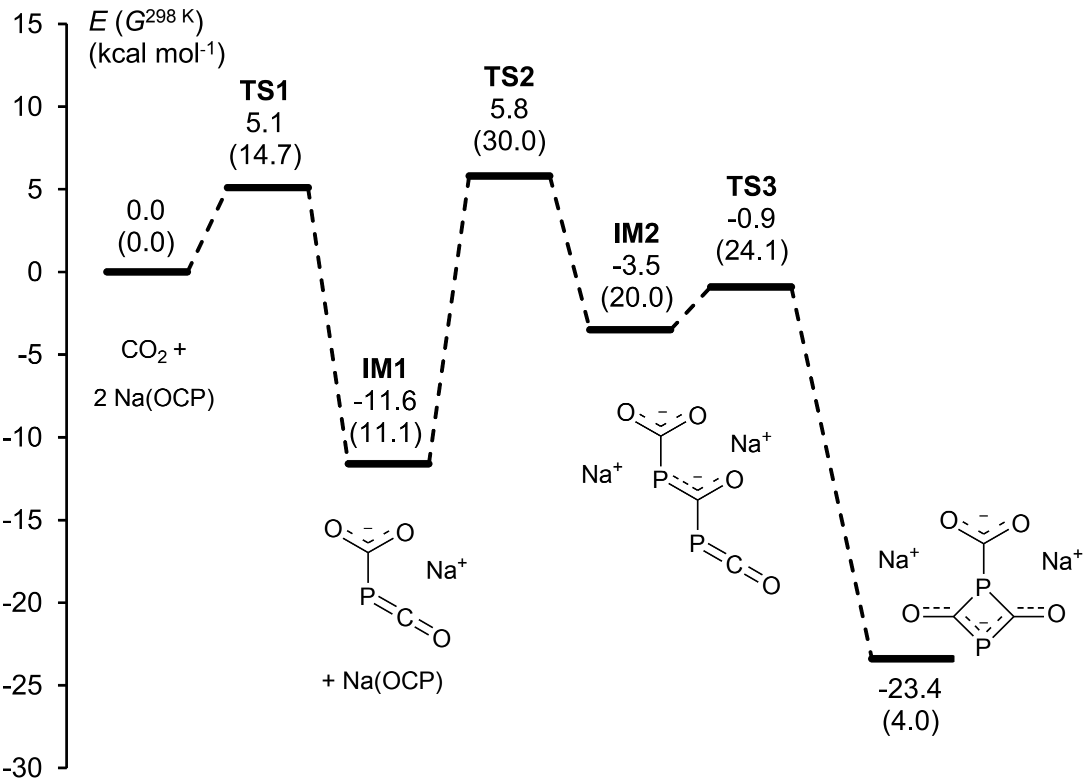

Figure 2.6 Minimum energy reaction pathway leading to dianion **4** at the B3LYP/6-31+G*(THF) level of theory. Relative Gibbs free energies ($G^{298\ K}$) are given in parentheses.

With respect to the starting materials, two Na(OCP) and CO_2, the formation of the adduct $[O_2C{-}PCO]^-$ (**IM1**) in the first reaction step is exothermic by $\Delta_rE = -11.6$ kcal mol^{-1} and proceeds via a rather low activation barrier of $\Delta E^{\ddagger} = 5.1$ kcal mol^{-1}. The next step is the addition of a second equivalent of Na(OCP). All attempts to locate a transition state for a direct and concerted [2+2] cycloaddition reaction failed. Instead, $(OCP)^-$ may attack the electrophilic carbon center of the phosphaketene unit in **IM1** to form the rather energy rich intermediate **IM2** [being 8.0 kcal mol^{-1} less stable than **IM1** + Na(OCP)]. According to these computations, this step is the rate determining one with $\Delta E^{\ddagger} = 17.4$ kcal mol^{-1}. The formed open dianion **IM2** undergoes a ring-closing reaction via a transition state of a very low energy ($\Delta E^{\ddagger} = 2.6$ kcal mol^{-1}) to give the final product **4**. This reaction is best viewed as an intramolecular nucleophilic attack of the central phosphorus atom on the electrophilic carbon center of the peripheral P=C=O group. Including entropy, all reaction steps become endergonic. Overall, the formation of the final product is weakly endergonic by $\Delta_rG^{298\,K} = +4.0$ kcal mol^{-1} (calculated at 298 K in the gas phase including solvent effects). Although these model calculations are rather approximate (e.g. the ionic interaction is different in the gas phase from the one in a solution, and solvation influences the entropy), the calculated $\Delta_rG^{298\,K} \approx 0$ value and the moderate activation barriers agree well with the results from the VT-NMR experiments, which indicate a rather slow (on the IR and even NMR time scale) equilibrium between **4**, CO_2 and two $(OCP)^-$ ions.

2.5 Reactivity studies

As mentioned above, the π-bonding in the $OC^BP^BC^BO$ moiety of **4** shows a significant degree of delocalization. While the negative charge is mainly located on the oxygen atoms, the HOMO of the dianion **4** is a π(p)-type orbital perpendicular to the ring plane and mainly located at the dicoordinated P^B atom with minor contributions from the oxygen atoms (Figure 2.7).

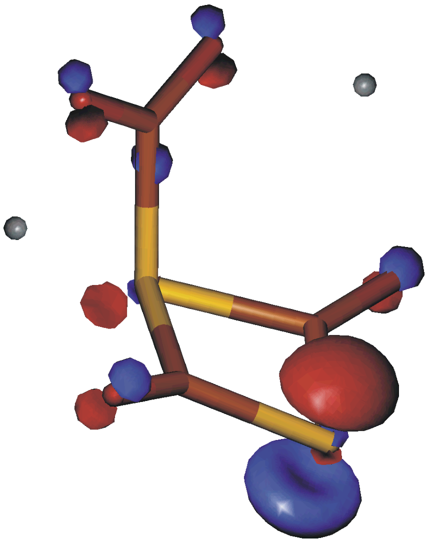

Figure 2.7 HOMO of dianion **4** with sodium counter ions (B3LYP/6-31G*).

Consequently, **4** should behave as a phosphorus centered nucleophile and some test reactions were performed to verify this assumption. All reaction products shown in Scheme 2.4 were characterized by ^{31}P-, ^{13}C-NMR spectroscopy and IR spectroscopy. In case of the product **2^{Tr*}** a structure analysis using single crystal X-ray diffraction was performed.

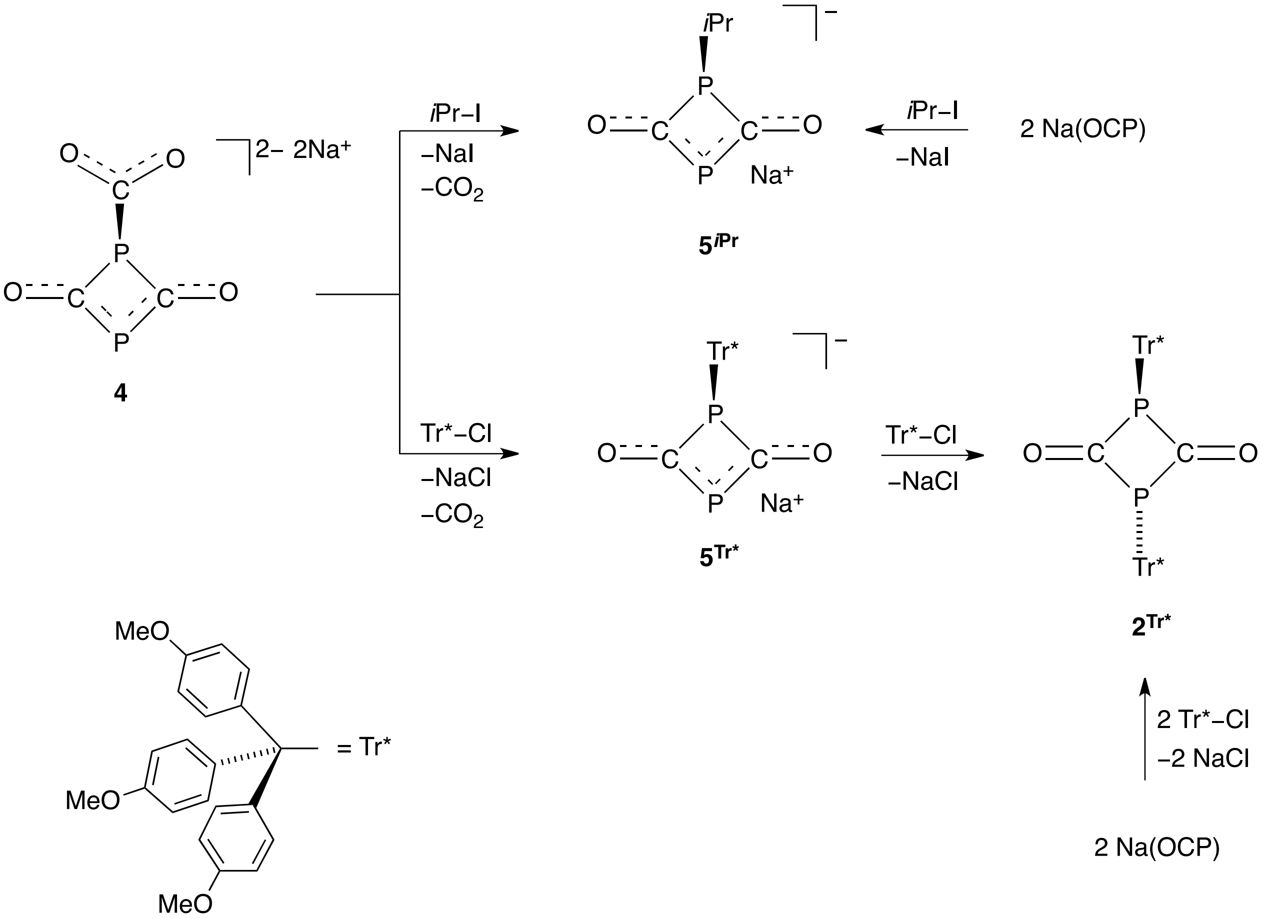

Scheme 2.4 Reactions of dianion **4** and Na(OCP) with 2-iodopropane and 4,4',4''-trimethoxytriphenylmethyl chloride.

The disodium salt of the dianion **4** reacts cleanly with one equivalent of 2-iodopropane or 4,4',4''-trimethoxytriphenylmethyl chloride (Tr*-Cl) forming the mono-anionic four-membered rings **5^{iPr}** and the rather unstable **5^{Tr*}**, respectively. One equivalent of CO_2 is released in these reactions (detected by IR-spectroscopy). While **5^{iPr}** does not react further with 2-iodopropane, **5^{Tr*}** cleanly reacts with an excess of Tr*-Cl to give the neutral 1,3-diphospha-2,4-dione $\mathbf{2}^{\mathbf{Tr*}}$. A related compound has been reported by Schmutzler *et al.* as a product from the reaction of $Ph_3C{-}PH_2$ with phosgene, $COCl_2$.[28] By slow evaporation of THF yellow diamond shaped crystals were obtained, which were analyzed by single crystal X-ray diffraction (Figure 2.8). The structure shows the expected planar centro-symmetric 1,3-diphosphetane-2,4-dione ring. For steric reasons a *trans* orientation of the Tr* substituents is observed and both phosphorus centers reside in pyramidal coordination sites [Σ°(P) = 308.4]. All bonding parameters are comparable to those of $\mathbf{2}^{\mathbf{Mes*}}$[26] and the calculated structure of $\mathbf{2}^{\mathbf{Me}}$ (see Table 2.2) with P-C single bond and C=O double bond lengths in the expected range.[39]

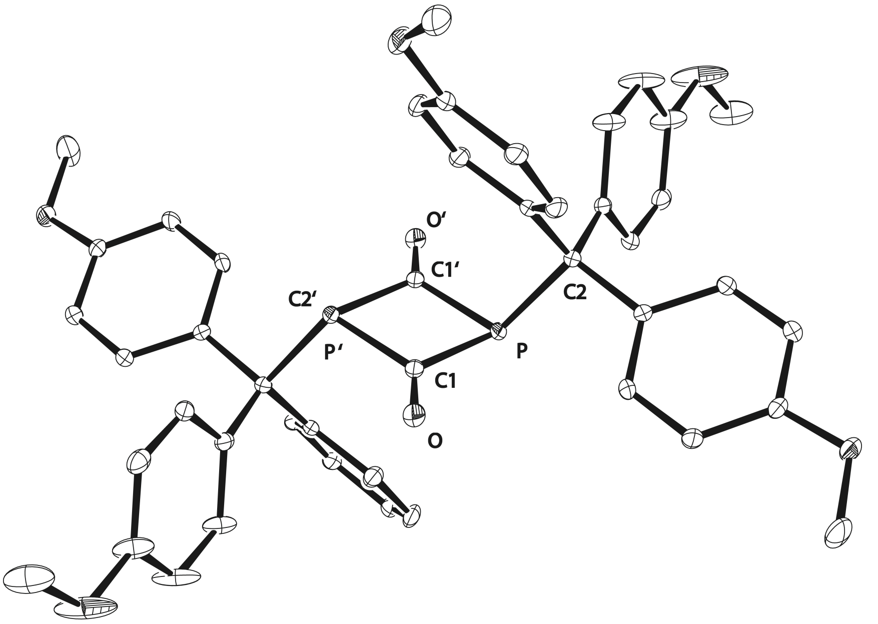

Figure 2.8 ORTEP plot of $\mathbf{2}^{\mathbf{Tr*}}$ (thermal ellipsoids are drawn at 30% probability). Hydrogen atoms and solvent molecules (THF) have been omitted for clarity. Selected bond lengths (Å) and angles (°): C1-P 1.858(3), C1-O 1.205(3), P-C2 1.906(2); P-C1-P' 97.6(1), C1-P1-C1' 82.4(1), Σ°(P) = 308.4, Σ°(C1) = 359.9.

Since in solution **4** is in equilibrium with Na(OCP), it cannot be excluded that $\mathbf{5}^{\boldsymbol{i}\mathbf{Pr}}$ and $\mathbf{5}^{\mathbf{Tr*}}$ are formed in reactions with Na(OCP). Indeed, the reaction between Na(OCP) and 2-iodopropane – even in excess – leads exclusively to $\mathbf{5}^{\boldsymbol{i}\mathbf{Pr}}$. However, the reaction between two equivalents Na(OCP) and the sterically encumbered but activated trityl chloride Tr*-Cl gives only $\mathbf{2}^{\mathbf{Tr^*}}$. Even at low temperatures the monoanionic heterocycle $\mathbf{5}^{\mathbf{Tr^*}}$ could not be detected. This species is hence only accessible from the CO_2 adduct **4** which behaves as an $(P_2C_2O_2)^{2-}$ transfer reagent most likely via a nucleophilic attack of the dicoordinated P center (see HOMO in Figure 2.7) and concomitant loss of CO_2.

2.6 Conclusion

Although the dimerization of $(OCP)^-$ is hampered by Coulomb repulsion, a CO_2 adduct of the hypothetic dimeric dianion $(P_2C_2O_2)^{2-}$ – to some extent an analogue of the squarate anion $(C_4O_4)^{2-}$ – can be synthesized. This adduct forms in an almost thermoneutral reaction and the experiments have shown that the disodium salt $Na_2(P_2C_3O_4)$ **4** is in equilibrium with CO_2 and Na(OCP). Computations allow to propose a reaction mechanism, which differs from a classical concerted [2+2] cycloaddition.[30] The first reaction step involves the attack of the CO_2 carbon center by the phosphorus center of $(OCP)^-$. In the following step the carbon center of the resulting phosphaketene ($[O_2C{-}P{=}C{=}O]^-$) is attacked by a second $(OCP)^-$ anion. The final step in the formation of the four-membered 1,3-diphospha-2,4-dionate ring can be described as an intramolecular nucleophilic ring closure reaction.

In its reactions with alkyl halides, however, dianion **4** serves as a $(P_2C_2O_2)^{2-}$ transfer reagent allowing the synthesis of mono-substituted four-membered ring anions $[R{-}P(CO)_2P]^-$. These anions can react further with alkyl halides to give neutral 1,3-diphospha-2,4-diones. Alternatively, these species can be obtained in the reaction between Na(OCP) and alkyl halides. The monoanions are not always accessible in the reactions with Na(OCP). Further studies could be carried out in order to explore the potential of these latter anionic species in the synthesis of phosphorus heterocycles.

3. Experimental proof for the ambident character of the $(OCP)^-$ anion: Reactions of Na(OCP) with triorganyl tetrel compounds

3.1 Introduction

Ambident nucleophiles have not only attracted scientific attention but also play an important role in various synthetic procedures. For example, enolate anions are remarkably useful synthons in a plethora of organic transformations. According to the HSAB concept, soft electrophiles (e.g. alkyl halides) can be attacked by the carbon center, which is widely utilized to construct a carbon-carbon bond.[40] On the contrary, silyl halides as hard electrophiles react at the oxygen site, which enables the application of silyl ethers as protecting groups for carbonyl compounds.[41] The driving force is the high oxophilicity of silicon, manifested in the exceptionally large bond energy of the Si−O σ-bond (111.2 kcal/mol), which exceeds the Si−C σ-bond energy (82.6 kcal/mol).[39] In accordance with the diagonal relationship between carbon and phosphorus, the ambident character of phosphaenolate anions has been reported in the literature, and the preference of the oxygen site was found in silylation reactions: A 1,3 silyl shift was described, whereby $Me_3Si{-}P{=}CR{-}O{-}SiMe_3$ was obtained from $(Me_3Si)_2P{-}CO{-}R$.[42, 43] This observation was explained by the weakness of the Si−P σ-bond (bond energy: 62.7 kcal/mol)[39] compared to the strength of the Si−O σ-bond.[44] Similarly, silyl migration was assumed in the reaction of $[(^iPr_3Si)(Me_3Si)_2P]$ with phosgene, however no details were reported.[45] The authors identified the product as $^iPr_3Si{-}O{-}C{\equiv}P$ by extensive ^{31}P-, ^{13}C-, ^{17}O-, ^{29}Si- and ^{1}H-NMR spectroscopic investigations and − among others – mentioned a surprisingly large $^3J_{PSi}$ coupling constant (51.3 Hz). Furthermore, it was reported that $^iPr_3Si{-}O{-}C{\equiv}P$ is not accessible directly from $^iPr_3SiCl$ and the lithium salt of the $(OCP)^-$ anion.[43, 45] On the contrary, the nitrogen analogue of the latter, $(^iPrNCP)^-$, reacts with R_3SiCl (R = Ph, Me) to form

^{i}Pr(R_3Si)N−C≡P.[46, 47] The formation of the Si−N bond was explained by the stronger affinity of silicon for nitrogen than for phosphorus (σ-bond energies: Si−N: 92.0 kcal/mol vs. Si−P: 62.7 kcal/mol).[39]

Different theoretical studies have already proposed the ambident character of the $(OCP)^-$ anion,[24, 48] however, there is no experimental evidence to date to verify this. The alkylation of this anion takes place on the phosphorus atom forming transient phosphaketenes (see Chapter 2). Furthermore, the first example of an $(OCP)^-$ transition metal complex, which is best described as a metallaphosphaketene [Triphos$(CO)_2$Re−P=C=O] has been reported.[24] In these reactions exclusively the phosphorus site of the $(OCP)^-$ anion attacks the electrophile. Therefore, the question arises whether the silylation of the $(OCP)^-$ anion also takes place on the phosphorous atom or − as assumed due to the high oxophilicity of silicon − on the oxygen atom. In this chapter, the results of the studies on the reactivity of Na(OCP) towards triorganyl tetrel compounds (R_3EX where E = Si, Ge, Sn, Pb; R = Ph or ^{i}Pr; X = Cl or OTf, trifluoromethanesulfonate) are discussed. A clarification is provided, which of the two isomers shown in Scheme 3.1 is formed.

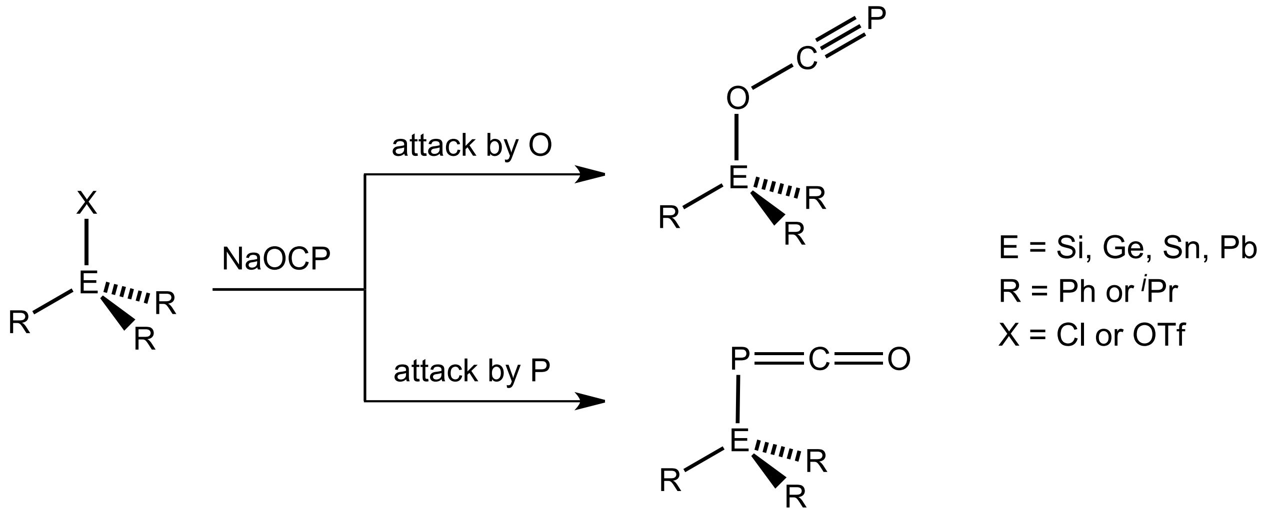

Scheme 3.1 Possible reactivity of Na(OCP) towards triorganyl tetrel compounds.

3.2 Oxyphosphaalkynes ($R_3E-O-C\equiv P$) vs. phospha-ketenes ($R_3E-P=C=O$)

Density functional calculations on the relative energy of the phosphaketene ($R_3E-P=C=O$, R = H, Ph) compared to the corresponding heterosubstituted oxyphosphaalkyne ($R_3E-O-C\equiv P$) were performed. At the B3LYP/cc-pVDZ(-PP) level of theory the phosphorus bonded analogues (phosphaketenes) are more stable than the oxygen bonded isomers for both R = H and Ph (Figure 3.1).

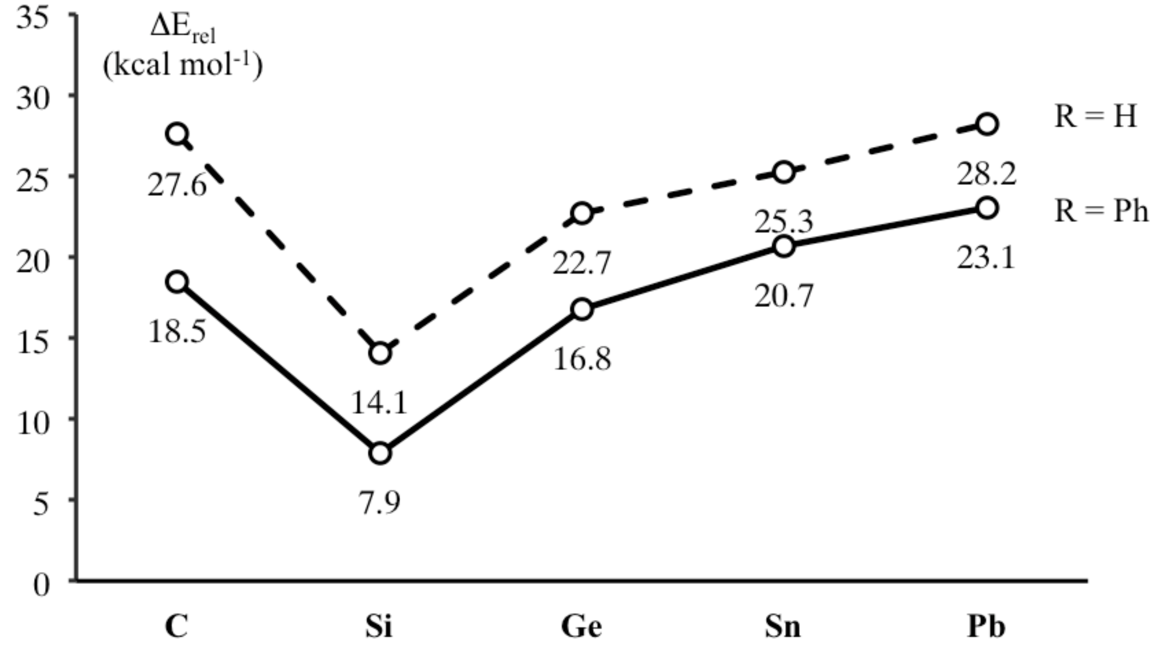

Figure 3.1 Relative energy of the oxyphosphaalkynes ($R_3E-O-C\equiv P$) compared to that of the corresponding phosphaketenes ($R_3E-P=C=O$) at the B3LYP/cc-pVDZ(-PP) level [E = C, Si, Ge, Sn, Pb; R = H (dotted line), Ph (solid line)].

In the case of carbon (E = C), the energy difference between the two isomers is remarkably large (e.g. 18.5 kcal/mol for R = Ph). This agrees with the experimental observations described in Chapter 2: The reaction of Na(OCP) with 4,4',4"-trimethoxytriphenylmethyl chloride delivers the four-membered ring dimer of the initially formed phosphaketene, which, however, could not be detected by NMR spectroscopy even at low temperature.

3.3 Silylphosphaketenes – Siloxyphosphaalkynes

Among the group 14 analogues the smallest relative energy difference between the two isomers is found in the case of the silicon compounds (E = Si). This energy difference (7.9 kcal/mol for R = Ph) is outside of the range of the computational error and thus the silyl phosphaketene is predicted to be more stable than the silyl oxyphosphaalkyne. These results are inconsistent with the previous experimental study carried out by Heckmann.[45] The authors stated that $^{i}Pr_3Si{-}O{-}C{\equiv}P$ was formed rather than conserving the P-Si bond of the precursor. In the light of our calculations, however, there is no thermodynamic driving force for the formation of the less stable oxyphosphaalkyne isomer. Previously, the reported compound could not be obtained from Li(OCP) and $^{i}Pr_3SiCl$.[45] Therefore, Na(OCP) was reacted with the more reactive R_3SiOTf (R = Ph, ^{i}Pr) in order to elucidate this contradiction. When the reaction was performed with $^{i}Pr_3SiOTf$ at room temperature in ethereal solvent, in the ^{31}P-NMR spectrum three singlets were observed: The resonance at −307.2 ppm has no Si satellites, while the ones at −371.3 and −368.4 ppm show Si satellites with coupling constants of 48.3 and 46.3 Hz, respectively. As it will be discussed below, the most downfield signal can be assigned unambiguously to $^{i}Pr_3Si{-}O{-}C{\equiv}P$ (**6**), while the two close upfield peaks represent two isomers of $^{i}Pr_3Si{-}P{=}C{=}O$ (**7** and the metastable **7’**) (Scheme 3.2). Although the NMR measurements did not reveal the exact structures of these two isomers, their very similar NMR characteristics suggest that **7** and **7’** are two rotamers of the same compound. The relative integrals of the peak areas revealed that at RT **6** is formed in 95%. However, when the reaction was performed at 45 °C, the rotamer **7** was formed exclusively.

$$^{i}\mathrm{Pr_3SiOTf} + \mathrm{NaOCP} \xrightarrow[\text{- NaOTf}]{\text{THF/Et}_2\text{O}} {}^{i}\mathrm{Pr_3Si{-}O{-}C{\equiv}P} + {}^{i}\mathrm{Pr_3Si{-}P{=}C{=}O}$$

	6	**7**
25°C	95%	5%*
45°C	0%	100%

Scheme 3.2: Reaction of ^{i}Pr$_3$SiOTf with NaOCP (*: amount of **7** and **7'** together).

The concomitant formation of the two constitutional isomers provides the first experimental evidence for the ambident character of the (OCP)$^-$ anion. **6** is not stable at room temperature, it rearranges slowly to **7**. This isomerization was monitored by ^{31}P-NMR spectroscopy at RT (see Figure 3.2) and the kinetic behavior was studied using non-linear regression to the data obtained by integration.

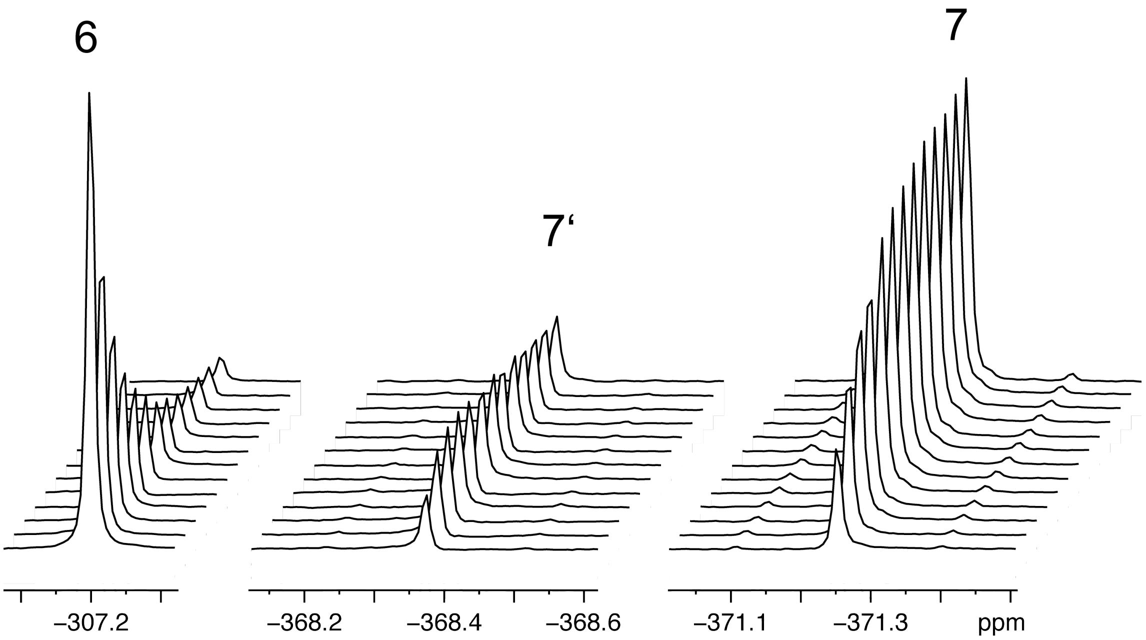

Figure 3.2 Details of the 162 MHz ^{31}P-NMR spectra for the isomerization reaction. The time difference between the spectra is 50 min.

According to the fitted model the decay of **6** follows first order kinetics with a half life of $t_{½} \approx 1.5$ h. Both phosphaketene rotamers **7'** and **7** form simultaneously from **6** with rate constants of $k_1 = 2.5 \times 10^{-3}$ min^{-1} and $k_2 = 4.8 \times 10^{-3}$ min^{-1}, respectively. Furthermore, the less stable rotamer **7'** slowly converts in a first order process to **7** ($k_3 = 1.3 \times 10^{-3}$ min^{-1}). Thus **7** can either form directly from the oxyphosphaalkyne or via the intermediate **7'**.

$$\begin{tikzcd}
 & \mathbf{7'} \arrow[d, "k_3"] \\
\mathbf{6} \arrow[ur, "k_1"] \arrow[r, "k_2"'] & \mathbf{7}
\end{tikzcd}$$

The oxyphosphaalkyne **6** is the kinetic and the silyl phosphaketene **7** the thermodynamic product of the nucleophilic substitution reaction (see Scheme 3.2), which is in agreement with the lower energy of the latter (*vide supra*). A simple explanation for the parallel formation of the two constitutional isomers is the following: Since the largest contribution in the HOMO of the (OCP)$^-$ anion is on the phosphorus atom (see Figure 3.3), the orbital controlled product is **7**. In contrast, **6** is the charge controlled reaction product, because the oxygen atom of the (OCP)$^-$ anion is slightly more negatively charged (NPA charges: O −0.65 e, P −0.44 e).[24]

6 and **7** were characterized by NMR- and IR-spectroscopy and the analytical data were compared to literature values of related compounds and verified by theoretical calculations (see Table 3.1). The NMR spectra of **7** were recorded in C_6D_6 for comparison with the literature data.

Table 3.1 Experimental and calculated spectroscopic data (in parentheses) of **6**, **7** and related literature known compounds. Chemical shifts (δ) are given in ppm and the absolute values of the coupling constants (J) are given in Hz. IR-vibrational frequencies ν_{asym} of the PCO unit are given in cm^{-1}.

	$\delta\ ^{31}$P	$\delta\ ^{13}$C	$^{1}J_{PC}$	$\delta\ ^{29}$Si	$^{1/3}J_{PSi}$	$\delta\ ^{17}$O	ν_{asym}
^{i}Pr$_3$SiOCP (**6**)[a]	−307.2 (−296.2)	145.5 (157.9)	9.8 (17.8)	30.2 (37.2)	-[b] (0.5)	- [c] (128.6)	1656 (1648)
^{i}Pr$_3$SiPCO (**7**)[d]	−370.1 (−353.7)	183.4 (199.1)	91.8 (150.9)	33.1 (43.2)	48.3 (87.8)	288.9 (345.3)	1947 (1963)
^{i}Pr$_3$SiOCP**Lit.**[d, e]	−369.9 (−330)[f]	183.2	91.9	33.1	48.3	4.9	-
Na(OCP)[g]	−392.0 (−428.1)	166.3 (181.1)	46.5 (101.9)	-	-	155.3 (210.4)	1755 (1817)
^{i}Pr(Me$_3$Si)NCP[d, h]	−137.6 (−114.5)	153.9 (167.0)	18.2 (1.0)	13.2 (11.2)	3.5 (1.9)	-	1588 (1606)
K(^{i}PrNCP)[h, i]	−226.1 (−224.9)	178.8 (189.9)	45.7 (60.8)	-	-	-	-

[a] in THF-d8/Et$_2$O mixture
[b] No J coupling detectable due to the large line width (40 Hz).
[c] No signal detectable due to instability of the compound.
[d] in C$_6$D$_6$
[e] Reported values for a compound, which was incorrectly described as ^{i}Pr$_3$SiOCP; for more information see text.
[f] Calculated for Me$_3$Si−O−C≡P at the HF/MP2/aug-cc-pVTZ level.[45, 48]
[g] Measured in THF-d8,[17] IR-spectrum measured with ATR unit.[17, 24]
[h] NMR data,[49] IR data[47]
[i] in THF-d8

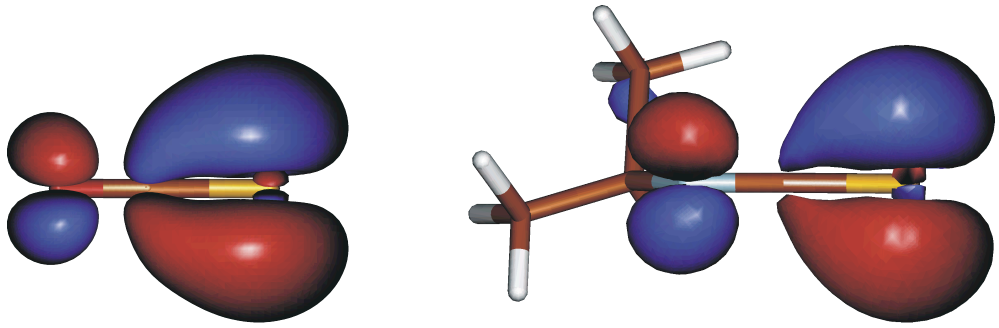

Figure 3.3 HOMO of (OCP)$^{-}$ (left) and (^{i}PrNCP)$^{-}$ (right) anions at the B3LYP/aug-cc-pVDZ level. Partial NPA charges: (OCP)$^{-}$: O −0.67, C +0.12, P −0.45 e; (^{i}PrNCP)$^{-}$: N −0.69, C −0.13, P −0.28 e.

Based on the similar charge distribution and HOMO orbital coefficients[46] (^{i}PrNCP)$^-$ is one of the most appropriate reference species for the (OCP)$^-$ anion (see Figure 3.3). Since the ^{31}P-NMR chemical shifts and $^1J_{PC}$ coupling constants of phosphaalkynes (R−C≡P) vary within a broad range, their values are not very informative.[3, 45] Therefore, the changes in the chemical shifts and coupling constants, which accompany the formation of ^{i}Pr$_3$Si−O−C≡P from (OCP)$^-$ and ^{i}Pr(Me$_3$Si)N−C≡P from (^{i}PrNCP)$^-$, Δδ = δ(silylated compound) – δ(anion), are compared. According to the ^{31}P-NMR spectra, silylation of (OCP)$^-$ to form **6** is accompanied by a chemical shift change of Δδ = 84.8 ppm to a higher frequency. Similarly, Δδ = 88.5 ppm is observed for the [^{i}PrNCP]$^-$ analogue. The ^{13}C-NMR spectra show similar shift changes, however, in this case to a lower frequency: Δδ = −11.8 ppm for the (OCP)$^-$ and Δδ = −24.9 ppm for the [^{i}PrNCP]$^-$ analogue. Furthermore, the $^1J_{PC}$ coupling constants are also comparable for **6** (9.8 Hz) and ^{i}Pr(Me$_3$Si)N−C≡P (18.2 Hz). In the IR-spectrum of **6** the frequency of ν = 1656 cm^{-1} can be assigned to the asymmetric stretching vibration of the O−C≡P unit.

These experimental findings contradict the previously reported data for ^{i}Pr$_3$Si−O−C≡P,[45] which is actually its constitutional isomer: ^{i}Pr$_3$Si−P=C=O. The arguments for this statement can be summarized as follows:

(**A**) The P-Si coupling constant of 48.3 Hz has the magnitude of typical $^1J_{PSi}$ values (15.5−73.0 Hz).[44, 50]

(**B**) The ^{13}C-NMR chemical shift of 182.5 ppm and the $^1J_{PC}$ value of 90.8 Hz compare to literature data of phosphaketenes (175.4 ppm, 91 Hz;[24] 206.9 ppm, 107.7 Hz[26]) and the $^1J_{PC}$ coupling constant is much larger than a usual $^1J_{PC}$ value for phosphaalkynes.[45]

(**C**) The measured ^{31}P-NMR chemical shift (−370.1 ppm) fits better the calculated value for ^{i}Pr$_3$Si−P=C=O (−353.7 ppm) than that for ^{i}Pr$_3$Si−O−C≡P (−296.2 ppm). In the previous report[45] the authors only used the calculated chemical shift of Me$_3$SiOCP (−330 ppm)[48] as a reference. Since the difference in the ^{31}P-NMR chemical shifts between the two possible isomers is in the range of the accuracy of the calculations, the values of both reference compounds are necessary to identify the product.

(**D**) The experimentally obtained ^{17}O-NMR chemical shift of **7** (288.9 ppm) (Figure 3.4) is consistent with the calculated value (345.3 ppm) and lies in the typical range of ketenes (e.g. 340 ppm for $Ph_2C{=}C{=}O$ [51] and 255.0 ppm for $Me_3Si{-}CH{=}C{=}O$ [52]). Presumably the authors assigned the peak of di-*n*-butyl ether (which was used as solvent during the synthetic procedure) to $^{i}Pr_3Si{-}O{-}C{\equiv}P$ (the ^{17}O-NMR spectrum of di-*n*-butyl ether in C_6D_6 shows a resonance at 5 ppm.)

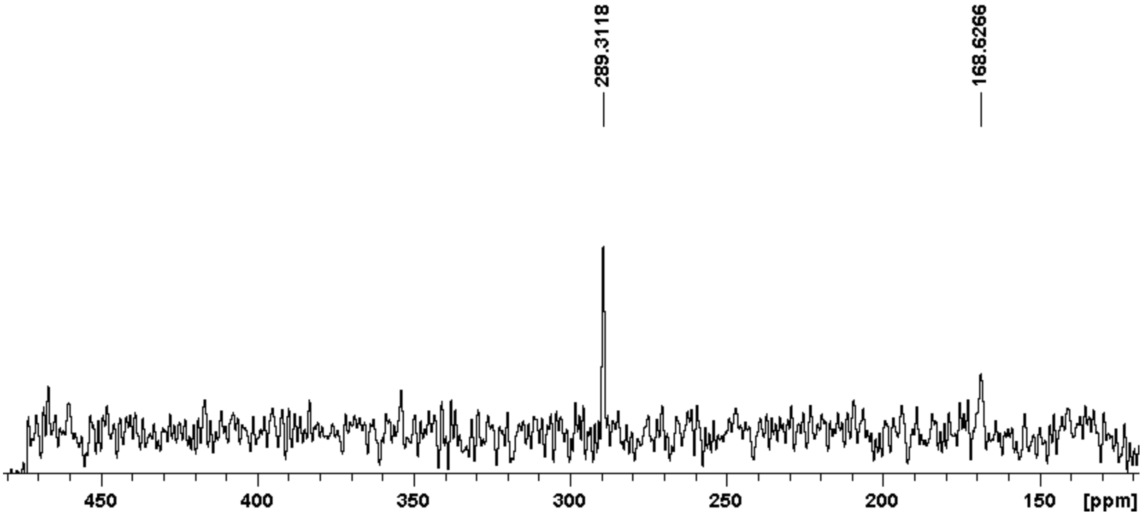

Figure 3.4 64.8 MHz ^{17}O-NMR spectrum of $^{i}Pr_3Si{-}P{=}C{=}O$. The peak at 168.6 ppm corresponds to $^{i}PrSiOTf$.

(**E**) The IR-spectrum indicates the characteristic band of a phosphaketene at ν = 1947 cm^{-1} (2,4,6-tri-*tert*-butylphenyl phosphaketene (Mes*−P=C=O): ν = 1970 cm^{-1}),[26] which is in good agreement with the calculated value (1963 cm^{-1}).

In analogy to the reaction of Na(OCP) with $^{i}Pr_3SiOTf$, both $Ph_3Si{-}O{-}C{\equiv}P$ (**8**) and $Ph_3Si{-}P{=}C{=}O$ (**9**) isomers can also be generated *in situ*. From the reaction of **9** with a further $(OCP)^{-}$ anion, the cycloaddition product **10** is formed, which appears as two doublets in the ^{31}P-NMR-spectrum (δ ^{31}P: 105.7 and 305.3 ppm, $^{2}J_{PP}$ = 18 Hz). The analogous anion bearing an isopropyl substituent instead of the silyl group can be obtained from Na(OCP) and 2-iodopropane (see Chapter 2).

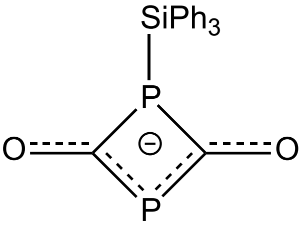

10

3.4 Heavier tetrel substituted phosphaketenes, $Ph_3E{-}P{=}C{=}O$ (Ge, Sn, Pb)

In contrast to the silyl compounds, the heavier triorganyl tetrel chlorides (R_3ECl, E = Ge, Sn, Pb) form exclusively the phosphaketene isomers, as predicted by the computations (see Figure 3.1). The germyl ($Ph_3Ge{-}P{=}C{=}O$, **11**) and stannyl ($Ph_3Sn{-}P{=}C{=}O$, **12**) phosphaketenes can be isolated in good yields as yellow powders, whereas the lead analogue ($Ph_3Pb{-}P{=}C{=}O$, **13**), even though it forms cleanly, decomposes during isolation. Interestingly no dimerization of any of these hetero phosphaketenes was observed (all known organyl phosphaketenes can form dimers, see chapter 2 and references [26-29]).

All the tests to grow single crystals remained unsuccessful because the compounds decompose in solution slowly (e.g. $(Ph_3Sn)_3P$ was identified as a decomposition product of **12**). Attempts to form pentacoordinated compounds using Lewis bases (e.g. pyridine-N-oxide) lead to consecutive reactions (see chapter 4). The vacuum sublimation of **11** resulted in an amorphous material, while **12** formed the corresponding tristannyl phosphane upon heating *in vacuo*. The compounds were thus characterized by extensive NMR- and IR-spectroscopy and for a systematic comparison the most important analytical data for $Ph_3E-P=C=O$ (E = Si, Ge, Sn, Pb) are collected in Table 3.2.

Table 3.2 NMR- and IR-spectroscopic data for $Ph_3E-P=C=O$ (E = Si, Ge, Sn, Pb). Chemical shifts (δ) are given in ppm and the absolute values of the coupling constants (*J*) are given in Hz. IR-vibrational frequencies ν_{asym} (PCO) are given in cm^{-1}. Calculated values are shown in parentheses (B3LYP/cc-pVDZ(-PP) level).

E	$\delta\,^{31}P$	$\delta\,^{13}C$	$^1J_{PC}$	ν_{asym} (PCO)
Si (**9**)	-343.6	184.5	99.1	1962 (1977)
Ge (**11**)	-344.0	182.5	105.0	1954 (1971)
Sn (**12**)	-378.0	180.6	108.0	1946 (1969)
Pb (**13**)	-364.0	181.7	110.0	1923 (1950)

The ^{31}P-NMR chemical shifts lie within a relatively narrow range (from −343.6 ppm to −378.0 ppm), which is remarkably shifted to a lower frequency compared to Mes*−P=C=O (−207.4 ppm).[25] The chemical shifts are influenced by the nature of the heteroatom E and correlate with the electronegativity values as defined by Allen[53] (see Figure 3.5).

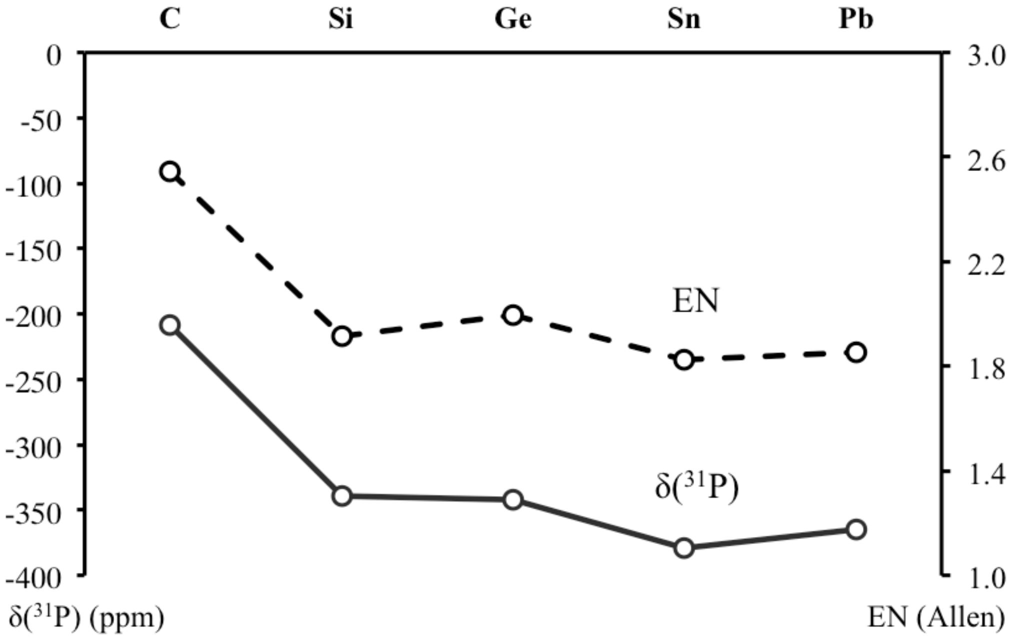

Figure 3.5 Correlation of the ^{31}P-NMR chemical shifts of the phosphaketenes (solid line) with the electronegativity of the heteroatom E (dotted line). The chemical shift for E = C is for Mes*−P=C=O.[25]

As expected, the ^{13}C-NMR chemical shifts are much less influenced by the heteroatom E and are somewhat shifted compared to Mes*−P=C=O (206.9 ppm).[25]

Similarly to conventional phosphaketenes, such as Mes*−P=C=O, the compounds **9**, **11**–**13** are typical heterocumulenes. When going down the column from Si to Pb, the slightly increasing $^{1}J_{PC}$ coupling constants indicate the moderate strengthening of the PC bond. On the other hand, the IR frequencies show the slight weakening of the CO bond in the direction Si to Pb. These tendencies are also reflected in the calculated bond lengths, even though the changes are minor (less than 0.01 Å). A simple explanation for these trends can be found in the neutral hyperconjugation,[52] which is the reason for the enhanced stability of silyl ketenes.[52, 54] The zwitterionic resonance structure in Figure 3.6 illustrates the hyperconjugative electron donation from the EP bond to the PCO moiety.

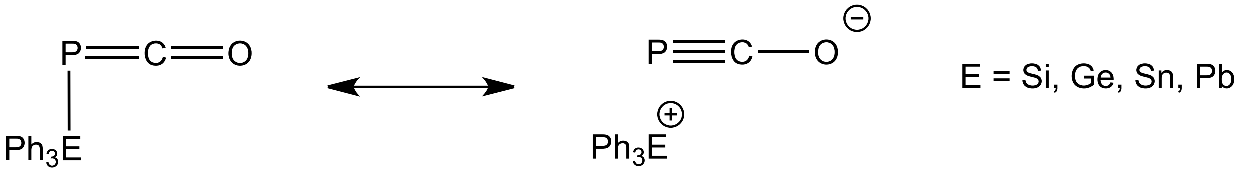

Figure 3.6 Two possible mesomeric structures of phosphaketenes.

When going from Si to Pb the weight of the zwitterionic resonance structure grows slightly due to the increasing donor ability of the EPh_3 group. Nevertheless these species are best described by the phosphaketene resonance structure.

3.5 The stability of phosphaketenes

Finally, the bonding structure shall be examined to find an answer, as to why the phosphaketenes are lower in energy than the oxyphosphaalkynes. As a simple principle, the formation of a strong chemical bond can be the driving force of a reaction. Consequently, due to the high affinity of the heteroelements E towards oxygen (oxophilicity), one would expect the oxyphosphaalkynes to be the more stable isomers. The EO bonds are indeed significantly stronger than the corresponding EP bonds (see Figure 3.7). To explain the higher stability of the phosphaketene isomers one must therefore consider additional stabilizing factors in the PCO moiety, which overcompensate the relative weakness of the EP bonds.

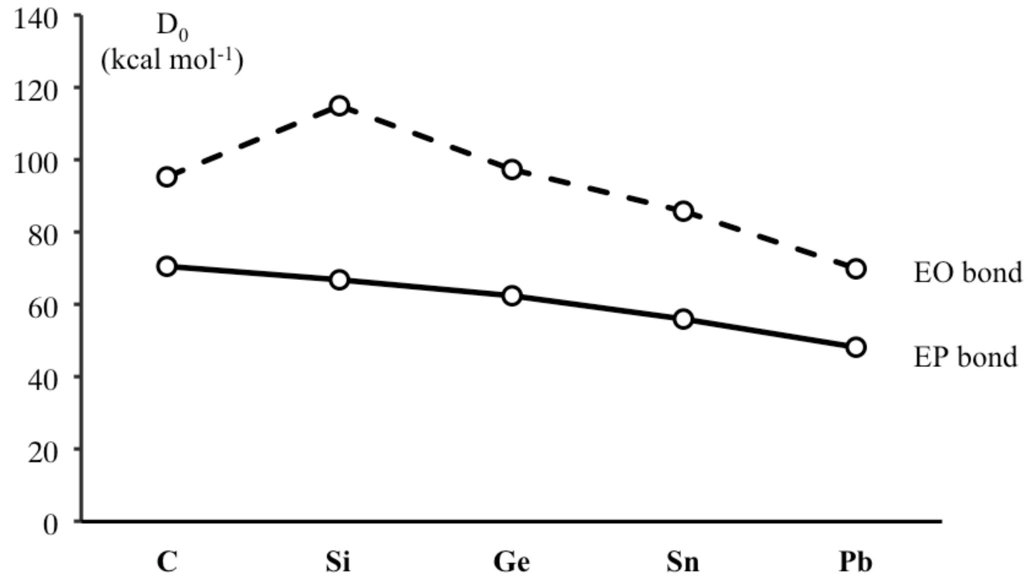

Figure 3.7 Bond dissociation energies (D_0) of the EO and EP σ-bonds (E = C−Pb) at the B3LYP/cc-pVDZ(-PP) level.

For an energy decomposition analysis first the Lewis structures of the two isomers are compared. Since the "O−C=P" moiety is part of both isomers the basic structural differences are the following: $R_3E{-}P{=}C{=}O$ contains an EP σ- and a CO π-bond, while an EO σ- and a "second" CP π_2-bond can be found in $R_3E{-}O{-}C{\equiv}P$. The σ-bond energies are estimated with the bond dissociation energies (D_0) of $H_3E{-}PH_2$ and $H_3E{-}OH$ (see Table 3.3). The CO π-bond energy in $R_3E{-}P{=}C{=}O$ is approximated by that of formaldehyde (H_2CO, 94.6 kcal/mol). For the estimation of the "second" CP π_2-bond energy in $R_3E{-}O{-}C{\equiv}P$, phosphaethyne was applied as a model compound ($H{-}C{\equiv}P$, 55.3 kcal/mol). These values are listed as E_π in Table 3.3.

Besides, the delocalization within the phosphorus-carbon-oxygen unit has to be taken into account. To gain quantitative information on the extent of delocalization, the energies (E_{deloc}) of the isodesmic reactions below (Scheme 3.3) were calculated.

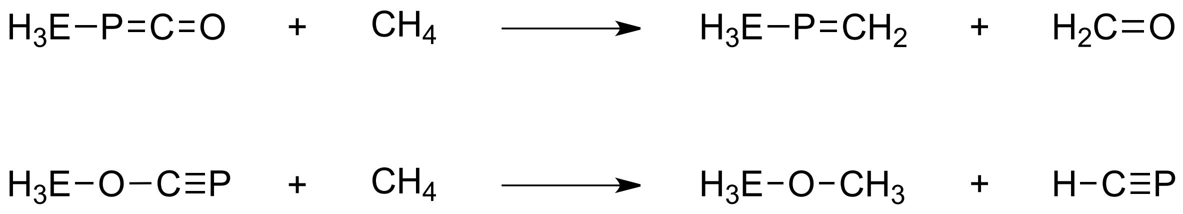

Scheme 3.3 Calculated isodesmic reactions, E = C, Si, Ge, Sn, Pb.

If the reaction energy has a large positive value it indicates a remarkable stabilization, which is due to delocalization in the phosphorus-carbon-oxygen unit. Indeed, the NBO analysis shows delocalization from the oxygen lone pairs into the π^*(CP) orbitals. The calculated isodesmic reaction energies (E_{deloc}) are collected in table 3.3. Thus, the total stabilization energy (E_{total}) can be obtained as the sum of the following increments: $E_{total} = D_0 + E_\pi + E_{deloc}$.

The reasons for the higher stability of phosphaketenes compared to the corresponding phosphaalkynes are: (a) the CO π-bond in $R_3E{-}P{=}C{=}O$ is much stronger (by 39.3 kcal/mol) than the second CP π_2-bond in $R_3E{-}O{-}C{\equiv}P$, (b) the delocalization energy (E_{deloc}) is substantially greater for all the phosphaketene isomers studied.

As a consequence of these two effects, which overcompensate the weakness of the PE bonds, all the phosphaketenes possess larger total stabilization energies compared to the corresponding oxyphosphaalkyne isomers.

The difference in the total stabilization energies (ΔE_{total}) correlates well with the relative energies of the two isomers (ΔE_{rel}) (see Table 3.3). This bolsters the feasibility of the energy decomposition procedure applied.

Table 3.3 Stabilization energy increments for $H_3E{-}P{=}C{=}O$ and $H_3C{-}O{-}C{\equiv}P$ at the B3LYP/cc-pVDZ(PP) level. D_0: bond dissociation energy of E−P and E−O bonds, E_π: CO π-bond energy for $H_3E{-}P{=}C{=}O$ and the CP π_2-bond energy for $H_3C{-}O{-}C{\equiv}P$, respectively. E_{deloc}: isodesmic reaction energies (see scheme 3.3). $E_{total} = D_0 + E_\pi + E_{deloc}$, $\Delta E_{total} = E_{total}(H_3E{-}P{=}C{=}O) - E_{total}(H_3E{-}O{-}C{\equiv}P)$. ΔE_{rel}: relative energy of $H_3E{-}O{-}C{\equiv}P$ compared to $H_3E{-}P{=}C{=}O$. All energies are given in kcal/mol.

E	Compound	D_0	E_π	E_{deloc}	E_{total}	ΔE_{total}	ΔE_{rel}
C	$H_3C{-}P{=}C{=}O$	70.6	94.6	26.4	191.7	28.1	27.6
	$H_3C{-}O{-}C{\equiv}P$	95.2	55.3	13.2	163.6		
Si	$H_3Si{-}P{=}C{=}O$	66.8	94.6	37.1	198.5	13.7	14.1
	$H_3Si{-}O{-}C{\equiv}P$	114.8	55.3	14.7	184.8		
Ge	$H_3Ge{-}P{=}C{=}O$	62.4	94.6	36.3	193.3	21.7	22.7
	$H_3Ge{-}O{-}C{\equiv}P$	97.4	55.3	18.8	171.6		
Sn	$H_3Sn{-}P{=}C{=}O$	55.9	94.6	38.5	189.0	24.4	25.3
	$H_3Sn{-}O{-}C{\equiv}P$	85.8	55.3	23.6	164.6		
Pb	$H_3Pb{-}P{=}C{=}O$	48.0	94.6	37.5	180.1	27.1	28.2
	$H_3Pb{-}O{-}C{\equiv}P$	70.0	55.3	27.7	153.0		

3.6 Conclusion

In this chapter the first experimental evidence for the ambident character of the $(OCP)^-$ anion has been described: The reaction of Na(OCP) with silyl triflates delivers both the $R_3Si{-}O{-}C{\equiv}P$ and $R_3Si{-}P{=}C{=}O$ isomers. The former is the kinetic product, while the latter is the thermodynamically favored isomer. This is in agreement with the DFT calculations, which also show that the phosphaketenes are lower in energy than the corresponding oxyphosphaalkynes. The analysis of spectroscopic data and comparison with calculated values revealed that the silylphosphaketene $^iPr_3Si{-}P{=}C{=}O$ was erroneously interpreted in the literature as siloxyphosphaalkyne ($^iPr_3Si{-}O{-}C{\equiv}P$). The triorganyl chlorides of the heavier group 14 elements Ph_3ECl (E = Ge, Sn, Pb), however, form exclusively the phosphaketene isomer ($Ph_3E{-}P{=}C{=}O$), which is – according to the calculated relative energies – more stable than the oxyphosphaalkyne isomer. As a simple estimation, the EP and the EO bond energies would predict the oxygen-bonded isomer to be more stable. However, two further factors have to be considered in order to understand the thermodynamic stability of the heterophosphaketenes: Firstly, the CO π-bond in the phosphaketenes is much stronger than the second CP π_2-bond in the corresponding phosphaalkyne. Secondly, the delocalization within the PCO unit of the phosphaketene delivers more stabilization energy than the interaction between the CP triple bond and the oxygen atom in the oxyphosphaalkyne. The reactivity of these heterophosphaketenes is discussed in the next chapter.

4. Synthesis of phosphorus heterocycles from heterophosphaketenes

4.1 Introduction

Although phosphaketenes ($R{-}P{=}C{=}O$) have been known for three decades,[25] their chemistry has remained limited. Likely, the reason for this is that phosphaketenes have an affinity to undergo dimerization to form 1,3-diphosphatane-2,4-dions. The stabilization of the monomeric form has been achieved in two different ways: Using steric protection[25] or by hetero substitution on the phosphorous atom (see Chapter 3 and reference).[24] A recent publication reports the monomeric methylphosphaketene in the coordination sphere of tungsten.[31] As described in the previous chapter, the $(OCP)^-$ anion provides an easy access to the tetrel substituted heterophosphaketenes ($R_3E{-}P{=}C{=}O$, E = Si, Ge, Sn, Pb) via nucleophilic substitution.

4.2 The "decomposition" of stannylphosphaketene in dimethyl sulfoxide

When the phosphaketene $Ph_3Sn{-}P{=}C{=}O$ (**12a**) was dissolved in a coordinating solvent like dimethyl sulfoxide, the color of the solution slowly changed from yellow to orange and a slight gas formation was observed. According to the NMR-spectroscopic data **12a** decomposes cleanly to form the anion **14a**, accompanied by the evolution of carbon monoxide (see Scheme 4.1).

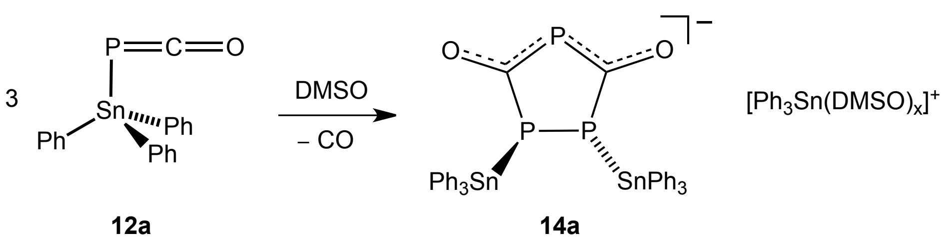

Scheme 4.1 Decomposition of **12a** in DMSO to **14a**.

In the ^{31}P-NMR spectrum the five-membered ring anion can be identified by a triplet at 124.5 ppm and a doublet at −68.3 ppm ($^{2}J_{PP}$ = 20.9 Hz). The ^{119}Sn-NMR spectrum shows a multiplet resonance at −129.3 ppm, which can be assigned to the stannyl groups of the heterocycle. Furthermore two singlets at −224.2 and −235.0 ppm were observed, which are in the range of solvent coordinated triphenyltin cations.[55] The formation of the same anion was observed when other strong electron pair donors (pyridine, HMPTA) were added to a THF solution of **12a**. Presumably, the Lewis base coordinates to the stannyl group of the phosphaketene forming a pentacoordinated tin species. As a result, the P-Sn bond strength decreases and thus it is more prone to heterolytic dissociation to form an $(OCP)^{-}$ anion and a organotin cation stabilized by the Lewis base. To prove whether the $(OCP)^{-}$ anion itself is involved in the decomposition reaction, $[Na(OCP)\times(dioxane)_{2.5}]$ was reacted in THF with two equivalents of $R_3Sn{-}P{=}C{=}O$ (**12**) (**12a**: R = Ph, **12b**: R = Cy). Based on the NMR data this reaction cleanly delivers the sodium salt of the heterocyclic anion **14** (**14a**: R = Ph, **14b**: R = Cy), observed in the decomposition of **12a** in the presence of Lewis bases (Scheme 4.2).

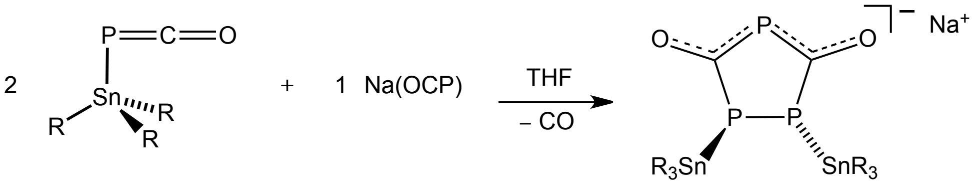

12

14

a: R = Ph
b: R = Cy

Na(OCP) = $[NaOCP\times(dioxane)_{2.5}]$

Scheme 4.2 Reaction of a triorganotin phosphaketene with the $(OCP)^{-}$ anion.

4.3 X-ray structures

Colorless single crystals of the sodium salts of **14a** and **14b** were obtained from saturated DME or THF solutions, respectively. The results of the X-ray diffraction studies are shown in Figure 4.1.

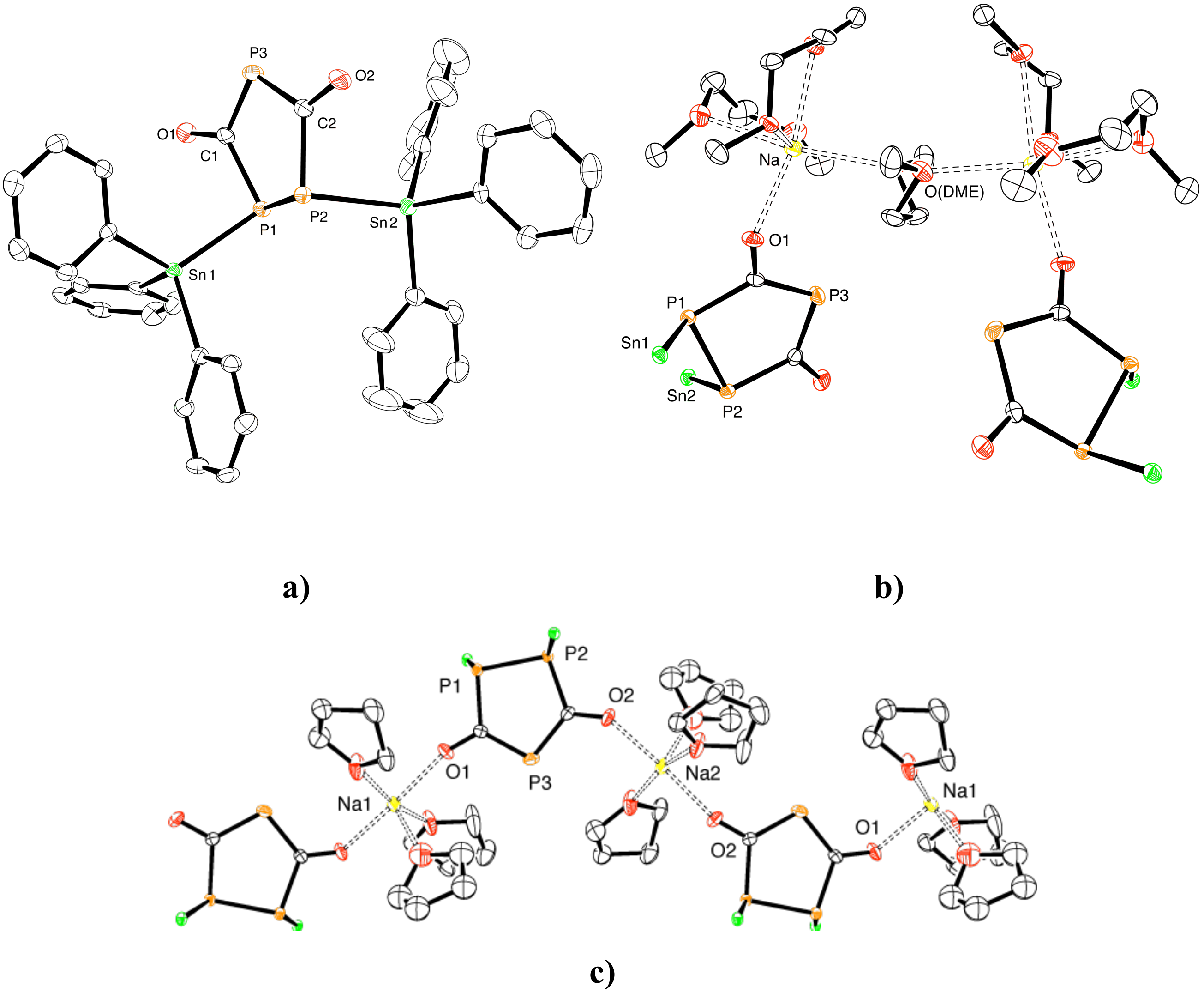

Figure 4.1 **a)** ORTEP pot of $[Na(DME)_2(\mathbf{14a})]_2$×(DME) (thermal ellipsoids are drawn at 50% probability). Hydrogen atoms and sodium cation with solvent molecules (DME) are omitted for clarity. Selected bond lengths (Å) and angles (°): P1-P2 2.197(1), P1-Sn1 2.498(9), P1-C1 1.891(3), C1-O1 1.241(4), C1-P3 1.790(3), P3-C2 1.778(3), C2-O2 1.257(4), C2-P2 1.876(3), P2-Sn2 2.502(9); P1-C1-P3 119.4(2), C1-P3-C2 100.0(2), P3-C2-P2 120.2(2), C2-P2-P1 96.6(1), P2-P1-C1 96.8(1). **b)** ORTEP plot of $[Na(DME)_2(\mathbf{14a})_2]$×(DME) (thermal ellipsoids are drawn at 50%

probability). Hydrogen atoms and phenyl rings at the tin atoms are omitted for clarity. Selected bond lengths (Å): O1-Na 2.336(2), Na-O(DME) 2.438(3). **c)** ORTEP plot of zig-zag array [Na(THF)$_3$(**14b**)]$_\infty$ (thermal ellipsoids are drawn at 50% probability). Hydrogen atoms and cyclohexyl rings at the tin atoms are omitted for clarity. Selected bond lengths (Å) and angles: Na1-O1 2.281(2), Na2-O2 2.305(2), P1-P2 2.189(7), P1-Sn1 2.522(5), P1-C1 1.876(2), C1-O1 1.245(3), C1-P3 1.779(2), P1-C2 1.784(2), C2-O2 1.248(3), C2-P2 1.878(2), P2-Sn2 2.530(6); P1-C1-P3 121.1(1), C1-P3-C2 100.6(1), P3-C2-P2 120.9(1), C2-P2-P1 98.2(7), P2-P1-C1 98.3(7).

[Na(DME)$_2$(**14a**)]$_2$×(DME) (Figure 4.1a, b) consists of two ion pairs, the Na$^+$ cations of which are linked by a μ_2-(κ^1*O*, κ^1*O*)-bridging DME molecule, and only the oxygen atom O1 of the heterocyclic anion **14a** coordinates to a sodium cation. On the other hand, [Na(THF)$_3$(**14b**)]$_\infty$ (Figure 4.1c) forms a regular polymeric zig-zag array, in which the quasi C_2 symmetric anion connects two solvent coordinated sodium cations in a μ_2-(κ^1*O*, κ^1*O*) fashion. In both structures the stannyl substituents are in *trans* orientation and the OCPCO units show π-delocalization similar to previously reported structures.[32, 56] The CO "double" bonds (1.24-1.26 Å) are elongated compared to the C=O bond in the related (Me$_3$Sn)$_2$P(Ad)C=O (1.217 Å),[46] whereas the PC bonds are slightly shorter (stronger) than in this reference compound (1.877 Å).

4.4 Investigations on the reaction mechanism

In order to understand the formation of anion **14**, ^{31}P and ^{119}Sn-NMR studies were performed at −40 °C on a sample of two equivalents of Ph$_3$Sn−P=C=O and one equivalent of Na(OCP) prepared in THF at −60 °C. The measured ^{31}P-NMR spectra and the structures of the corresponding intermediates are shown in Figure 4.2. The assignment of the signals is based on comparison with literature data and DFT calculations on model compounds (see Figure 4.2). The simulated spectra are included in the appendix of this thesis.

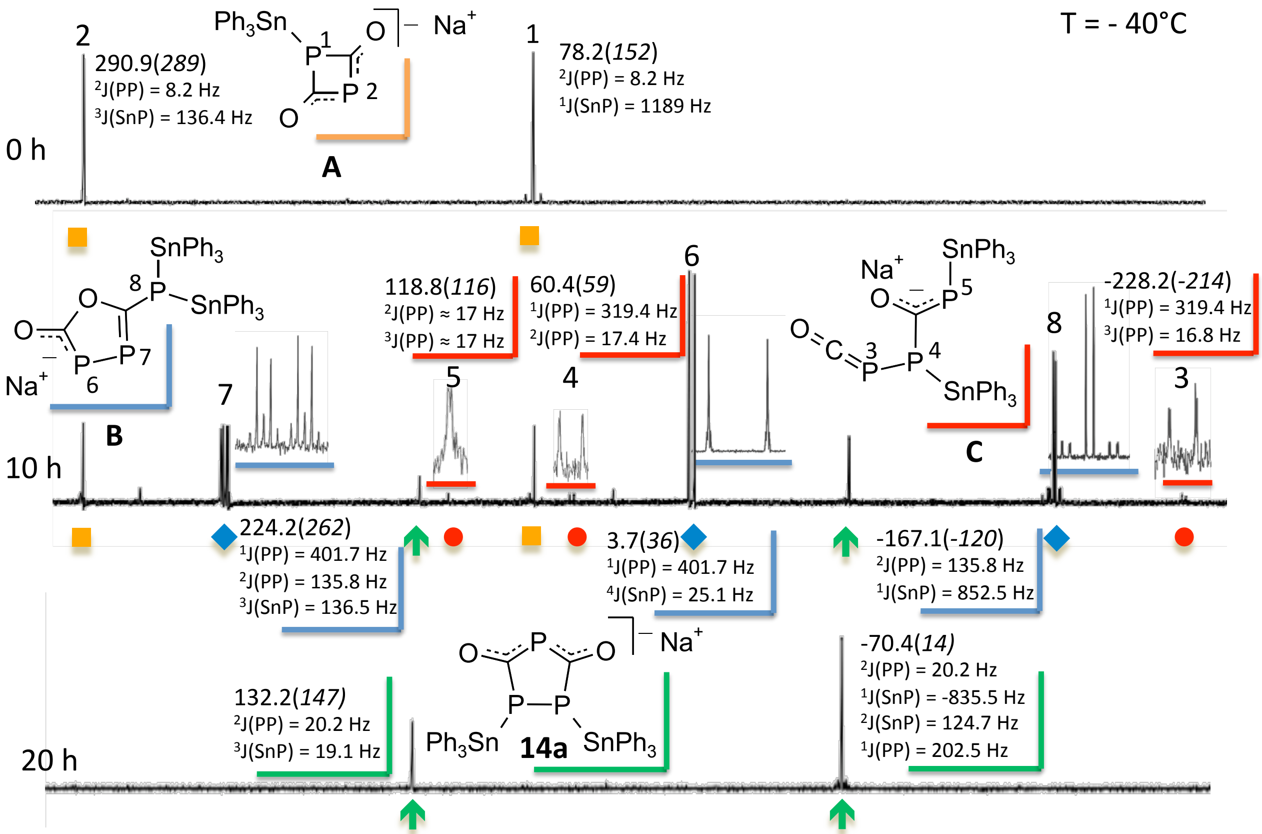

Figure 4.2 ^{31}P-NMR spectra (THF-d8/–40°C) at three reaction coordinates showing the intermediates **A** (orange) **B** (blue), **C** (red) and the final product **14a** (green). Calculated chemical shifts (B3LYP/aug-cc-pVDZ(-PP)) are given in parentheses.

In the ^{31}P-NMR spectrum of the reaction mixture at –40 °C no Na(OCP) was observed, only the four-membered ring adduct **A** (similar structures were reported in Chapter 2 and 3) and $Ph_3Sn{-}P{=}C{=}O$ were detected. While the concentrations of **A** and $Ph_3Sn{-}P{=}C{=}O$ decreased continuously, the parallel formation of two further species (**B** and **C**, showing the typical time dependence of intermediates) and the final product **14a** was observed. Anion **B** features a five-membered ring consisting of two OCP units (compare 1,3,4-oxadiphospholonide 159.2 ppm and –35.5 ppm, $^1J_{PP}$ = 361.0 Hz)[57] and a distannylphosphino moiety, which shows a characteristic chemical shift (δ = –127.1 ppm) and satellite pattern ($(Me_3Sn)_2P(Ad)C{=}O$ –120.4 ppm, $^1J_{SnP}$ = 617.2 Hz).[46]

In a much lower concentration intermediate **C** was observed, containing a phosphaketene group with a chemical shift comparable to Mes*−P=C=O (δ = −206.9 ppm).[25] Intermediates **B** and **C** are structural isomers of the final product **14a** and a comparison of the structures reveals that stannyl group migration and ring opening/closing steps should be considered in the transformation from these intermediates to the final product. Seemingly the reaction mechanism is more complicated than a simple cycloaddition; therefore DFT calculations were performed on possible reaction pathways (see Figure 4.3).

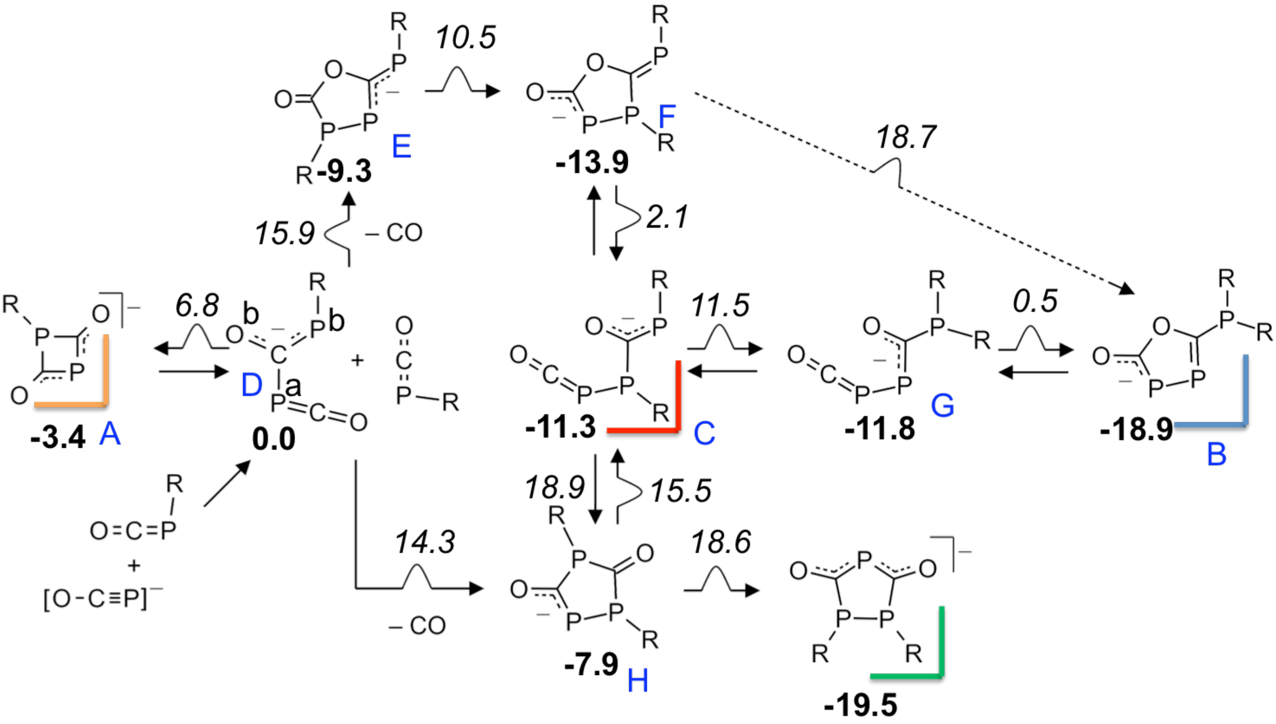

Figure 4.3 Calculated reaction pathways on model compounds (R = SnH_3) at B3LYP/aug-cc-pVDZ(PP) level of theory. The relative energies of the intermediates are given compared to [**D** + R−P=C=O]. The activation barriers are given compared to the starting material of that particular process, which is shown with the arrow. The sodium cations and additional carbon monoxide molecules are omitted for clarity.

The first reaction step is a nucleophilic attack of an $(OCP)^-$ anion on the carbon atom of a stannylphosphaketene to form **D**, which is supposedly in an equilibrium with the slightly more stable **A**. **A** is observable on NMR time scale and acts as a reservoir for the reactive species **D**, which can undergo two different 1,3-dipolar [3+2] cycloadditions with a stannylphosphaketene, to form either **E** or **H**. The PP bond of these rings is constructed from a stannylphosphaketene and the P^a=C=O unit of **D** under the loss of carbon monoxide from the latter. No direct [3+2] pathway was found leading directly from **D** to the final product. If **D** reacts as a dipole including the atoms P^a and O^b, the heterocycle **E** is formed, while the cycloaddition involving the P^aCP^b moiety delivers **H**. Either **E** or **H** can lead to the observed intermediates **B**, **C** and the final product. According to the similar relative energies and activation barriers both pathways involving either **E** or **H** should be considered. As shown in the upper section of Figure 4.3, the rearrangement of anion **E** via a 1,2 stannyl migration leads to **F**. Although the 1,3 stannyl shift forming **B** directly from **F** is feasible, a ring opening step of **F** yielding **C** is more likely due to the much lower activation barrier of the latter process. The two-step formation of **B** from **C** through **G** is expected to be reversible, because all three species have similar relative energies and all the activation barriers in the processes **C**⇌**G** and **G**⇌**B** are rather low. Moreover, **C** is also in equilibrium with **H**, which can form the final product via a 1,3 stannyl shift. The formation of the final product from **H** is thermodynamically preferred compared to the ring opening leading reversibly to **C**, however, the former process has a somewhat higher activation barrier ($E^‡$ = 18.6 vs. 15.5 kcal/mol). **H** is therefore slowly and irreversibly converted to the final product (note that $E^‡$ = 30.2 kcal/mol for the reverse reaction from the final product to **H**). Hence, the species **B** and **C** act as reservoirs for **H**.

4.5 The reaction of Ph₃Ge−P=C=O with Na(OCP)

The investigations were extended to the lighter group 14 analogues. Surprisingly, the germanium analogue of cycle **14a** is not accessible from Ph_3GePCO and Na(OCP). At −70 °C the germanium analogue of intermediate **A** is formed, which slowly isomerizes at temperatures above −50 °C to the sodium salt of 1-germyl-1,2-diphosphetane-3,4-dione (see Scheme 4.3). These species could not be isolated because of their decomposition at room temperature.

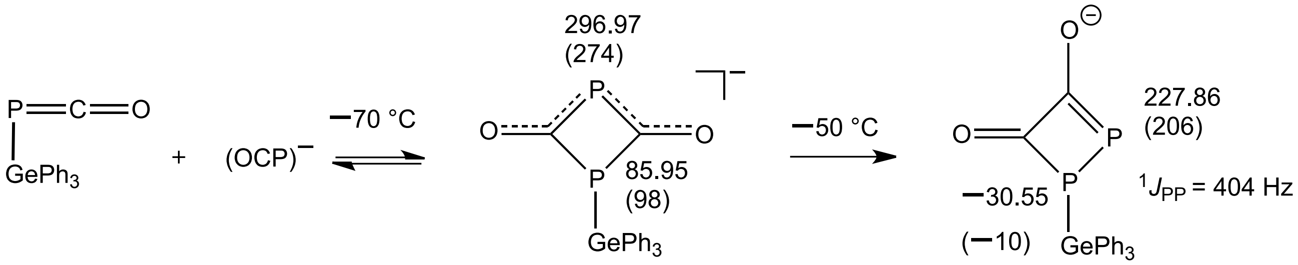

Scheme 4.3 Reaction of $Ph_3Ge{-}P{=}C{=}O$ with Na(OCP). Calculated chemical shifts at the B3LYP/aug-cc-pVDZ level of theory are given in parentheses.

4.6 Synthesis of a siloxy substituted 1,2,4-triphospholide

When trimethylsilylazide is reacted with Na(OCP) in a ratio of 2:3 the ^{31}P-NMR spectrum exhibits again a triplet and a doublet, but the chemical shifts (t 186.1, d 173.4 ppm, $^{2}J_{PP}$ = 55.2 Hz) indicate a remarkable structural difference with respect to **14**. The obtained anion **15** was unequivocally identified as 3,5-bis(trimethylsiloxy)-1,2,4-triphospholide (see Scheme 4.4). Low temperature ^{31}P-NMR investigations on the formation of **15** reveal the silyl analogue of **A** (see Figure 4.3) as an intermediate (resonances at 78.3 and 309.3 ppm). Only one further intermediate, assigned to the dimer of the silyl phosphaketene, was detected (singlet at 176 ppm).

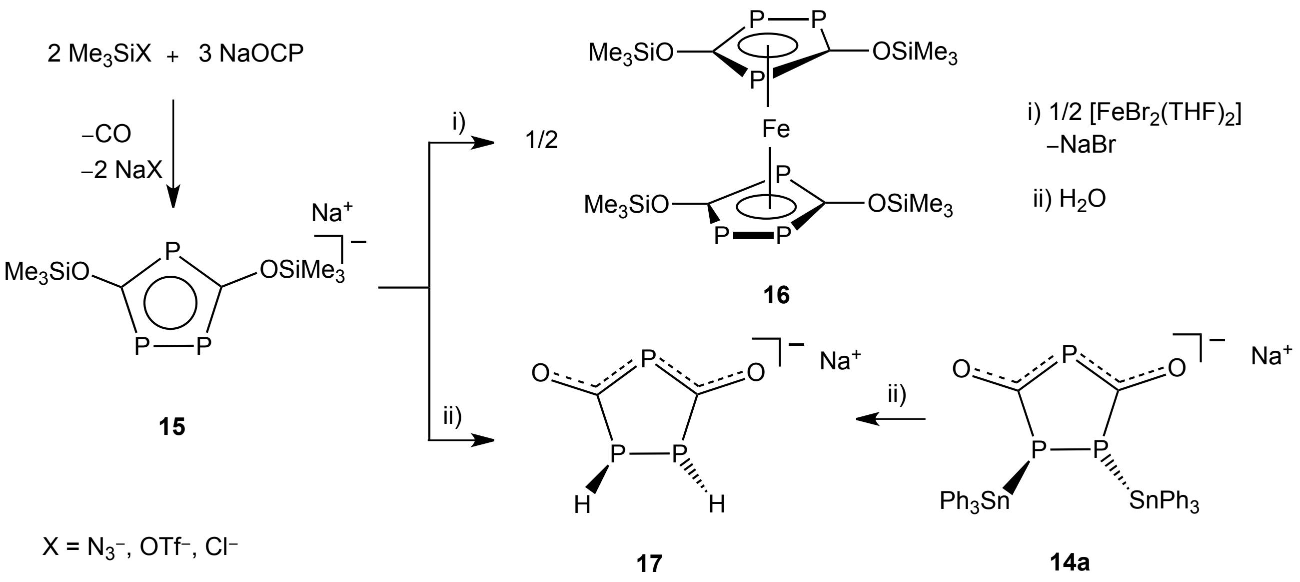

Scheme 4.4 Formation and reactivity of anion **15**.

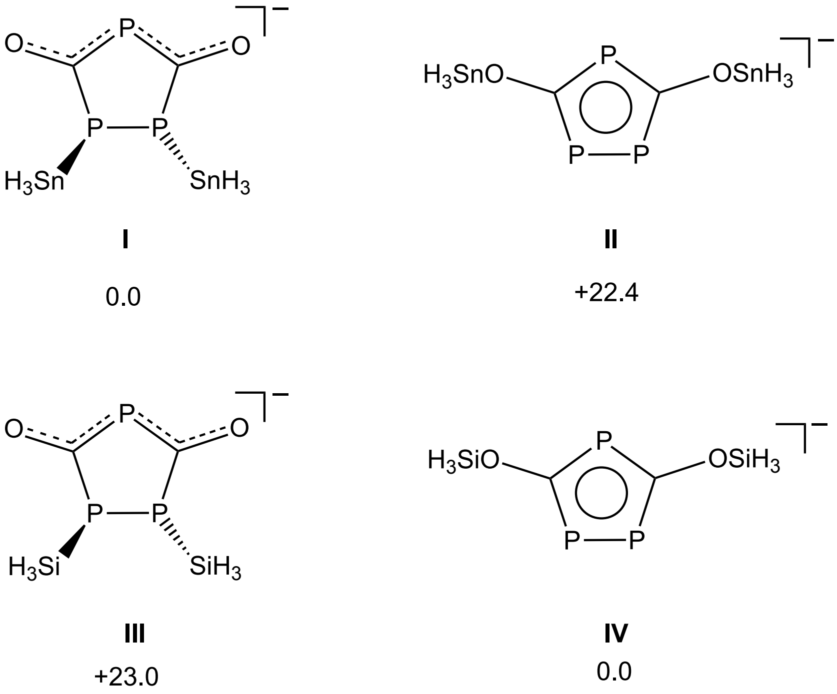

Figure 4.4 Relative energy of anions **II** and **III** compared to anions **I** and **IV**, respectively at the B3LYP/aug-cc-pVDZ(-PP) level of theory.

The unexpected formation of **15** instead of the silicon analogue of **14** can be explained as a result of competing stabilization effects. The calculated relative energies of model anions (see Figure 4.4) also bolster the thermodynamic stability of **I** and **IV** compared to the corresponding isomers **II** and **III**, respectively. As a simple model one can compare the bond energies and delocalization effects in the anions. A Sn-P single bond is much weaker than a Sn-O bond (bond dissociation energy: 55.9 vs. 85.8 kcal/mol, see chapter 3). The higher stability of **I** proposes that the π-delocalization in the OCPCO unit (of anion **I**) is able to overcompensate the weakness of the Sn-P bonds and thus offers more energetic stabilization than the aromaticity in **II**. The difference between the Si-O and Si-P bond dissociation energies (114.8 vs. 66.8 kcal/mol, see chapter 3) is much larger than in the case of Sn-O and Sn-P bonds. Thus, the remarkable strength of the Si-O bond together with the high aromaticity gives more stabilization in **IV** than the Si-P bonds and the delocalization within the OCPCO π system in **III**.

4.7 Reactivity of the siloxy substituted 1,2,4-triphospholide

Significantly, **15** is easily accessible in excellent yield starting from Na(OCP), which can be prepared in a one-pot synthesis. In contrast, the *tert*-butyl analogue $[(^tBuC)_2P_3]^-$, which is the starting material for a plethora of complexes and cage compounds, can only be obtained via multistep syntheses in moderate yields.[11, 58, 59]

In preliminary test reactions **15** has shown a reactivity similar to $[(^tBuC)_2P_3]^-$ (Scheme 4.4). The reaction of **15** with $[FeBr_2(THF)_2]$ cleanly affords the sandwich complex **16** (1,1’,2,2’,4,4’-hexaphopsphaferrocene). Furthermore, when **15** reacts with water, the hydrolysis of the silyl groups delivers anion **17** (parent analogue of **14**), which is stable in THF solution for several days. Anion **17**, which can be regarded as the simplest heavier analogue of the urazolide anion $[(HN)_2(CO)_2N]^-$, is alternatively accessible from **14** and H_2O. Interestingly, the protonation takes place on the two neighboring phosphorous centers and not on the oxygen atoms. This is a further example for the preferred formation of an OCPCO π system instead of an aromatic delocalization.

4.8 Conclusion

In summary, the decomposition of phosphaketene **12a** leads to an ion pair of a hypervalent tin cation and the heterocyclic anion **14a**, which can also be formed directly from Na(OCP) and Ph_3SnCl. Mechanistic studies have revealed that this seemingly simple reaction involves several rearrangement steps and stannyl shifts. Anion **14** is mainly stabilized by π delocalization in the OCPCO fragment. In contrast, the silyl analogue of **14** cannot be synthesized but the aromatic triphospholide anion **15** is formed instead, offering an easily accessible alternative for 1,2,4-triphospholides. **15** is a viable precursor for η^5 complexes, which allowed the synthesis of the siloxy substituted hexaphosphaferrocene **16**. The siloxy groups offer the possibility of further functionalization. The formation of the anions **14** and **15** shows that the $(OCP)^-$ ion can also act as a P^- transfer reagent accompanied by the loss of carbon monoxide. This type of reactivity will be further discussed in the next chapter.

5. A simple access to 1,2,4-oxadiphospholes

5.1 Introduction

Decarbonylation reactions, such as the transformation of aldehydes into hydrocarbons are widely utilized for the removal of carbonyl groups in organic syntheses.[60, 61] As special congeners of carbonyl compounds, ketenes can undergo photochemical decarbonylation yielding carbenes as reactive species.[62] Analogously, decarbonylation reactions of phosphaketenes R−P=C=O have been described.[63, 64] These photochemical[26] or transition metal assisted[65-68] reactions deliver – via the cleavage of the PC double bond – transient phosphinidenes or phosphinidene complexes, respectively. As already discussed in Chapter 2, the weight of the phosphaethynolate mesomeric structure **1b** is slightly larger than that of **1a** (Figure 5.1).[24] Beside these two predominant structures, though with a much smaller contribution, structure **1c** was found.

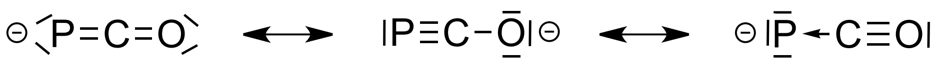

$$^{\ominus}P{=}C{=}O \longleftrightarrow P{\equiv}C{-}O^{\ominus} \longleftrightarrow {}^{\ominus}P{\leftarrow}C{\equiv}O$$

1a **1b** **1c**

40.2 % 51.7% 7.1%

Figure 5.1 Resonance structures of the phosphaethynolate anion.

The delocalization of the negative charge hampers the spontaneous decarbonylation of the $(OCP)^{-}$ ion, however, the contribution of mesomeric structure **1c** suggests that this anion may act as a (formal) P^{-} transfer reagent. As a proof of this principle, recently it was demonstrated that the reaction of an imidazolium salt with Na(OCP) forms the adduct of the parent phosphinidene (P−H) with the corresponding N-heterocyclic carbene.[69] According to the proposed mechanism, in this reaction the parent phosphaketene (H−P=C=O) is formed as intermediate, which delivers the PH fragment in a concerted reaction step under the extrusion of CO. Furthermore, a substituted phospholide was obtained as a side product in the reaction of Na(OCP) and diethyl but-2-ynediolate accompanied by the loss of carbon monoxide.[57] In the previous chapter the role of $(OCP)^-$ as a P^- transfer reagent in the formation of five-membered anionic rings was discussed. In this chapter the investigations on the reactivity of Na(OCP) towards acyl chlorides are presented. The mechanistic understanding of a rather complex but selective reaction, which employs the $(OCP)^-$ anion as both P nucleophile and P^- precursor is provided.

5.2 Synthesis of ester-functionalized 1,2,4-oxadiphospholes

Acyl phosphaketenes RC(O)(P=C=O) are the heavier analogues of acyl isocyanates. Knowing that sterically demanding groups are needed to stabilize a phosphaketene in a monomeric form,[25, 27, 28] in the first experiment $Na(OCP)(dioxane)_{2.5}$ was reacted with the rather bulky 2,4,6-trimethylbenzoyl chloride (MesC(O)Cl) in a 1:1 ratio. The precipitation of sodium chloride and a slight gas evolution were observed during the reaction. Subsequent investigation of the reaction solution by ^{31}P-NMR spectroscopy showed no resonance in the expected chemical shift range for mesitoyl phosphaketene. (The calculated chemical shift of MesC(O)(P=C=O) is −110 ppm at the B3LYP/aug-cc-pVDZ level of theory.) Instead, two doublet resonances at 112 and 253 ppm with the same coupling constant ($J = 46$ Hz) were observed. The ^{13}C-NMR spectrum and an X-ray diffraction analysis revealed the formation of the ester substituted 1,2,4-oxadiphosphole **19**, which was isolated as a light sensitive, yellow solid in 68% yield (Scheme 5.1).

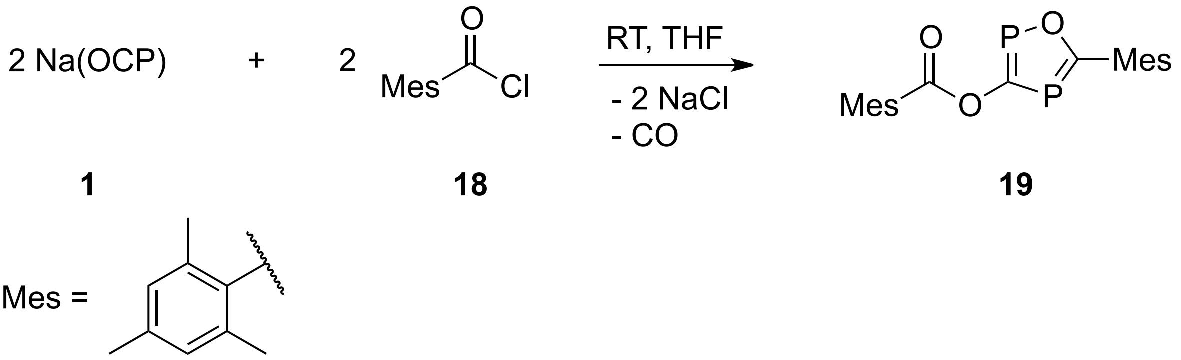

Scheme 5.1 Formation of the ester substituted 1,2,4-oxadiphosphole **19**.

There are only a handful of synthetic procedures for 1,2,4-oxadiphospholes and they enable only poor to moderate yields.[70-73] These methods usually involve several reaction steps and complicated techniques are needed to separate the product from the large amount of byproducts. The reaction of the easily accessible Na(OCP) with MesC(O)Cl offers a straightforward synthesis with a good atom economy regarding the phosphorous. Similarly, clean reactions were observed with other aromatic acyl chlorides (e.g. *o*-toluoyl chloride, 2,6-difluorobenzoyl chloride). Applying aliphatic acyl chlorides, however, the formation of the 1,2,4-oxadiphospholes was accompanied by unidentified byproducts.

5.3 X-ray structure of the 1,2,4-oxadiphosphole

The structure of **19** was verified by a single crystal X-ray analysis (Figure 5.2). The oxadiphosphole ring and the attached ester moiety are coplanar, while the mesityl rings are rotated out of this plane by 44.2 and 84.5 degrees. The PC and CO bond lengths of the P_2C_2O ring are comparable to those in other 1,3-oxaphospholes.[74-76] The first structural characterized 1,2,4-oxadiphosphole was published by Ionkin *et al.*,[72] however, the highly disordered structure does not allow any comparison.

Although the PC bond lengths reflect a Lewis drawing with alternating single (C1-P2) and double bonds (C1-P1 and C2-P2), to some extent bond length equalization can be observed, which indicates a moderate aromatic delocalization. This is in agreement with previous theoretical studies, which stated that the aromaticity of the parent 1,2,4-oxadiphosphole is just slightly smaller than that of furan and other phosphasubstituted furanes.[77-80] Nuclear independent chemical shift[81] calculations revealed that the ester substituent has only very little influence on the aromaticity of the five-membered ring. (The NICS(0) value for **19’** bearing methyl instead of mesityl groups is −9.9 ppm at the B3LYP/6-311+G** level of theory. The replacement of the ester function by a hydrogen results in a NICS(0) value of −10.8 ppm.)

A striking feature of the structure shown in Figure 5.2 is the rather short P1-O3 distance (2.5 Å), which is significantly smaller than the sum of the van der Waals radii of phosphorous and oxygen (3.32 Å),[82, 83] indicating a secondary interaction. Note that the oxygen atom O3 of the carbonyl group faces the phosphorous atom P1, which is positively polarized by the neighboring O1 atom. As computational evidence, the topological analysis[84] of the electron density on a model system **19’** revealed a bond critical point between P1 and O3 (see Figure 5.3). The corresponding electron density of ρ = 0.029 a.u. indicates a relatively strong interaction in the range of hydrogen bonds.

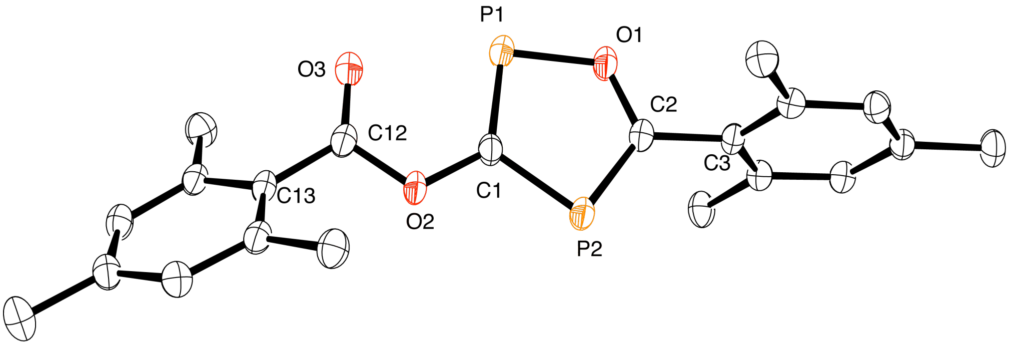

Figure 5.2: ORTEP plot of **19** (thermal ellipsoids are drawn at 50% probability). Hydrogen atoms have been omitted for clarity. Selected bond lengths (Å) and angles (°): P1-C1 1.716(3), C1-P2 1.780(2), C2-P2 1.715(2), C2-O1 1.346(3), O1-P1 1.696(2), C2-C3 1.497(3), C1-O2 1.395(3), C12-O3 1.219(3), C12-C13 1.489(3); C1-P1-O1 93.0(1), P1-O1-C2 118.7(2), O1-C2-P2 119.2(2), C2-P2-C1 90.9(1), C1-O2-C12 116.0(2), O2-C12-C13 112.7(2), O3-C12-C13 127.0(2).

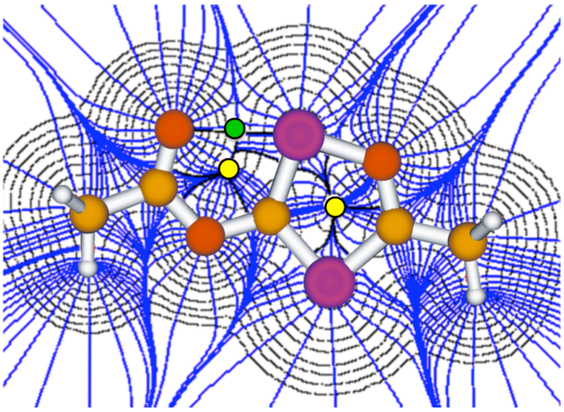

Figure 5.3 Atoms in molecules (AIM) plot of **19’** at the B3LYP/6-311+G** level of theory. The green and yellow dots represent the bond and ring critical points, respectively.

5.4 Investigations on the reaction mechanism

Since the formation of **19** involves four reactants (2 MesCOCl + 2 Na(OCP)), an elaborate mechanism can be expected for this reaction. To explore the reaction sequence, first low temperature ^{31}P-NMR measurements were performed (the reaction completes instantaneously at room temperature). Applying *in situ* monitoring, a THF solution containing the starting materials (in stoichiometric amounts) was gradually allowed to warm from −50 °C to room temperature. At −35 °C the parallel formation of the two intermediates **A** and **B** was observed (Figure 5.4). Further NMR investigations at different temperatures indicated that **B** is in equilibrium with **A** and an $(OCP)^{-}$ anion. Besides Na(OCP), intermediates **A** and **B** as well as the final product **19** no other species were observed in the ^{31}P-NMR spectra. These low temperature NMR experiments were repeated using different stoichiometric ratios of the starting materials, but no further insights were gained.

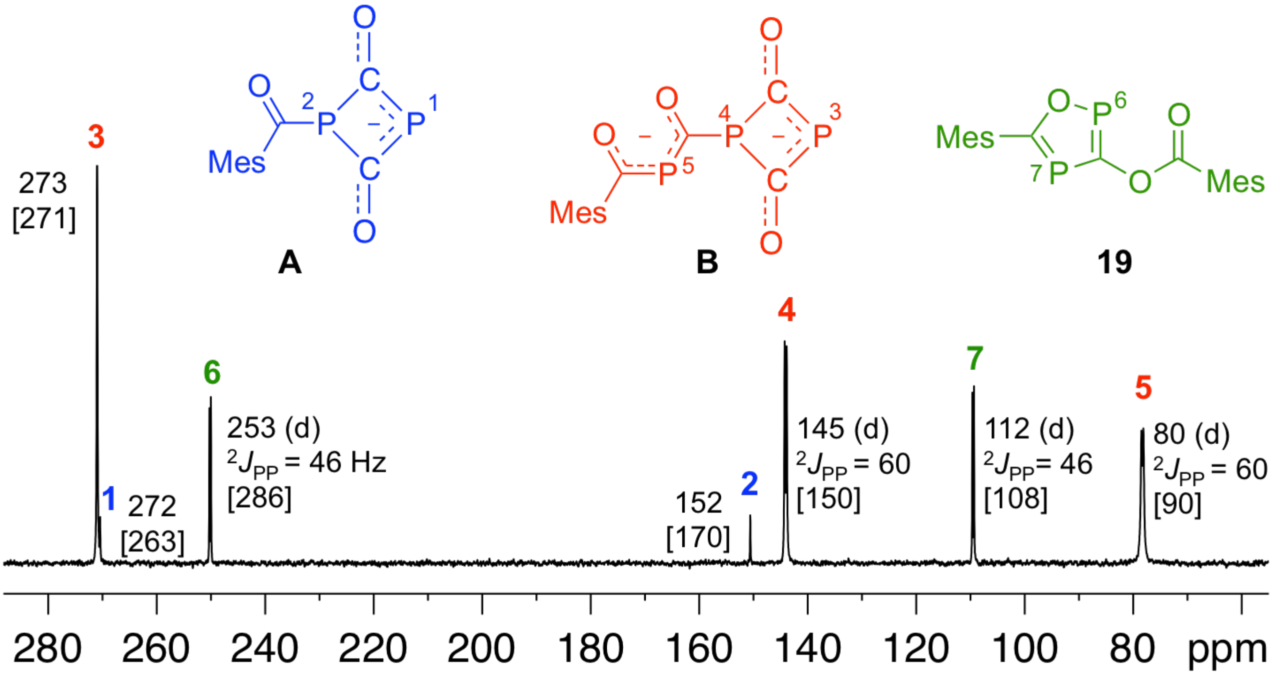

Figure 5.4 ^{31}P-NMR spectrum at −35°C after 17 h reaction time showing intermediates **A**, **B** and the final product **19**. Chemical shifts are given in ppm, coupling constants (*J*) in Hz. Calculated chemical shifts at the GIAO/B3LYP/aug-cc-pVDZ level are given in brackets.

Anion **A** and dianion **B**, identified using GIAO chemical shift calculations, are adducts of a mesitoyl phosphaketene molecule with one and two $(OCP)^-$ ions, respectively. This indirectly proves the initial formation of mesitoyl phosphaketene, MesC(O)(P=C=O). The common structural motif of **A** and **B** is the four-membered $P(CO)_2P$ ring, which was first described for $[O_2C–P(CO)_2P]^{2-}$, the adduct of a CO_2 molecule and two $(OCP)^-$ ions (see Chapter 2). The ^{31}P-NMR chemical shifts of this adduct (279 and 102 ppm) are indeed similar to those of the rings in **A** and **B**. The ^{31}P-NMR chemical shift of the P5 atom (80 ppm) in **B** matches well that of bismesitoyl phosphide $[P(COMes)_2]^-$, 86 ppm).[85]

At this point of the discussion it is not obvious how the intermediates **A** and **B** are involved in the formation of **19**. Important information was obtained from the reaction of 2,4,6-trimethylbenzothioyl chloride (**20**) with Na(OCP) – preformed by R. Suter in our working group[86] – which resulted in the formation of anion **21** (see Scheme 5.2).

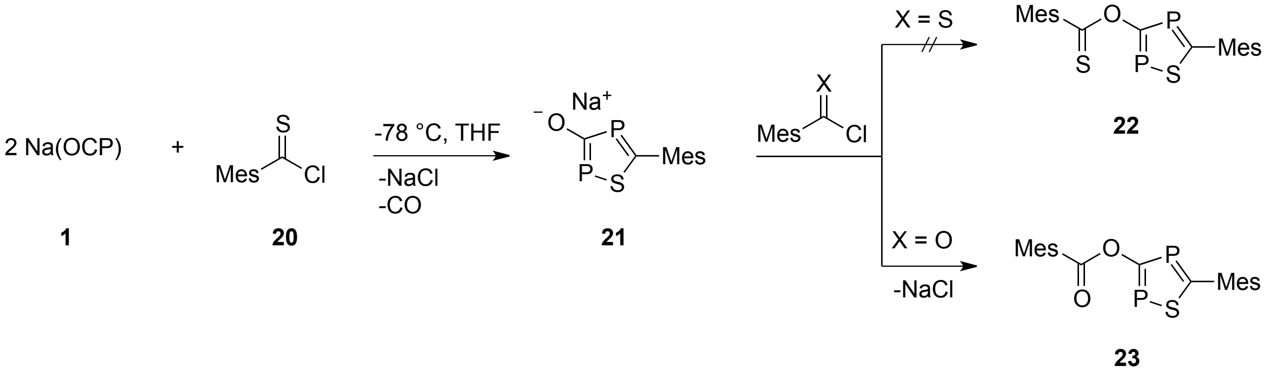

Scheme 5.2 Formation of sodium 1,2,4-thiadiphosphol-3-olate (**21**) and its reaction with (thio)acyl chloride.[86]

Compound **22**, which is the disulfur analogue of **19** was not formed, even when the thioacyl chloride was applied in excess. However, when **21** was reacted with mesitoyl chloride, compound **23**, the monosulfur analogue of **19** was obtained.[86] 1,2,4-thiadiphospholes have been reported in the literature.[87-89]

The different outcome of these experiments can be explained by the differing electrophilicity of thioacyl chlorides and acyl chlorides. These results also shed further light on the formation mechanism of the oxadiphosphole **19**. It is likely that in the last step a mesitoyl chloride molecule reacts with a 1,2,4-oxadiphosphol-3-olate anion, which is the oxygen analogue of **21**. However, this anion could not be observed in the ^{31}P-NMR spectrum, which implies that this nucleophilic substitution proceeds rather fast.

The direct observation of intermediates **A** and **B** as well as the indirect evidence for the 1,2,4-oxadiphosphol-3-olate anion allow a proposition for the reaction sequence of the formation of **19** (Scheme 5.3).

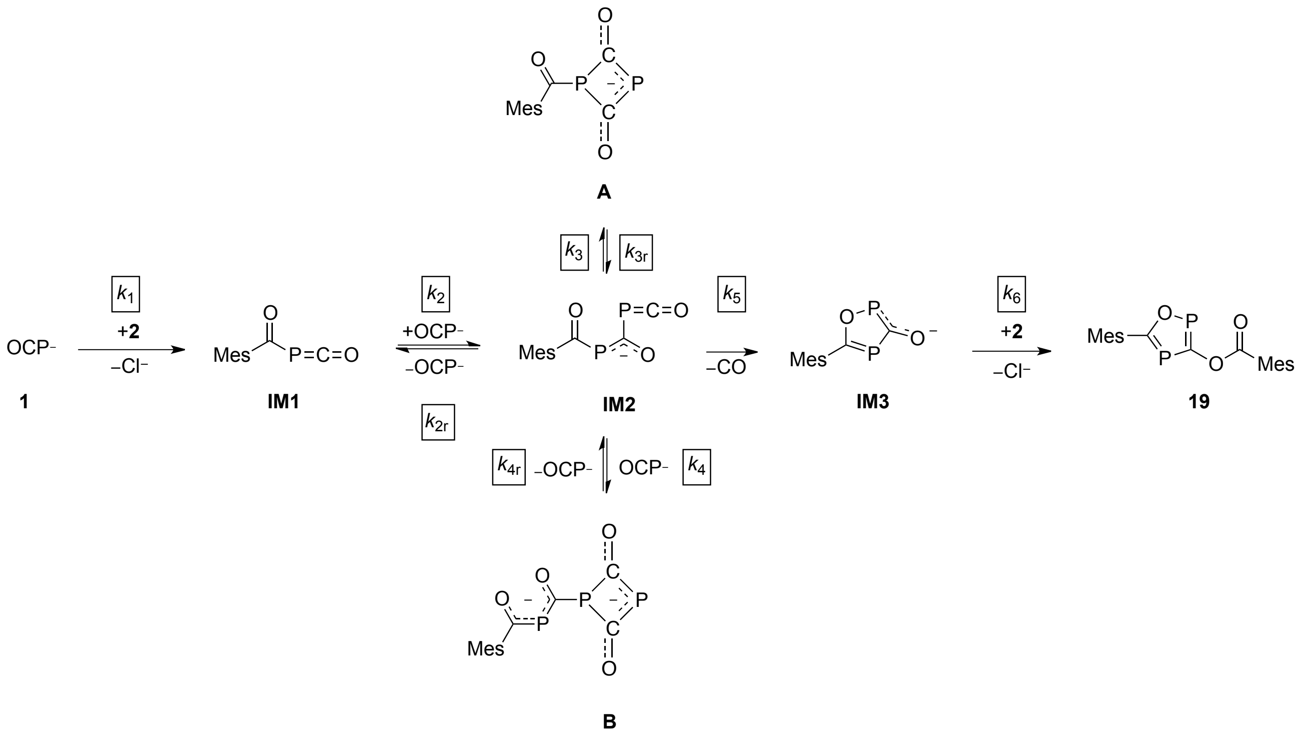

Scheme 5.3 Proposed reaction mechanism leading to **19**.

The starting step is the formation of the acyl phosphaketene **IM1**, which is then attacked by an (OCP)$^-$ ion, leading to **IM2**. From intermediate **IM2**, which was not observed experimentally, the cyclic anions **A**, **B** and **IM3** can be formed. A ring closure of **IM2** leads to its isomer **A**, while a formal cycloaddition of **IM2** with another (OCP)$^-$ ion delivers intermediate **B**. Presumably, the reactions leading from **IM1** to **IM2** as well as from **IM2** to the intermediates **A** and **B** are reversible. This is bolstered by the experimentally observed equilibrium between **A**, an (OCP)$^-$ anion and **B** (*vide supra*). Furthermore, **IM2** can undergo a cyclization under the loss of CO yielding **IM3**. In the final step, the nucleophilic substitution on an acyl chloride with **IM3** gives the final product **19**.

To validate the reaction mechanism shown in Scheme 5.3 and gain information on the rate of the processes, a kinetic study was carried out. The reaction progress was followed at −35 °C by ^{31}P-NMR spectroscopy and the concentrations of Na(OCP), **A**, **B** and the final product **19** were determined from the relative integrals of the corresponding peak areas (see Figure 5.5). Applying non-linear fitting to these data, the rate constants for the reaction steps shown in Scheme 5.3 could be estimated (see Table 5.1). As certain species could not be included in the fitting (either they are not observable on the NMR time scale or do not contain P atoms), this method cannot exclude the possibility of other (slightly different) reaction pathways. However, the fitted model reasonably describes the time dependency of the system.

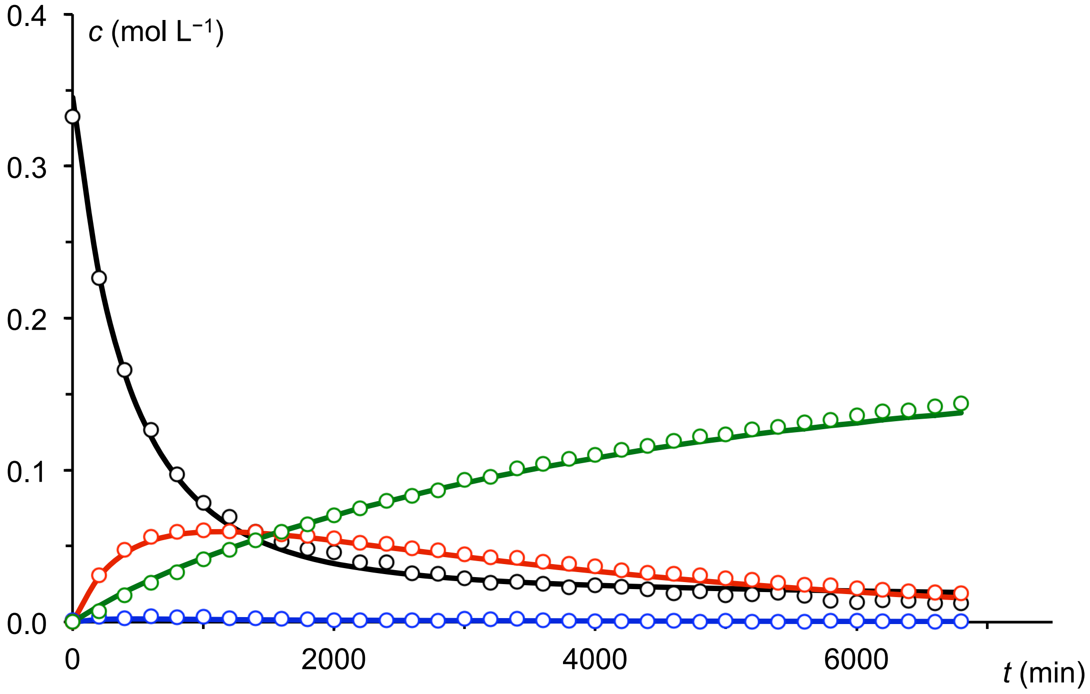

Figure 5.5 Measured (dots) and fitted (solid lines) concentrations of Na(OCP) (black), **A** (blue), **B** (red) and **19** (green).

Table 5.1 Estimated rate constants (for first order reactions in min^{-1}, for second order in $\text{L mol}^{-1}\text{ min}^{-1}$), see Scheme 5.3. The last step of the reaction is instantaneous, thus k_6 is not listed.

Forward reaction		Reverse reaction	
k_1	2.36×10^{-3}		
k_2	4.98	k_{2r}	1.47
k_3	2.08×10^{-2}	k_{3r}	5.02×10^{-3}
k_4	8.40×10^{-1}	k_{4r}	3.64×10^{-4}
k_5	8.19×10^{-2}		

The slowest step in this four-step reaction cascade leading to **19** (via **IM1**, **IM2** and **IM3**) is the first nucleophilic substitution ($k_1 < k_5 << k_2$ and the last **IM3→19** step proceeds instantaneously), which is followed by a very quick and reversible step delivering **IM2**. The reaction chain is perturbed by the two side reactions leading to **A** and **B**. Starting from **IM2**, the formation of **B** is much faster than that of **IM3** and **A**. Thus the concentration of **B** increases steeply in the beginning of the reaction (in the first ca. 15 hours). Since the formation of **B** from **IM2** is reversible and **IM2** is consumed in an irreversible step to form **IM3**, **IM2** can be recovered continuously via the ring opening of **B**. The rate constant of the reaction leading to **B** is three orders of magnitude larger than that of the reverse reaction ($k_4 >> k_{4r}$), hence species **B** acts as a reservoir for **IM2**. Similarly, **A** is a conserved form of **IM2**, however in this case the accumulation effect is much less pronounced (k_3 is similar to k_{3r}). Indeed, the concentration of **A** is small and approximately constant during the entire observed period.

The formation of **IM3** from **IM2** deserves a closer look. High-level calculations revealed that this reaction follows a concerted mechanism and the activation barrier was found to be low (4.0 kcal/mol at the CCSD(T)/aug-cc-pVDZ//B3LYP/6-31+G*level of theory). The structure of the corresponding transition state is shown in Figure 5.6 and the geometrical parameters indicate a late transition state. The cleavage of the PC double bond of the phosphaketene moiety occurs simultaneously with the formation of the PO bond. A continuous change in the atom distances was observed along the reaction coordinate. In this process, the starting material, which consists of a phosphaketene unit and a separate delocalized OCPCO moiety, transforms to a moderately aromatic system. The increase in aromaticity is reflected by NICS(0) values depicted as a function of the reaction coordinate, which become continuously more negative. Since there is an exocyclic part involved in this bond transformation process, this reaction should be described as a coarctate reaction.

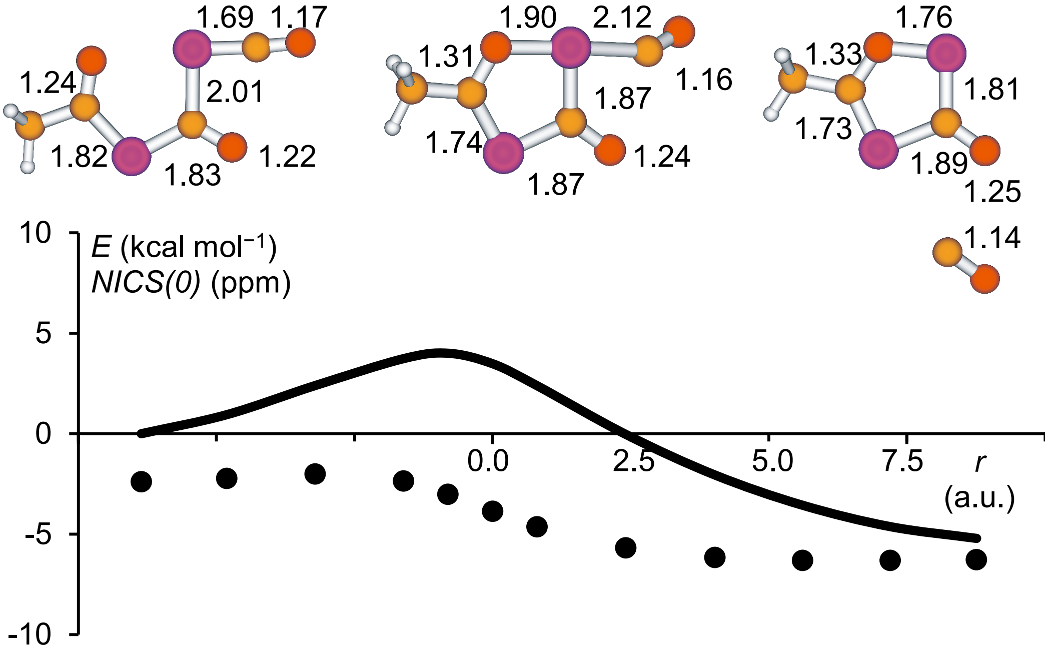

Figure 5.6 Relative energy (solid line, CCSD(T)/aug-cc-pVDZ//B3LYP/6-31+G*) and NICS(0) values (dots, B3LYP/6-311+G**//B3LYP/6-31+G*) along the reaction coordinate for the ring closure reaction leading from **IM2** to **IM3**. Selected atom distances are given in Å for **IM2**, the transition state and **IM3**.

Beside the classical linear and pericyclic reactions, a third group of reactions was classified by Herges as coarctate.[90-93] The coarctate (or complex) reactions proceed in a concerted manner by breaking and making two bonds at one (or more) atoms at a time. In a pericyclic reaction the bond making and bond breaking occurs simultaneously in a cyclic pathway. On the contrary, the coarctate transition state exhibits a so-called coarctate atom (see Figure 5.7a), at which the loop of overlapping orbitals is compressed (coarctated). Analogous to the pericyclic reactions, the transition state of the coarctate reactions is stabilized by orbital interactions, which can be either of the Hückel or Möbius type. The transition state leading to **IM3** is stabilized by a Möbius type eight-electron interaction and the coarctation of the orbital loop is at the P atom (see Figure 5.7b). Coarctate reactions can be further classified as real or pseudocoarctate reactions, in the latter the electron delocalization includes a disconnection. Pseudocoarctate reactions typically exhibit planar transition states and low activation barriers. Since the transition state **TS(IM2→IM3)** is almost planar and the barrier is very small, this reaction has pseudocoarctate character. Similarly, the fragmentation of 3-azidoacrylaldehyde to isoxazol and dinitrogen has been described and classified as a pseudocoarctate process.[94]

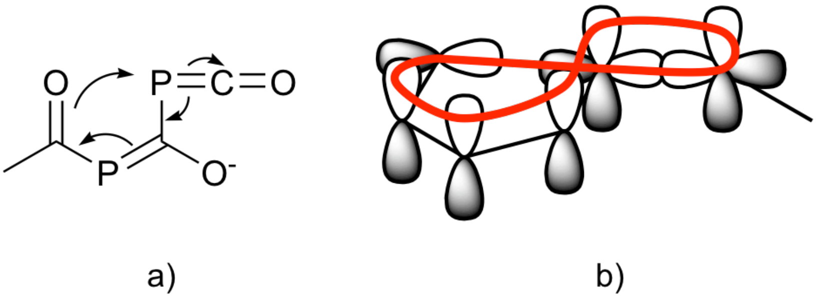

Figure 5.7 a) Coarctation at the P atom of the phosphaketene unit; b) Möbius type eight-electron interaction.

5.5 Conclusion

A one-pot synthesis for substituted 1,2,4-oxadiphospholes, utilizing Na(OCP) as phosphorous source has been presented. The reaction is remarkably selective and atom economic with respect to phosphorous, furthermore, excellent yields can be obtained. The stepwise reaction mechanism was deciphered applying low temperature ^{31}P-NMR spectroscopy, kinetic measurements and theoretical calculations. The $(OCP)^{-}$ anion was found to react as a nucleophile and P^{-} transfer reagent. Moreover, its formal [2+2] cycloaddition products act as reservoirs for the initially formed, highly reactive mesitoyl phosphaketene. The formation of the oxadiphosphole ring proceeds in a concerted, pseudocoarctate reaction step. The 1,2,4-oxadiphosphole **19** offers the possibility of further modifications: its reactivity in cycloadditions and in coordination chemistry can be expected to lead to new ester functionalized phosphorous compounds and complexes.

6. Interconversion of a monocyclic phosphide anion and an annulated diazaphospholenium cation

6.1 Introduction

In this chapter, the potential of the phosphaethynolate anion $(OCP)^-$ in cycloadditions will be further manifested and its reactivity towards dicyclohexylcarbodiimide (DCC) will be presented.

Regarding the activity of the $(OCP)^-$ anion towards activated alkynes and bulky carbodiimides only a few examples have been reported. The [4+2] addition of $(OCP)^-$ with 2*H*-pyran-2-one followed by the extrusion of CO_2 delivers the phosphinin-2-olate anion.[57] Furthermore, substituted phosphinin-4-olates are accessible from activated alkynes and $(OCP)^-$. As an intermediate the [2+2] adduct of $(OCP)^-$ and an alkyne molecule, the four-membered ring anion **I**, was observed (see figure below).[57] Subsequently, **I** undergoes a cycloaddition with a second alkyne moiety, yielding the six-membered heterocyclic product. Jupp and Goicoechea reported the formation of the [2+2] adducts of [K([18]crown-6)](OCP) and diphenylketene or bis(2,6-diisopropylphenyl)carbodiimide.[18] The anion of the latter adduct (**II**) is a four-membered PC_2N ring bearing a carbonyl and an imine group. The authors stated that the reaction of [K([18]crown-6)]OCP with N,N'-dicyclohexylcarbodiimide (DCC) showed no evidence of the cycloaddition product being formed even after prolonged heating.

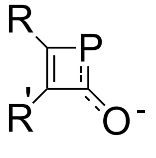

I

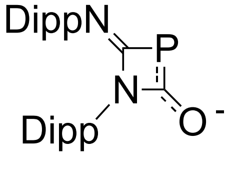

II

6.2 Reaction of Na(OCP) with dicyclohexylcarbodiimide (DCC)

In contrast to the earlier results by Jupp and Goicoechea, a clean reaction was observed when [Na(OCP)(dioxane)$_x$] (**1**) and DCC (**24**) were reacted in a ratio of 2:1 in refluxing THF. In the ^{31}P-NMR spectrum the observed singlet resonance at −44.2 ppm is remarkably shifted to a lower frequency compared to that of **II** (+18.6 ppm), which propounds a significantly different environment around the P atom. Indeed, the ^{13}C-NMR spectrum and an X-ray diffraction study (*vide infra*) revealed the formation of the six-membered ring anion **25** (Scheme 6.1). Note that the analogous compounds bearing *p*-tolyl rests as well as isopropyl rests were also isolated, for experimental details see chapter 9.

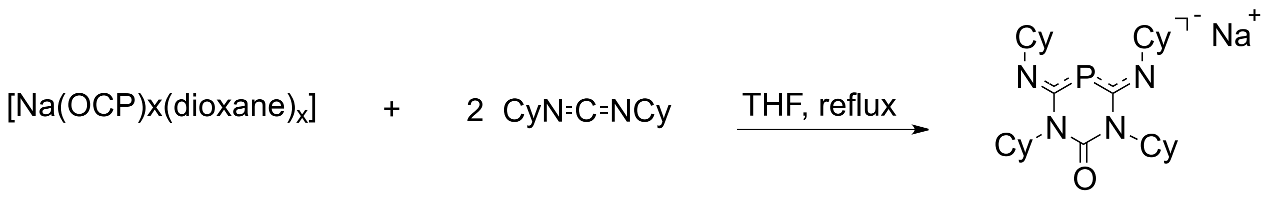

1 **24** [Na][**25**]

Scheme 6.1 Formation of six-membered ring anion **25**.

6.3 Mechanistic studies on the formation of the 1,3,5-diazaphosphinane anion

No reaction was observed when Na(OCP) and DCC were reacted in THF at room temperature. The reaction shown in Scheme 6.1 proceeds only upon refluxing of the reaction solution. Monitoring of the reaction proceeding by ^{31}P-NMR spectroscopy did not reveal any observable intermediate leading to **25**.

To understand the unexpected formation of **25** instead of the cyclohexyl analogue of **II**, theoretical calculations were performed. The minimum energy reaction pathway (MERP) of the reaction between Na(OCP) and two dimethyl carbodiimide molecules is shown in Figure 6.1.

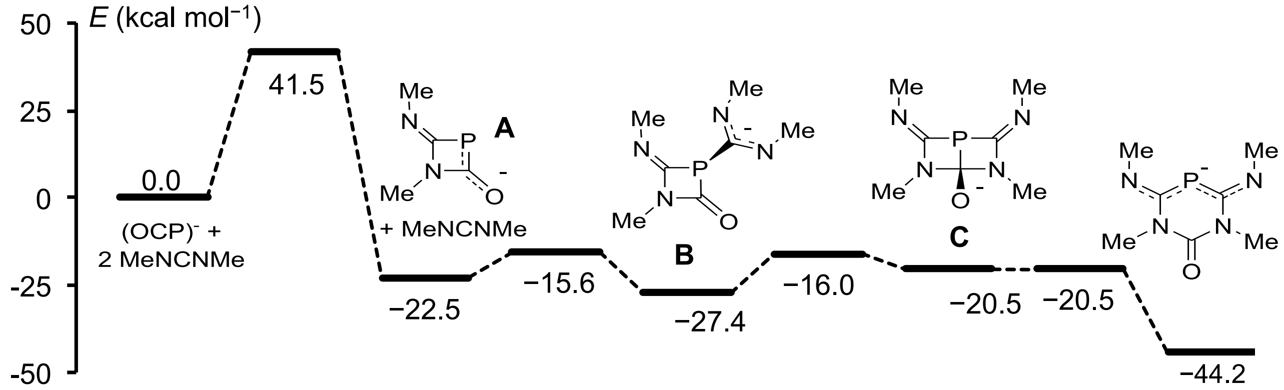

Figure 6.1 Minimum energy reaction pathway (MERP) of the reaction between Na(OCP) and two dimethyl carbodiimide molecules at the CBS-QB3 level. Na^+ ions were included in the computations but are not shown.

Formally, the first reaction step is a [2+2] cycloaddition delivering anion **A** (the methyl analogue of **II**), which is slightly more stable than the starting materials. In the next step, the phosphorous center of **A** attacks the central carbon atom of another carbodiimide molecule. The formed adduct **B** undergoes an intramolecular nucleophilic attack resulting in the rather energy-rich Dewar-benzene type intermediate **C**. To reduce the ring strain, **C** rearranges to the final product in a practically barrierless process. The comparison of the activation barriers indicates that the rate-determining step in this process is the formation of intermediate **A**. The rather high activation barrier of this step (41.5 kcal/mol) agrees with the experimental observation that the reaction proceeds only at high temperature. Since the activation barriers of the consecutive steps are remarkably smaller, the reaction does not terminate at the formation of **A**. Based on further ^{31}P-NMR spectroscopic studies there is no experimental evidence for the formation of the [2+2] adduct or any other intermediates. Nevertheless, the fact that **A** is isolable with the sterically encumbering Dipp groups (cf. anion **II**) bolsters the proposed mechanism.

6.4 Oxidation of the anionic 1,3,5-diazaphosphinane

In an attempt to obtain a persistent phosphorous centered radical species, [Na][**25**] was reacted with stoichiometric amounts of oxidizing reagents such as ferrocenium hexafluorophosphate or trityl chloride. Instead of the desired radical only the corresponding diphosphane **26** obtained was obtained (Scheme 6.2), which was observed as a singlet at –84 ppm in the ^{31}P-NMR spectrum.

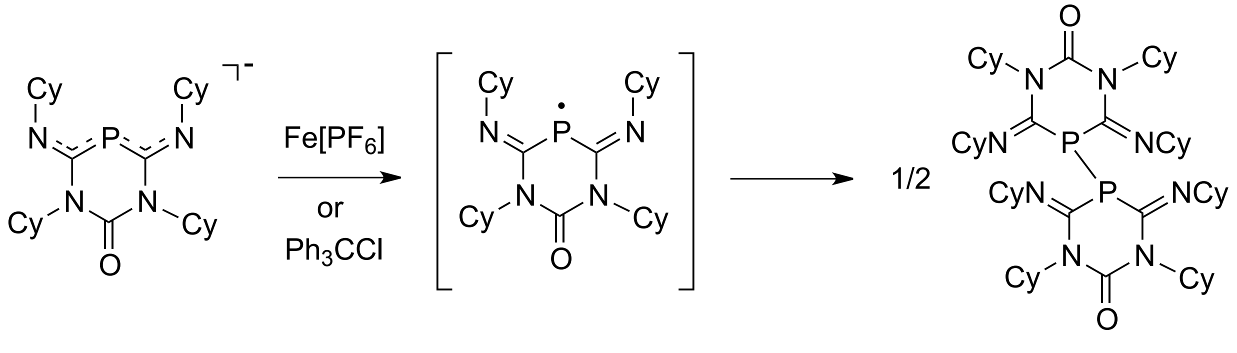

25 **26**

Scheme 6.2 Oxidation of anion **25** and subsequent dimerization of the initially formed radical species.

It is known that the PP bond of diphosphanes bearing bulky substituents can undergo reversible homolytic dissociation.[95-100] In the temperature range of 133 K to 323 K no signals could be detected in the EPR measurement of a solution containing **26**. This indicates that **26** cannot generate measurable amounts of the corresponding P centered radical.

Surprisingly, when the oxidation of [Na][**25**] was performed with an excess of elemental iodine, the formation of a species with a singlet ^{31}P-NMR resonance at 196.3 ppm was observed (Scheme 6.3). This low field chemical shift (in the range of unsaturated P atoms) indicates a remarkable structural change with respect to [Na][**25**] or the diphosphane **26**. The X-ray diffraction study (see below) of the red single crystals obtained from the reaction solution revealed that the oxidation product is built up by annulated 1,3,2-diazaphospholenium cations **28** and triiodide counter anions (in a 1:1 ratio). By sequential addition of small amounts of iodine to [Na][**25**] it was possible to identify two intermediates. Similarly to the oxidations mentioned above, first the diphosphane **26** is formed. The PP bond of **26** can be cleaved by iodine[101] and the formed iodophosphane **27** was observed as a singlet at –87.4 ppm in the ^{31}P-NMR spectrum. **27** is stable in solution and can only be converted to the final product by the addition of a further equivalent of iodine.

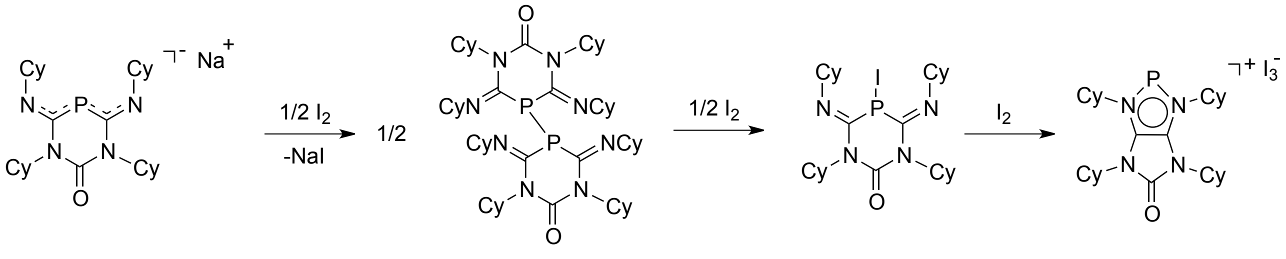

[25][Na] **26** **27** **[28][I$_3$]**

Scheme 6.3 Oxidation of the six-membered ring anion **25** with iodine to the diazaphospholenium cation **28**.

The reduction of cation **28** with elemental sodium or potassium leads in the first step quantitatively to the corresponding bis(diazaphosphane) ($\delta\,^{31}$P = 122.7 ppm) (Scheme 6.4). However, subsequent reduction attempts only deliver small amounts of anion **25** along with a black precipitate, which was not investigated further.

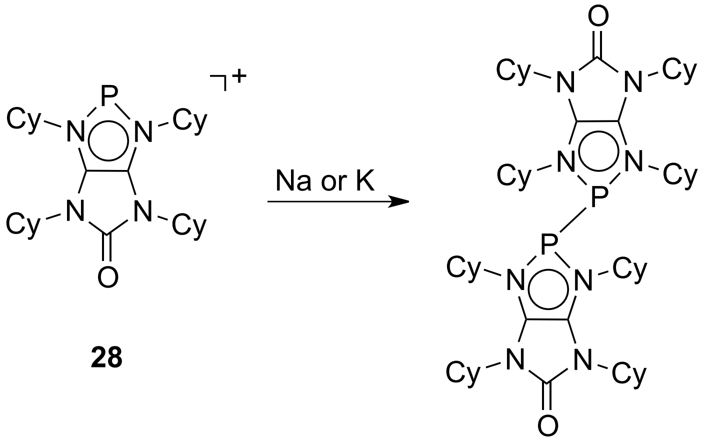

Scheme 6.4 Reduction of cation **25** with Na or K delivering the corresponding bis(diazaphosphane).

On the other hand, using elemental magnesium, cation **28** can cleanly be reduced to the magnesium salt of anion **25**, which was proven by spectroscopic methods (Scheme 6.5). Note that [Mg][**25**]$_2$ can also be obtained by an ion exchange reaction between [Na][**25**] and $MgCl_2$ (Scheme 6.6). Monitoring of the reaction by ^{31}P-NMR spectroscopy revealed the formation of the monoiodide [**28**][I] (δ ^{31}P = 186.7 ppm) and in this case the bis(diazaphosphane) was not observed.

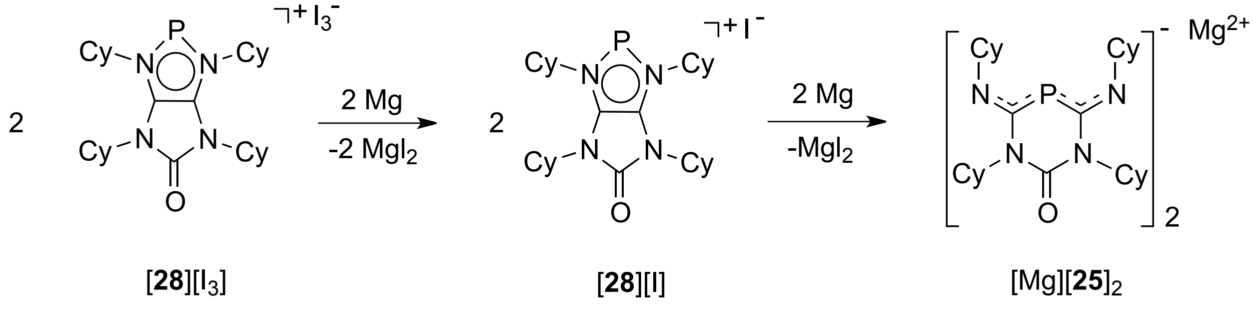

Scheme 6.5 Reduction of diazaphospholenium cation **28** with Mg to the magnesium salt of anion **25**.

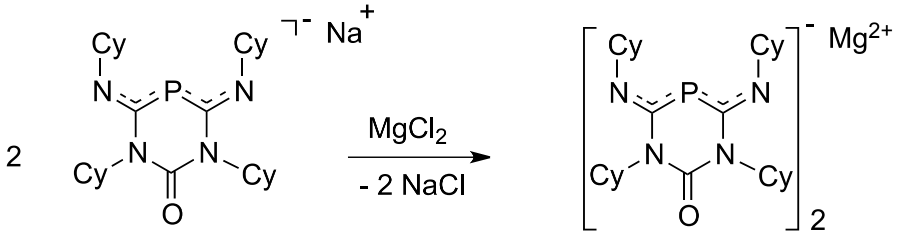

[Na][**25**]

[Mg][**25**]$_2$

Scheme 6.6 Generation of the magnesium salt of anion **25** by cation exchange from [Na][**25**].

6.5 X-ray structures

The X-ray structures of [Na][**25**] × 4 THF and [**28**][I_3], (see Figures 6.2a) and b), respectively) are both built up by contact ion pairs, which show no remarkable aggregation. The six-membered ring of phosphide **25** is non-planar, the maximum deviation from planarity is 0.254 Å. The solvent coordinated Na^+ ion binds to the oxygen atom of anion **25**. Compared to **II**, the exocyclic C=N bonds are slightly elongated (1.29 Å vs. 1.27 Å in **II**), while the PC bonds are somewhat shorter (1.80 Å vs. 1.84 Å in **II**). This indicates a stabilizing π-delocalization within the N=C−P−C=N moiety due to donor-acceptor interactions between the out of plane phosphorous lone pair and the π*(C=N) orbitals. In contrast to the twisted conformation of **25**, the two fused five-membered rings in **28** are co-planar. The bond lengths in the C_2N_2P ring of cation **28** are very similar to those of known diazaphospholenium cations, such as in 1,3-dicyclohexyl-1,3,2-diazaphospholenium triiodide (average bond lengths PN: 1.67 Å, CC: 1.34 Å, CN: 1.38 Å).[102] All the endocyclic CN bonds (1.36 – 1.41 Å) are significantly shorter than the exocyclic ones (1.48 – 1.50 Å), suggesting a conjugation within both the five-membered rings. Similarly, the length of the fusion CC bond (1.38 Å) is between that of a single and a double bond.

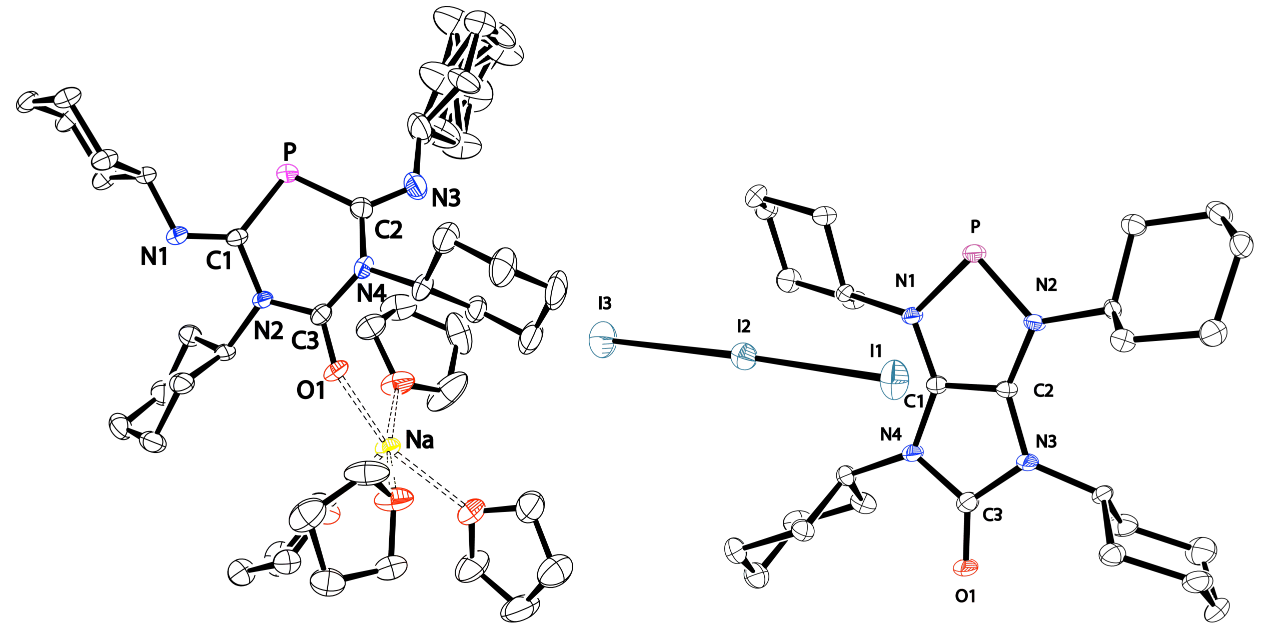

a) b)

Figure 6.2 **a)** ORTEP plot of [Na][**25**] × 4 THF (thermal ellipsoids are drawn at 50% probability). Hydrogen atoms have been omitted for clarity. Selected bond lengths (Å) and angles (°): P-C1 1.802(2), P-C2 1.798(2), C2-N4 1.445(3), N4-C3 1.374(3), C3-O1 1.245(3), O1-Na 2.246(2), C3-N2 1.365(3), N2-C1 1.441(2), C1-P 1.802(2), C1-N1 1.286(3), C2-N3 1.280(3); C1-P-C2 98.7(1), P-C2-N4 119.7(2), C2-N4-C3 121.8(2), N4-C3-N2 119.7(2), C3-N2-C1 123.1(2), N2-C1-P 118.2(1); **b)** ORTEP plot of [**28**][I$_3$] (thermal ellipsoids are drawn at 50% probability). Hydrogen atoms have been omitted for clarity. Selected bond lengths (Å) and angles (°): P-N1 1.699(3), N1-C1 1.354(4), C1-N4 1.381(4), N4-C3 1.411(4), C3-O1 1.217(4), C3-N3 1.409(4), N3-C2 1.374(5), C2-N2 1.360(5), N2-P 1.707(3), I1-I2 2.924(4) I2-I3 2.900(4), C1-C2 1.379(5); N1-P-N2 90.6(2), C1-N1-P 112.2(2), C2-N2P 112.0(2), C1-N4-C3 107.1(3), N3-C3-N4 107.3(3), C2-N2-P 112.0(2), I1-I2-I3 178.1(1);

6.6 Computational investigations on the rearrangement reactions

The alternating electronegativities of the neighboring atoms suggest that both the heterocycles **25** and **28** feature charge stabilization. This is also reflected in the partial charges and molecular electrostatic potential maps calculated for model species **25'** and **28’** (Me instead of Cy groups, see Figure 6.3), which indicate alternating positive and negative charges throughout the molecular skeletons.

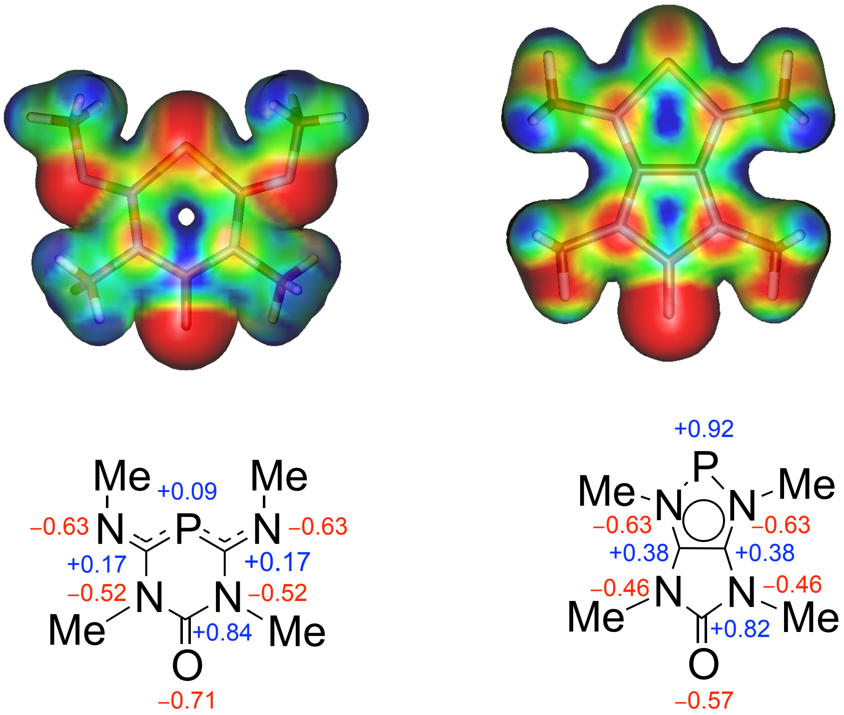

Figure 6.3 Molecular electrostatic potential maps and partial charges of ions **25’** (left) and **28’** (right) at the B3LYP/6-311+G** level.

The six-membered ring in **25’** is non-aromatic, as shown by the small negative value of the nucleus independent chemical shift 1 Å above the ring center (NICS(1) = −1.5 ppm) (for comparison NICS(1) = −10.2 ppm for benzene).[81, 103] As for cation **28’**, it has been established that the diazaphospholenium cations are stabilized by aromaticity. As expected, the aromaticity of the annulated PN_2C_2 ring in **28’** (NICS(1) = −8.6 ppm) is similar to that of an isolated diazaphospholenium cation (NICS(1) = −10.4 ppm). Compared to the PN_2C_2 ring, however, the C_2N_2(CO) fragment is much less aromatic (NICS(1) = −4.8 ppm, for 1*H*-imidazol-2(3*H*)-one: NICS(1) = −5.0 ppm).

To understand the rearrangement processes shown in Schemes 6.3 and 6.5 theoretical computations on model systems were carried out (applying Me groups instead of Cy groups). As discussed above, one equivalent of iodine is needed to convert the monoiodide **27** to the cation **28**. It is known that Lewis acids (eg. $AlCl_3$, $GaCl_3$, I_2) can accomplish the heterolytic cleavage of phosphorous halogen bonds to form phosphenium cations.[104] Hence, it is likely that an iodine molecule polarizes the PI bond of **27**, thereby increasing the positive partial charge on the P atom. To demonstrate a possible pathway for this transformation isolated cations as model species were investigated (see Figure 6.4).

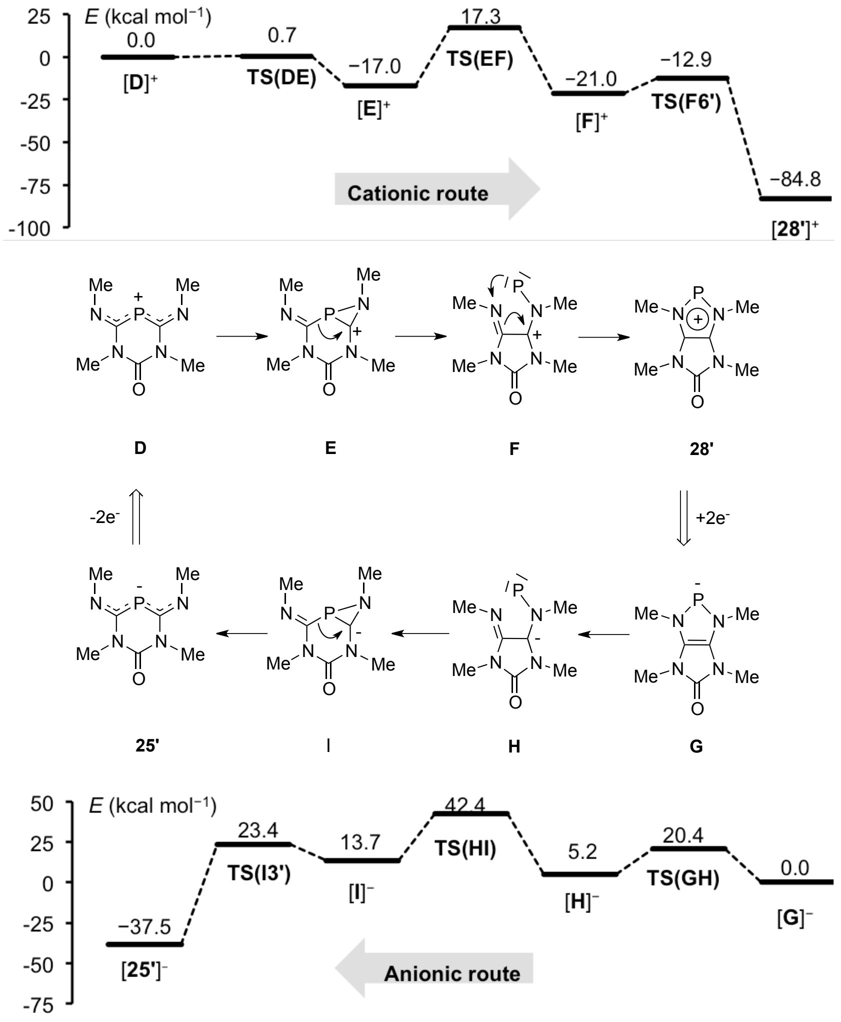

Figure 6.4 Possible rearrangement processes leading to **28’** and **25’**. Calculated relative energies at the CBS-QB3 level.

Starting from cation **D**, the first rearrangement step involves a ring closure giving the annulated azaphosphirane **E**. This is followed by the formation of **F**, which is an amino substituted phosphinidene. The highly exergonic cyclization of **F** leads to the cation **28'**, providing the thermodynamic driving force for this rearrangement process.Since it is known that halophosphanes can be reduced to phosphides using alkaline and earth alkaline metals,[101] it is proposed that the anion formed via a two-electron reduction of **28** is the starting point of the rearrangement sequence leading to anion **25**. This process (depicted in Figure 6.4 as **G→25'**) shows remarkable similarity to the formation of **28'** from **D**. The constitutions of the anionic intermediates **H** and **I** are analogous to the ones of **F** and **E**, respectively. The thermodynamic feasibility of the transformation **G→25'** is bolstered by the significantly negative Gibbs free energy value of −37.5 kcal/mol.

6.7 Conclusion

In summary, in this chapter the straightforward syntheses of the six-membered ring anion **25** and the annulated diazaphospholenium cation **28** have been presented. Note that these two oppositely charged ions have the same elemental composition, however, their constitutions are remarkably different (apart from the charge they are structural isomers). Moreover, **25** and **28** can be interconverted by redox processes. The theoretical investigations suggest that both rearrangement reactions include phosphinidenes as intermediates. Both of these heterocyclic ions are expected to offer applications as prototype redox active ligands in coordination chemistry. Due to several possible coordination sites **25** and **28** may be employed as building blocks in supramolecular networks.

7. Oligorization of isocyanates around a P^- anion: the reaction of $(OCP)^-$ with isocyanates

7.1 Introduction

Rigid polyurethane foams, the reaction products of diisocyanates, polyols and water, are commonly applied as durable structural and insulating materials.[105] The thermal and mechanical properties of these polymeric networks are crucially influenced by the degree of crosslinking, which can be achieved by incorporation of isocyanate cyclo-trimers. Lewis bases such as the fluoride anion,[106] N-heterocyclic carbenes[107] and acyclic[108, 109] or cyclic[110-112] phosphanes are well known to catalyze the cyclo-oligomerization of isocyanates (**29**) to form cyclic dimers (uretdiones **30**) and trimers (isocyanurates **31** and iminooxadiazinediones **32**) (Figure 7.1).

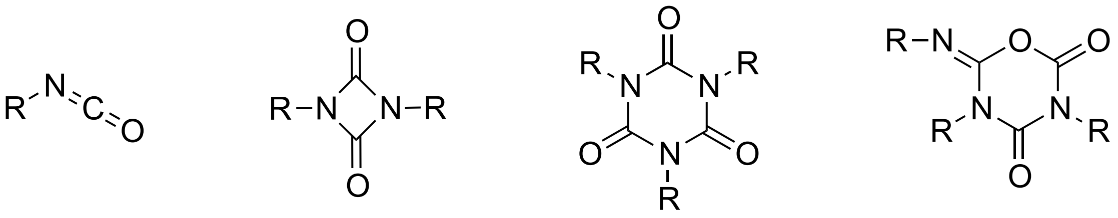

29 **30** **31** **32**

Figure 7.1 Isocyanates (**29**) and their oligomers (**30**-**32**).

The reactivity of isocyanates towards phosphides (PR_2^-) and phosphido complexes has barely been investigated. In the reported examples, the insertion of isocyanates into the transition metal-phosphorous bond of phosphido complexes has been observed.[113-115] Some yttrium-phosphido complexes were found to catalyze the cyclo-trimerization of isocyanates,[113] however, relatively high catalyst loadings are required to reach full conversion.

7.2 Reaction of Na(OCP) with 2,6-diisopropylphenyl isocyanate

The dihydrogenphosphide anion (PH_2^-) reacts with carbon monoxide or alternative CO-sources (esters of carbonic acid, iron pentacarbonyl) to form the phosphaethynolate ion $(OCP)^-$.[17] Extending this thought, isocyanates were also tested as CO-sources. Screening of the reaction between $NaPH_2$ and isocyanates indeed indicated the formation of Na(OCP). As it will be discussed in this chapter, depending on the substituent of the isocyanate and the molar ratio of the starting materials, different further reaction products were observed.

Sodium phosphaethynolate Na(OCP) was obtained as the main reaction product when the rather bulky 2,6-diisopropylphenyl isocyanate (Dipp−NCO **29a**) was reacted with $NaPH_2$ at 85 °C in a ratio of 2:1. During this reaction it was possible to detect the intermediates **I1** ($\delta\,^{31}P$: −150 ppm (t), $^1J_{PH} = 207$ Hz) and **I2** (two isomers: $\delta\,^{31}P$: −70 ppm (d), $^1J_{PH} = 260$ Hz; −83 ppm (d), $^1J_{PH} = 240$ Hz) by NMR-spectroscopy (Scheme 7.1). Similar data were reported by Becker for $H_3C{-}O{-}C(O){-}PH_2$ ($\delta^{31}P$: −138.6 ppm, $^1J_{PH} = 218$ Hz) and $[H_3C{-}O{-}C(O)PH]Li$ ($\delta\,^{31}P$: −83.8 ppm, $^1J_{PH} = 219$ Hz).[116]

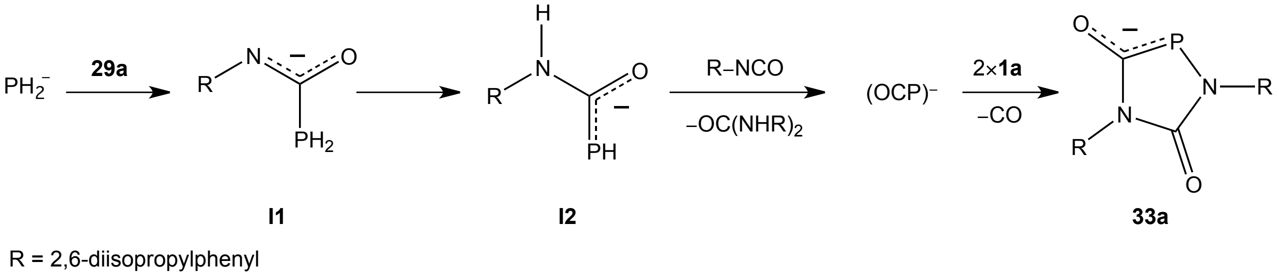

Scheme 7.1 Reaction between $NaPH_2$ and Dipp−N=C=O (**29a**).

When an excess of 2,6-diisopropylphenyl isocyanate was added to $NaPH_2$ or alternatively to Na(OCP), the orange colored sodium salt of 1,4,2-diazaphospholidine-3,5-dione (**33a**) ($\delta^{31}P$: 117 ppm) was formed (Scheme 7.1). The result of an X-ray diffraction study on single crystals of $[Na(THF)_2($**33a**$)]$ is shown in Figure 7.2 (for the discussion of the structure parameters see below). The lithium salt of **33a** has previously been mentioned (in a conference abstract),[117] however, neither analytical data nor evidence for the intermediate formation of the (OCP)$^-$ anion was given.

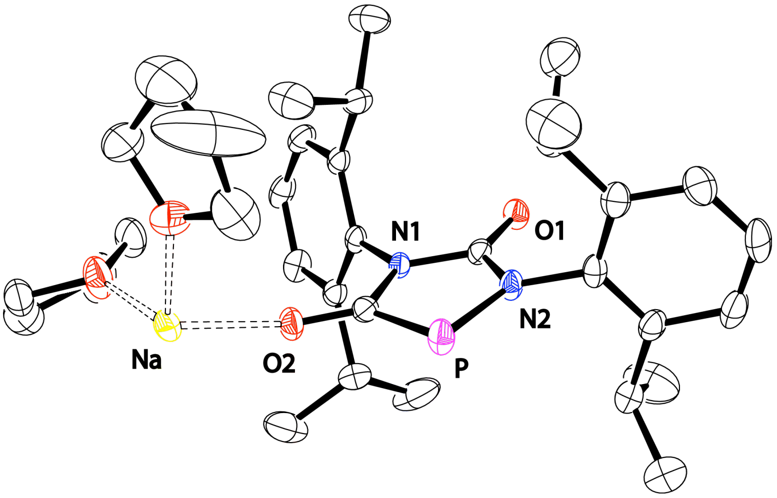

Figure 7.2 ORTEP plot of [Na(THF)$_2$(**33a**)] (thermal ellipsoids are drawn at 50% probability). Hydrogen atoms have been omitted for clarity. Selected bond lengths (Å) and angles (°): C1-N1 1.378(3), N1-C2 1.425(3), C2-P 1.756(3), C2-O2 1.254(3), P-N2 1.779(2), N2-C1 1.347(3), C1-O1 1.245(3); C1-N1-C2 115.9(2), N1-C2-P 110.0(2), C2-P-N2 88.3(1), P-N2-C1 115.8(2), N2-C1-N1 110.1(2).

7.3 Reaction of Na(OCP) with sterically less demanding isocyanates (PhNCO, CyNCO, *n*-BuNCO)

Na(OCP) was also obtained in the reaction of $NaPH_2$ with the sterically less demanding phenyl isocyanate **29b** (ratio 1 : 2), however, the reaction mixture contained further products: anions **34b** and **35b** as well as isocyanurate **31b** (Scheme 7.2).

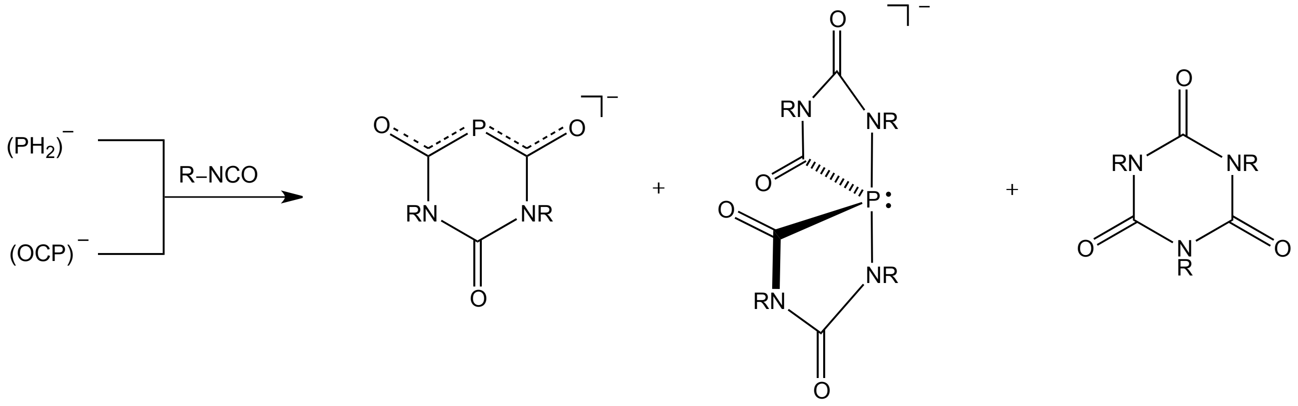

R = Ph (**b**), Cy (**c**), n-Bu (**d**)

34 **35** **31**

Scheme 7.2 Reaction of isocyanates with phosphide or phosphaethynolate ions.

The reaction between Na(OCP) and phenyl isocyanate (**29b**) also delivers **31b**, **34b** and **35b** (Scheme 7.2). This observation proves that Na(OCP) is the primary product in the reaction of sodium phosphide with isocyanates. Therefore, the investigations were continued employing Na(OCP) as starting material in the reaction with different isocyanates (R–NCO, R = Cy (**29c**), *n*-Bu (**29d**)). All of these reactions, again lead to the formation of **31**, **34** and **35**. The spiro phosphoranide **35**, which was unambiguously identified by single crystal X-ray diffraction (see below), is a formal adduct of four isocyanate moieties and a P^- anion. Likely, for sterical reasons the analogous spiro compound cannot form in the case of Dipp–NCO (Chapter 7.2). The six-membered heterocycle **34**, which formally consists of an $(OCP)^-$ anion and two isocyanate fragments, was identified spectroscopically.

In order to form selectively either of the products shown in Scheme 7.2, further test reactions have been performed. Varying the reaction conditions (solvent, temperature and concentration), however, did not result in a clean reaction. Generally, in all the reactions, the amount of **34** was much smaller than that of **35**. The complete separation of **34**, **35** and **31** was not successful because of the very similar physical properties of these compounds. **35** was obtained as colorless powder containing 20% decomposition product, which was identified as the five-membered ring anion **33**. Furthermore, for the full conversion of Na(OCP) an excess of isocyanate was needed since the isocyanurates (**31b**-**d**) were formed as byproducts. The addition of a catalytic amount (1 mol%) of Na(OCP) to phenyl isocyanate at room temperature resulted in the selective formation of triphenyl isocyanurate **31b**, which was isolated in excellent yield (92%). In the ^{31}P-NMR spectrum of the reaction suspension only **34b** and **35b** were observed. In another experiment, 1 mol% of the isolated **35c** also catalyzed the trimerization of phenyl isocyanate resulting in a comparable yield.

7.4 Catalytic activity of anionic species in the trimerization process of isocyanates

Experimental and theoretical studies have previously established that the oligomerization of isocyanates proceeds via sequential addition of isocyanates to the Lewis base-activated linear oligomer.[109, 118-120] On the basis of these findings, the reaction sequence shown in Figure 7.3a is proposed. The feasibility of this mechanism is bolstered by DFT model calculations using a simplified isocyanate (Me−N=C=O, **29e**).

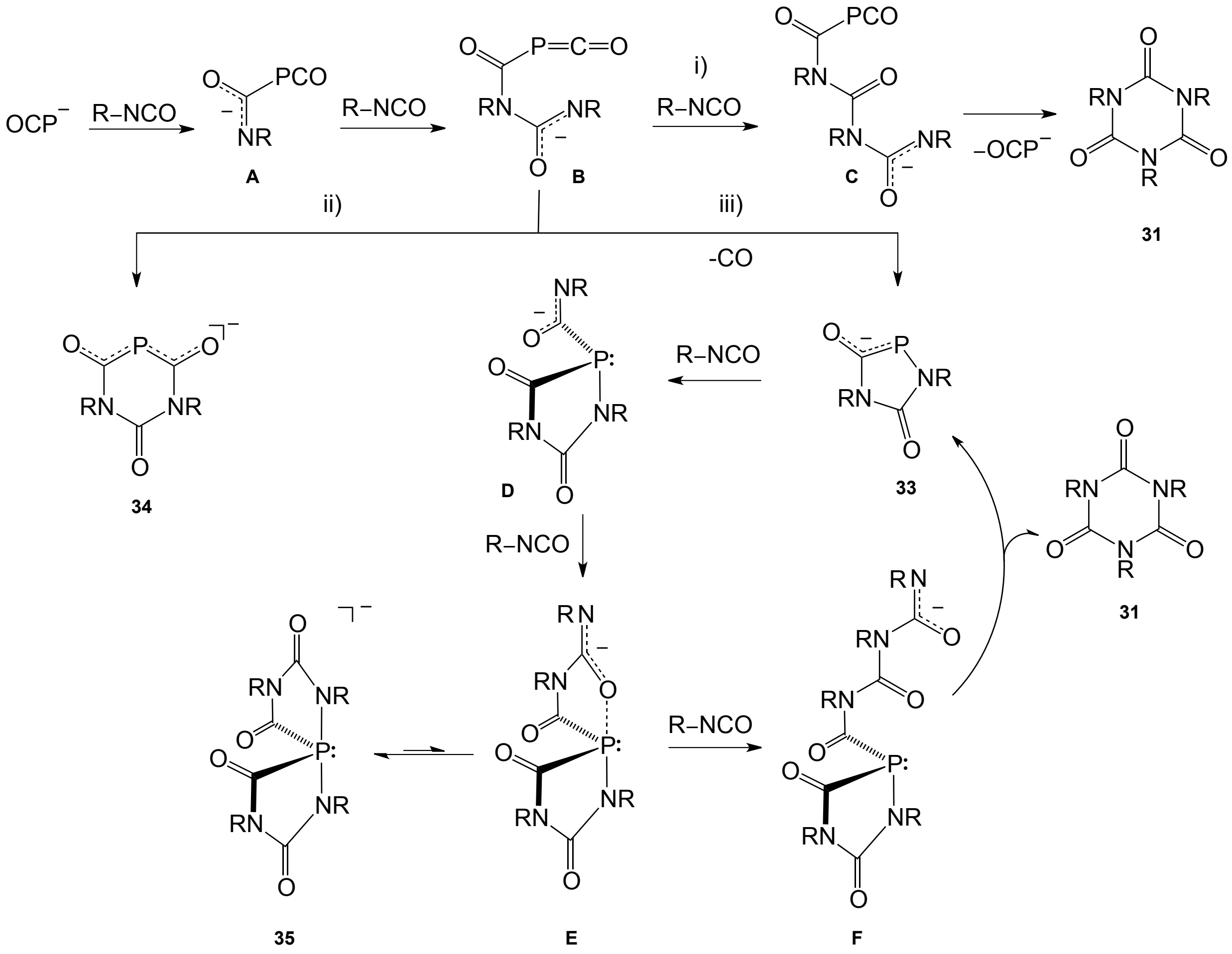

a)

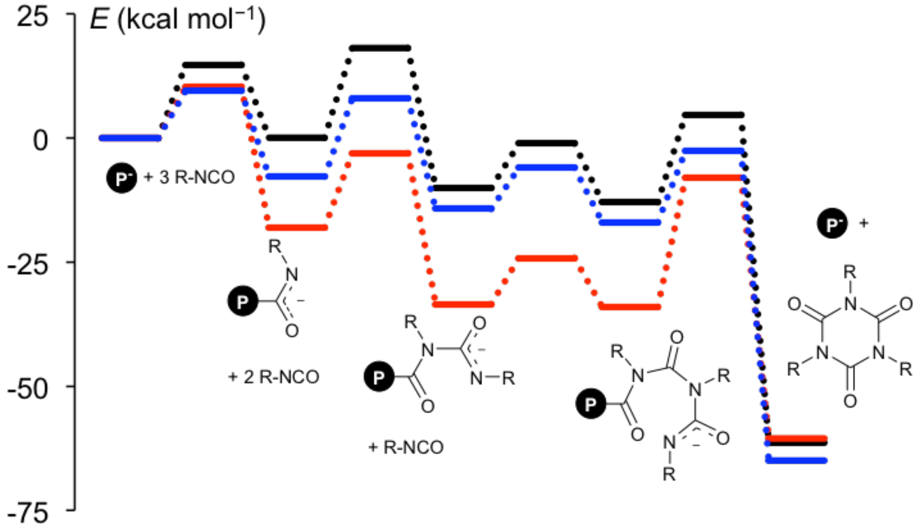

b)

Figure 7.3 **a)** Proposed catalytic cycles leading to **31**. **b)** MERPs for the formation of **31** from three isocyanate molecules catalyzed by $(OCP)^{-}$ (black), **33** (red) or **34** (blue).

The addition of two molecules of isocyanate to $(OCP)^-$ leads to **B**. This intermediate can react with a third isocyanate, delivering the trimer **31** and $(OCP)^-$ (see Figure 7.3a, route i). Alternatively, **B** can react in two further ways: The nucleophilic attack of the dicoordinated nitrogen atom on the carbon center of the PCO unit leads to the six-membered ring **34** (route ii). Furthermore the cyclization under the release of carbon monoxide delivers **33** (route iii), which is the precursor to **35**. Since the activation barriers **B→C** (9 kcal/mol), **B→34** (7 kcal/mol), **B→33** (5 kcal/mol) calculated on the model system are comparable and small, all three pathways can be considered kinetically feasible. The addition of two isocyanates to **33** results in **E**, which is an isomer of the spiroanion **35**. Hence, **35** is an inactive form of the catalytically active species **E** and can be "reactivated" by the cleavage of the PN bond. (Similarly, the ring opening of oxygen substituted phosphoranides has been shown.[121, 122]) **E** can react further with an isocyanate molecule to give **F**. In the final step **31** and **33** are formed from **F** and the catalytic cycle is restarted. As Lewis bases, the anions $(OCP)^-$, **33** and **34** are possible oligomerization catalysts. The minimum energy reaction pathways (MERPs) have been calculated for the trimerization with each of the three species (Figure 7.3b) and the reaction profiles are comparable to those reported for neutral proazaphosphatranes.[118] As the reaction profiles are very similar, all three anions can act as oligomerization catalyst. The spiro compound alone can catalyze the trimerization (see above), thus the $(OCP)^-$ anion can also be regarded as a precatalyst.

To enable the catalytic activity of **35** one of the PN bonds has to break. In order to gain more insight into this bond cleavage, it is instructive to inspect the X-ray structure of the spiro phosphoranides (Figure 7.4).

7.5 Single crystal X-ray diffraction studies

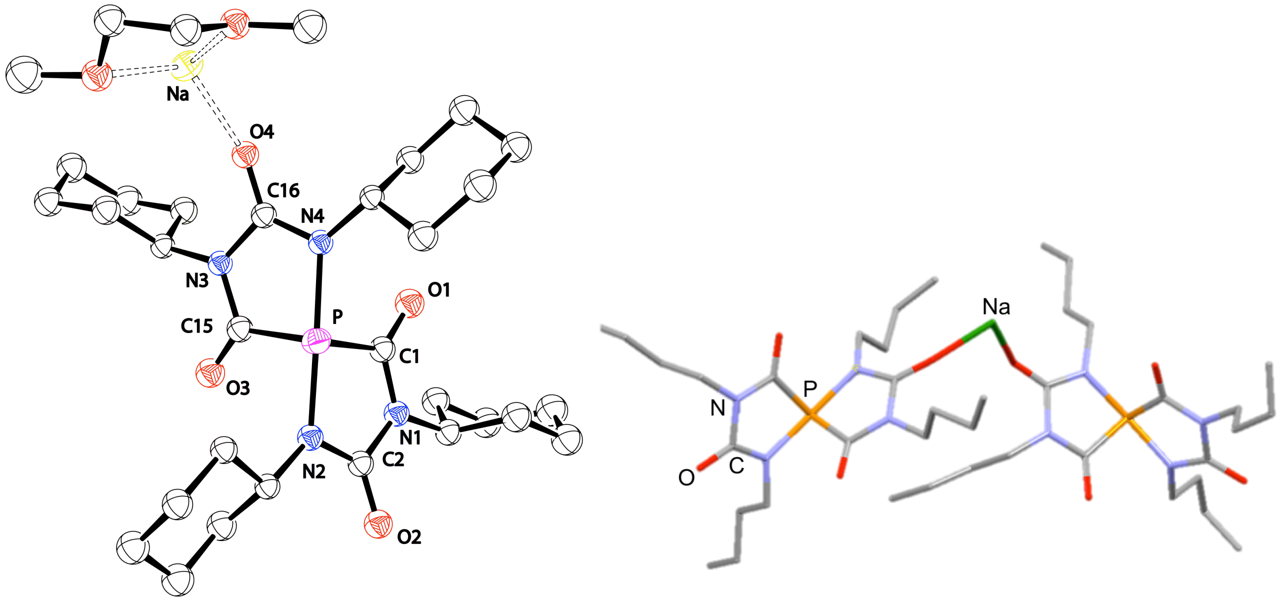

a) **b)**

Figure 7.4 **a)** ORTEP plot of [(Na(**35c**)(DME))$_\infty$] (thermal ellipsoids are drawn at 50% probability). Hydrogen atoms have been omitted for clarity. Selected bond lengths (Å) and angles (°): P-C1 1.860(7), C1-O1 1.209(7), C1-N1 1.380(7), N1-C2 1.424(7), C2-O2 1.255(6), C2-N2 1.305(7), N2-P 1.941(5), P-N4 1.917(6), N4-C16 1.318(7), C16-O4 1.252(7), C16-N3 1.423(8), N3-C15 1.365(7), C15-O3 1.221(7), C15-P 1.870(7); N2-P1-N4 170.8(2), N4-P1-C15 82.9(3), P1-C15-N3 112.8(5), C15-N3-C16 115.9(5), N3-C16-N4 111.24(6), P-C1-N1 112.1(5), C1-N1-C2 115.7(5), N1-C2-N2 112.4(6), C2-N2-P 113.6(4). Angle between the two ring planes: 131.3°. **b)** Detail of the X-ray structure of two enantiomers of [(Na(**35d**)(THF))$_\infty$]. Hydrogen atoms, selected sodium atoms and solvent molecules have been omitted for clarity. The two enantiomers are connected by sodium atoms and form an alternating chain.

The structures of the chiral phosphoranides [(Na(**35c**)(DME))$_\infty$] and [(Na(**35d**)(THF))$_\infty$] have been confirmed by X-ray diffraction (Figure 7.4). In both structures the sodium cations (each bearing one solvent molecule) with the spiro anions form three-dimensional networks. The crystal of [(Na(**35c**)(DME))$_\infty$] contains only one enantiomer (*Δ*), however, the crystal of [(Na(**35d**)(THF))$_{\infty}$] is a racemic mixture of the two enantiomers. Because of their similarity only the structure of [(Na(**35c**)(DME))$_{\infty}$] is discussed. The spiro anion **35c** consists of two identical five-membered rings connected through the 10-P-4 phosphorus atom, and the angle between the two ring planes is 102°. As expected from VSEPD considerations, the lone pair and the carbonyl carbons occupy the equatorial positions in the pseudo-trigonalbipyramidal arrangement (Ψ-TBP) around the phosphorus atom (HOMO see Figure 7.5). Due to their high electronegativity the two nitrogen atoms N2 and N4 are in the axial positions (apicophilicity), forming an almost linear N2-P-N4 arrangement ($\alpha = 170°$). Compared to the monocyclic anion **33a** (Figure 7.2) the PN bonds in **35c** are considerably elongated (1.941 Å and 1.917 Å vs. 1.779 Å in **33a**). Moreover, the phosphorus nitrogen bond lengths in **35c** are significantly longer than the axial PN bonds in neutral phosphoranes. For neutral 1,3,5,7-tetramethyl-1,3,5,7-tetraaza-4-phosphaspiro[3.3]heptane-2.6-dions (Figure 7.5) axial PN bond lengths from 1.74 Å to 1.80 Å were reported in the literature.[123] Note that similar extremely long axial bonds were found for the anionic 10-P-4 species in [Li(THF)(cyclenP)]$_x$ as well (1.94 Å and 2.01 Å) where cyclen is 1,4,7,10-tetraazacyclododecan (Figure 7.5).[124]

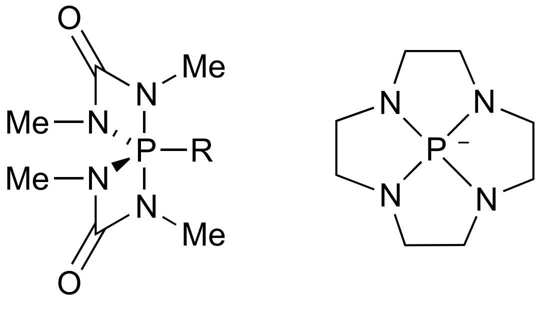

a) **b)**

Figure 7.5 **a)** 1,3,5,7-tetramethyl-1,3,5,7-tetraaza-4-phosphaspiro[3.3]heptane-2.6-dion, **b)** (cyclenP)$^{-}$.

The weakening of the PN bonds also reflects in the Wiberg bond order of 0.48. According to the natural bond orbital (NBO) calculations the P-N bond predominantly originates from the nitrogen atomic hybrid (with a contribution of 87%). The negative charges are mainly located on the oxygens and the P atom is positively charged (+0.80 e) (molecular electrostatic potential map in Figure 7.6). Therefore, anion **35** is best described as a donor acceptor complex between a phosphenium cation and two Schiff bases (Figure 7.6).

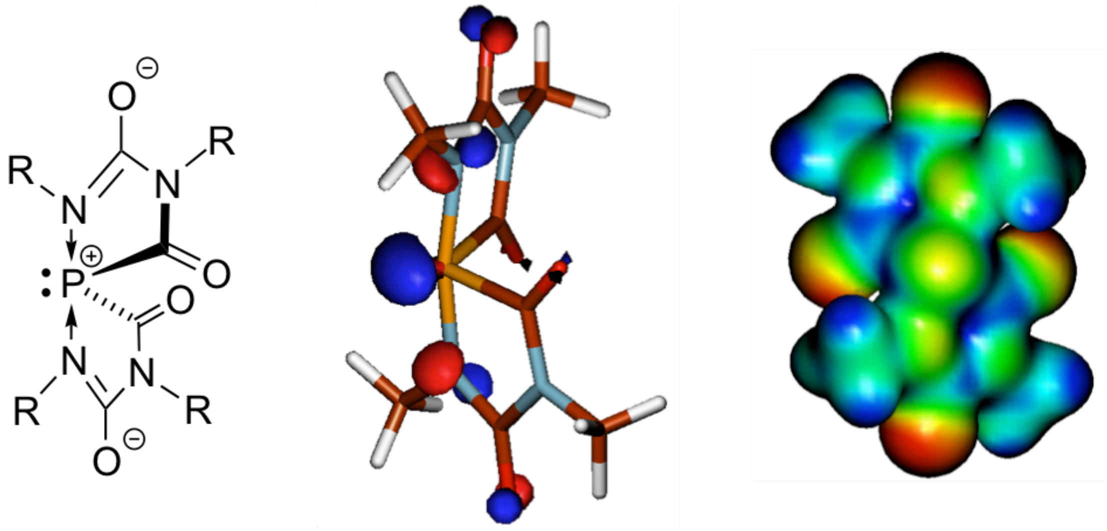

a) **b)** **c)**

Figure 7.6 **a)** Resonance structure describing **35** as an adduct of a phosphenium cation and two (anionic) Schiff bases, **b)** HOMO of **35**, and **c)** molecular electrostatic potential map of anion **35**.

7.6 VT-NMR study of a 2,6-difluorophenyl substituted phosphoranide

The lability of the PN bond was investigated on a model system by NMR spectroscopy. At 233 K the ^{19}F-NMR spectrum of the *in situ* generated 2,6-difluorophenyl analogue **35f** shows four resonances (each corresponding to two F atoms): three singlets (−116.53, −117.39, −118.95 ppm) and a doublet (−118.65 ppm,

J_{PF} = 126 Hz). In the ^{31}P-NMR spectrum a triplet (−67.4 ppm, J_{PF} = 126 Hz) is observed. This large coupling arises from the spatial proximity of the phosphorous and two fluorine atoms F^A (through-space coupling) (see Figure 7.7). At 283 K a dynamic phenomenon was observed. The ^{31}P-NMR spectrum now shows a quintet (−65.8 ppm, J_{PF} = 61 Hz) resulting from the coupling with four equivalent fluorine atoms F^A and F^B, which appear as a broad singlet in the ^{19}F-NMR spectrum. The F^C and F^D atoms remain nonequivalent (represented by two sharp singlets). Most likely, the exchange between F^A and F^B is caused by the free rotation of the 2,6-difluorophenyl rings. According to DFT calculations this rotation has a small barrier (11.1 kcal/mol) and is accompanied by the breaking of a PN bond. However, the exchange of F^C and F^D at 283 K is hindered due to the high rotation barrier (25.8 kcal/mol).

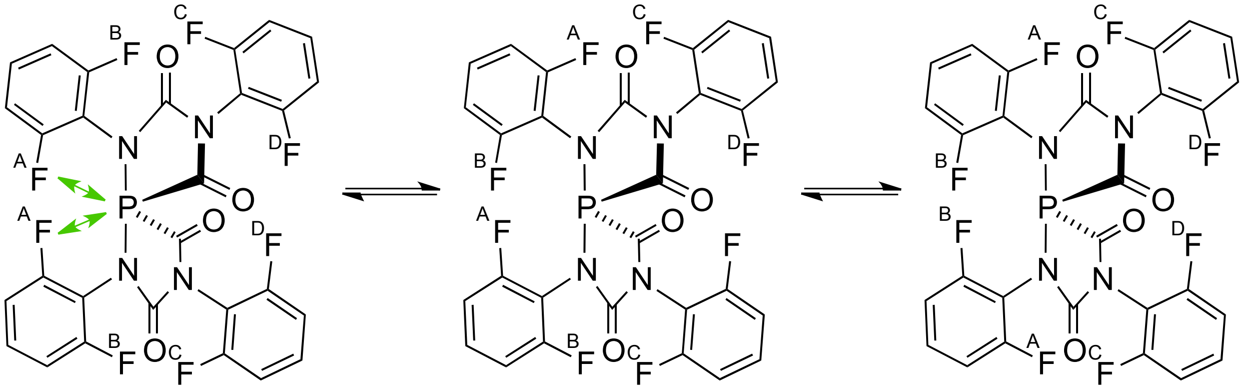

Figure 7.7: Dynamic behavior of anion **35f**.

7.7 Exchange of isocyanate moieties on a P¯ anion

According to Figure 7.3a, the ring opening of **35** followed by the reaction with an isocyanate molecule delivers the trimer **31** and anion **33**. As **33** has a strong affinity for isocyanates, **35** is continuously recovered. Thus it may be expected, that the addition of a different isocyanate to **35** leads to a new spiro anion. To prove this idea, **35c** was reacted with phenyl isocyanate (**29b**) and the formation of **35b** accompanied by a mixture of isocyanurates was observed (Scheme 7.3). No example was found in the literature, which is similar to this formal P^- transfer from one spiro anion to another. In this stepwise process, all the bonds to the P atom are broken and then reformed with another isocyanate. This exchange reaction depends on the nature of the involved isocyanates: Isocyanate moieties can only be replaced by more reactive isocyanates.

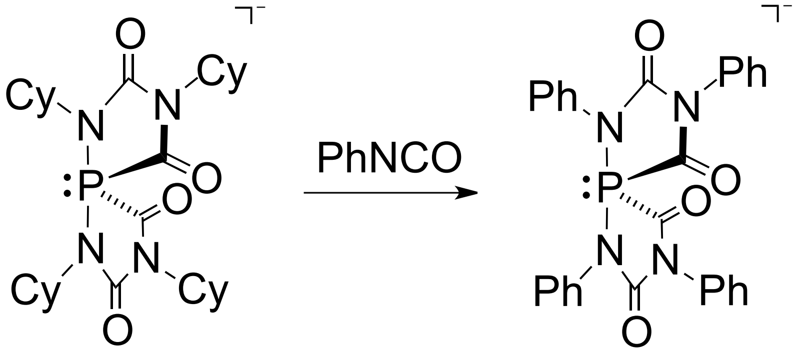

Scheme 7.3 Formal P^- transfer from **35c** to **35b**. The reaction is accompanied by the formation of different isocyanurates bearing Ph and Cy groups.

7.8 Reaction of Na(OCP) with diisocyanates

The concept of this exchange reaction can be extended to other aromatic isocyanates and diisocyanates. The reaction of Na(OCP) with industrially applied diisocyanates (e.g. toluene diisocyanate TDI, methylenediphenyl diisocyanate MDI) results in highly cross-linked materials, which are insoluble in most common solvents. The more controlled exchange reactions with diisocyanates offer an easy access to soluble spiro anions bearing free isocyanate functions. The reaction product of TDI with **35c** was reacted further with cyclohexane-1,4-dimethanol and the obtained polyurethane system, which is soluble in THF, still shows the characteristic chemical shift of the embedded spiro phosphoranide (br s, −58 to −77 ppm). The activity of this polymer as isocyanate trimerization catalyst was tested using PhNCO and the obtained **31b** was identified by X-ray diffraction analysis. On the contrary to the conventional approach to cross-linked polyurethanes, in which the diisocyanates are first partially trimerized, this method enables the synthesis of polyurethanes functionalized with an oligomerization catalyst.

7.9 Conclusion

In conclusion, Na(OCP) is a simple and easily accessible catalyst for the trimerization of isocyanates. The spiro phosphoranide **35**, which was proven to be the latent form of a catalytic species, is a formal adduct of a P^- anion and four isocyanate moieties. The isocyanate fragments of **35** can be substituted by a different (more reactive) isocyanate. Applying this method phosphoranides can be embedded into polyurethanes.

8. Summary and Outlook

The present work shows the high potential of the phosphaethynolate anion, $(OCP)^-$, as a building block in phospha-organic chemistry. Three different types of reactivity have been observed:

Firstly, this anion can take part in cycloadditions, providing a simple synthetic access to four-, five- and six-membered heterocyclic anions. The reaction of Na(OCP) with different types of heteroallenes (CO_2, isocyanates, phosphaketenes and carbodiimides) can yield entirely different molecular frameworks. Applying other heteroallenes to the $(OCP)^-$ anion might engender further unique cycloaddition products. In addition to this, the possible further functionalization of anionic heterocycles can in the future lead to a large variety of new phosphorous heterocycles. The application of these cycles as ligands in transition metal complexes is expected to open new perspectives for catalytic research.

Secondly, $(OCP)^-$ was proven to be an ambident nucleophile. However, preferably it reacts on the P atom with an electrophile. Simple salt metathesis reactions paved the way to several monomeric heterophosphaketenes. It is known that the photolysis of certain phosphaketenes delivers highly reactive phosphinidenes, which themselves are in the focus of scientific interest. They might also be accessible from the herein reported heterophosphaketenes. The present work also gives a few concrete examples illustrating the versatile reactivity of phosphaketenes towards nucleophiles (such as $(OCP)^-$) as well as heteroallenes. In the future, reactions of Na(OCP) with various types of electrophiles may lead to a comprehensive library of phosphaketenes.

Finally, $(OCP)^-$ was found to react as a P^- transfer reagent, being accompanied by the loss of carbon monoxide. This reactivity was demonstrated in the unexpected formation of new heterocycles. Considering the high atom economy regarding phosphorous and the advantages of the gaseous byproduct carbon monoxide, the usage of the phosphaethynolate anion as a P^- source gains in importance. The selective and single introduction of P^- anions into molecular frameworks, supra molecular networks or functional materials prospectively may be achieved by the application of Na(OCP) to the respective system.

The very different reaction mechanisms and reaction products discussed in the present work have already shown the versatile chemical behavior of the $(OCP)^-$ anion. Compared to its lighter analogue, the cyanate anion $(OCN)^-$, the phosphaethynolate anion $(OCP)^-$, shows a fairly unique character and delivers unpredictable reaction products. As an example, in the majority of the cases carbon monoxide is released during the reaction (e.g. leading to oxadiphospholes), however, sometimes a CO group is introduced into the molecule (e.g. reaction with carbodiimides).

Reaction sequences combining the versatile reactivity of the $(OCP)^-$ anion (ambident nucleophile, cycloaddition reagent and P^- source) may in the future yield numerous unexpected molecules in phospha-organic chemistry.

9. Experimental procedures

9.1 General remarks

Unless otherwise stated, all reactions were performed using standard Schlenk techniques under a dry argon atmosphere. Alternatively, reactions on small scale were performed in a glove box under argon atmosphere. Sensitive chemicals were stored and weighed in a glove box under argon atmosphere.

THF, diethylether, toluene and *n*-hexane were distilled from a sodium/benzophenone mixture under argon and stored over molecular sieves prior to use. Dichloromethane was distilled from CaH_2.

Solution NMR spectra were recorded on Bruker Avance 200, 250, 300, 400, 500 and 700 MHz NMR machines. Chemical shifts are given in ppm relative to Me_4Si (^1H, ^{13}C, ^{29}Si), 85 % H_3PO_4(aq.) (^{31}P), D_2O (^{17}O), CCl_3F (^{19}F), Me_4Sn (^{119}Sn) and Me_4Pb (^{102}Pb).

The multiplicity of the signals is indicated as s, d, t, q or m for singlets, doublets, triplets, quartets, quintet or multiplets. The abbreviation br describes broadened signals.

IR spectra were recorded on a Perkin-Elmer-Spectrum 2000 FT-IR spectrometer. Spectra in solid state were collected using an ATR device under inert atmosphere. The absorption bands are described as follows: very strong (vs), strong (s), medium (m) and weak (w); br stands for broad.

UV/VIS Spectra were recorded on a UV/VIS Lambda 19 spectrometer.

Elemental analyses were performed by the ETH Zürich Chemistry Microanalysis laboratory.

Melting points were measured with a Büchi melting point apparatus.

Singe crystals X-ray measurements were performed on Bruker SMART (ApexI or APEXII detector) machines or on an Oxford XCalibur diffractometer (CCD detector, CCD MoK$_\alpha$ radiation (0.71073 Å).

Mass-spectra were recorded by the Mass Spectrometry Service Facility at the Laboratory of Organic Chemistry , ETH Zürich

Computations

All calculations were performed by Dr. Zoltán Benkő.

The computations were carried out with the Gaussian 09 program package.[125] NMR chemical shifts were computed with the Gauge-Independent Atomic Orbital (GIAO) method. For the harmonic vibrational frequencies a scaling factor of 0.970 was applied. The ^{31}P chemical shifts were determined following the method in Ref[126]. The NBO analysis was performed with the NBO 5.0 program.[127] For visualization of the molecules the Molden program was used.[128]

9.2 Experimental procedures for Chapter 2

Synthesis of [Na(OCP)(dioxane)$_x$] (1)

The literature known synthesis of Na(OCP)[17] was slightly modified and simplified. DME, THF, dioxane and *tert*-butanol were degassed with argon prior to use. For the last purification step of the product, dry solvents were used only. Red phosphorus (7.0 g, 0.23 mol), sodium (16.0 g, 0.70 mol) and naphthalene (1.5 g, 0.012 mol) were suspended in DME (500 mL) and the reaction mixture was stirred for 12 h at RT. The resulting black suspension was cooled with an ice bath and *tert*-butanol (42 mL, 0.44 mol) was added dropwise via a syringe. Subsequently the reaction mixture was allowed to warm to RT and stirred for 1 h. Ethylene carbonate (20.0 g, 0.23 mol) in DME (50 mL) was added at 0 °C over a period of 1 h. The suspension was stirred for 12 h at RT and the solvent was removed under reduced pressure. The remaining solid was dissolved in THF (500 mL) and the mixture was filtered over a G4 glass frit. The solid was washed with THF (20 mL) and the yellow filtrate was concentrated to a volume of 200 mL. To this solution dioxane (200 mL) was added to precipitate the reaction product as a colorless fine powder. The precipitate was quickly filtered on air over a G4 glass frit and then quickly dried *in vacuo*. The raw product, a white powder, was purified further by precipitating from dry THF/dioxane once again. For analytical data see.[17]

Determination of the dioxane content of [Na(OCP)(dioxane)$_x$] (1)

The isolated reaction product contains coordinated dioxane molecules.[17] For further reactions the exact ratio of Na(OCP) and dioxane is essential. ^{31}P-NMR spectroscopy was found to be the best method to determine this value. The relaxation time of Na(OCP) was determined performing a standard T_1 relaxation time NMR experiment at RT: 1.7 s. For triphenylphosphane T_1 is 26 s.[129] Known amounts of [Na(OCP)(dioxane)$_x$] and triphenylphosphane were dissolved in THF (0.5 mL) and an inversed gated, ^{1}H decoupled ^{31}P-NMR spectrum with a recycle delay of 120 s and a 90° pulse sequence was recorded in order to obtain reliable integrals. The ratio Na(OCP)/dioxane was calculated from the relative integrals. Since this ratio can vary, it is recommended to determine it for each new batch. The feasibility of this method was proven by integration of a sample containing known amounts of PPh_3 and $O{=}PPh_3$.

Synthesis of [($Na_2P_2C_3O_4$)(Na(OCP))$_x$(dioxane)$_y$(THF)$_z$] (sodium salt of 4)

Carbon dioxide was purified and dried prior to use.

A continuous stream of carbon dioxide (1 bar) was passed through a solution of [Na(OCP)(dioxane)$_{2.5}$] (1.7 g, 5.6 mmol) in THF (15 mL) for 1 hour at RT. Quickly a color change of the solution from colorless to yellow was observed. Removing the solvent under reduced pressure gave a fine yellow powder.

^{31}P{^{1}H}-NMR (101.26 MHz, THF, 293 K): δ (ppm)= 270 ($\nu_{½}$ ≈ 4500 Hz), 105 ($\nu_{½}$ ≈ 4500 Hz);

Due to dynamic exchange no ^{13}C-NMR data is available for this compound.

IR (ATR): ν = 1559 (s, $\nu(C^AO_2)_{asym}$), 1479 (s, $\nu(C^BO)_{asym}$), 1292 cm^{-1} (vs, $\nu(C^AO_2)_{sym}$);

From the elemental analysis (%) (C 31.52, H 3.42, O 31.12, P 19.91) the average chemical composition is [($Na_2P_2C_3O_4$)(NaOCP)$_{0.34}$(dioxane)$_{1.91}$(THF)$_{0.37}$].

Salt exchange experiment

The sodium salt of **4** (70 mg, 0.16 mmol) in THF (2 mL) was added slowly at RT to a suspension of barium triflate (140 mg, 0.32 mmol) in THF (2mL) and a clear yellow solution was obtained. The solvent was removed under reduced pressure. After washing with pentane the reaction product was dried *in vacuo*. The yellow powder contains the by-product sodium triflate.

^{31}P{^{1}H}-NMR (161.98 MHz, THF-d8, 293 K): δ (ppm) = 274.8 (br s), 99.7 (br s);

^{13}C{^{1}H}-NMR (100.63 MHz, THF-d8, 293 K): δ (ppm) = 232.5 (dd, $^{1}J_{P(A)C(A)} = 60$ Hz, $^{3}J_{P(B)C(A)} = 25$ Hz, C^{B}), 183 (d, $^{1}J_{P(A)C(A)} = 45$ Hz, C^{A});

IR (ATR): ν = 1532 (s, $\nu(C^{A}O_2)_{asym}$), 1464 (s, $\nu(C^{B}O)_{asym}$), 1235 cm^{-1} (vs, $\nu(C^{A}O_2)_{sym}$).

NMR study on the equilibrium between the sodium salt of 4, CO_2 and Na(OCP) (1)

A sample of the sodium salt of **4** (30.4 mg) in THF (0.5 mL) with PPh_3 (21.9 mg) was prepared in a J. Young NMR tube. Since there was no CO_2 in the atmosphere above the dissolved **4**, the sample was shortly warmed to 313 K to generate CO_2(g). Then at 298 K the relaxation of the system was monitored by ^{31}P-NMR using the same settings as described above until the equilibrium was reached (no change in the integrals). The same monitoring was repeated at 313, 328 and again 298 K.

Boiling of this solution for 18 h led to a mixture in which the following compounds were identified: $Na_2(P_4C_4O_4)$: ^{31}P-NMR (161.98 MHz, THF-d8, 293 K): δ (ppm) = 43 (t, $^{2}J_{PP} = 32$ Hz), 83 (t, $^{2}J_{PP} = 32$ Hz), (lit.[19] in DME-d10: 40.8 (t, $^{2}J_{PP} = 31.5$ Hz), 86.6 (t, $^{2}J_{PP} = 31.5$ Hz)); CO: ^{13}C-NMR (100.63 MHz, THF-d8, 293 K): δ (ppm) = 184 (s) (lit.[130] in THF-d8: 185); oxalate ion: IR (ATR): ν = 1655 (s), 1350 (shoulder) and 802 cm^{-1} (s) (lit.[131] 1667, 1340 and 781) and carbonate ion: IR (ATR): ν = 1431 (br s) and 878 cm^{-1} (s) (lit.[131] 1458 and 880). A broad band at 1431 cm^{-1} results from a superposition of $Na_2(P_4C_4O_4)$, sodium carbonate and unreacted **4**.

Synthesis of 5^{iPr}

Synthesis from the sodium salt of **4**:

2-Iodopropane (120 mg, 0.7 mmol) in THF (2 mL) was added dropwise at RT to a solution of the sodium salt of **4** (150 mg, 0.35 mmol) in THF (2 mL). After 1 h stirring at RT the reaction mixture was filtered, the solvent was removed under reduced pressure and the obtained yellow solid was washed three times with *n*-hexane. The obtained yellow powder was dried *in vacuo*.

Synthesis from [Na(OCP)(dioxane)$_{2.5}$]:

2-Iodopropane (1.10 g, 6.2 mmol) was added dropwise at RT to a solution of [Na(OCP)(dioxane)$_{2.5}$] (1.25 g, 4.1 mmol) in THF (5 mL). After 1 h stirring at RT the reaction mixture was filtered, the solvent was removed under reduced pressure and the obtained yellow solid was washed three times with *n*-hexane. The obtained yellow powder was dried *in vacuo*.

^{31}P{^{1}H}-NMR (121.53 MHz, THF-d8, 293 K): δ = 288.4 (d, $^2J_{PP}$ = 6 Hz, $\lambda^3\sigma^2$-P), 131.2 (d, ^{2}J$_{PP}$ = 6 Hz, $\lambda^3\sigma^3$-P);

^{13}C{^{1}H}-NMR (62.92 MHz, THF, 293 K): δ (ppm) = 233.7 (dd, $^1J_{PC}$ = 55 Hz, $^1J_{PC}$ = 23 Hz, *C*=O), 28.37 (dd, $^1J_{PC}$= 35 Hz, $^3J_{PC}$= 8 Hz, CH), 17.45 (d, $^2J_{PC}$ = 8 Hz, CH$_3$);

^{1}H-NMR (300.13 MHz, THF-d8, 293 K): δ (ppm) = 1.96 (sept d, $^3J_{HH(Met)}$ = 7.1 Hz, $^2J_{PH}$ = 0.7 Hz, 1H, CH), 1.05 (dd, $^3J_{HH(Met)}$ = 7.1 Hz, $^3J_{PH}$ = 11.5 Hz, 6H, CH$_3$);

IR (THF): ν = 2964 (vs, CH), 1640 (w, ν_{sym}(CO)), 1520 cm^{-1} (vs, ν_{asym}(CO)); CH deformation bands cannot be assigned due to overlapping with coordinating THF.

Generation of 5^{Tr^*}

4,4',4"-trimethoxytriphenylmethyl chloride (50 mg, 0.136 mmol) in THF (1 mL) was added dropwise at RT to a solution of the sodium salt of **4** (59 mg, 0.136 mmol) in THF (1 mL). The reaction mixture was stirred for 5 min. Due to its instability, the compound could not be isolated but was characterized in solution.

^{31}P{^{1}H}-NMR (121.5 MHz, THF-d8, 293 K): δ (ppm) = 281.7 (d, $^2J_{PP}$ = 22 Hz, $\lambda^3\sigma^2$-P), 120.5 (d, $^2J_{PP}$ = 22 Hz, $\lambda^3\sigma^3$-P);

^{13}C{^{1}H}-NMR (125.8 MHz, THF, 293 K): δ (ppm) = 235 (dd, $^1J_{PC}$ = 54 Hz, $^1J_{PC}$ = 36.8 Hz, C=O), 167.7 (d, $^1J_{PC}$ = 51 Hz, C$_{trityl}$), 157.7 (s, C$_{arom-p}$), 138.7 (s, $^3J_{PC}$ = 6 Hz, C$_{arom\text{-}o}$), 131.2 (s, $^{2}J_{PC}$ = 8.4 Hz, $^{4}J_{PC}$ = 5.7 Hz, C$_{arom\text{-}ipso}$), 112.5 (s, C$_{arom\text{-}m}$), 54.5 (s, OCH_3);

^{1}H-NMR (300.13MHz, THF-d8, 293 K): δ (ppm) = 7.84-6.59 (overlapping m, 12H, H$_{arom}$), 3.77 (s, 9H, CH_3);

IR (THF): ν = 1885.3 (w), 1757 (w), 1606 (w), 1578 (w), 1510 (s, C=O), 1164 (vs), 842 (vs, CH$_{arom}$), 750 cm^{-1} (vs, CH$_{arom}$).

Synthesis of **2^{Tr*}**

A solution of 4,4',4''-trimethoxytriphenylmethyl chloride (100 mg, 0.272 mmol) in THF (1.5 mL) was added dropwise to a solution of [Na(OCP)(dioxane)$_{2.5}$] (74 mg, 0.244 mmol) in THF (1.5 mL) at RT. The yellow reaction mixture was stirred for 15 min at RT. After filtration the solvent was removed under reduced pressure. The obtained orange solid was washed twice with diethyl ether and dried *in vacuo* to yield a fine yellow powder (40 mg, 42%). Yellow, diamond-shaped single crystals of **2^{Tr*}** were obtained by slow evaporation of the solvent. Single crystals of the composition **2^{Tr*}** × 2 THF suitable for an X-ray diffraction analysis were obtained by slow evaporation of THF at RT.

^{31}P{^{1}H}-NMR (202.50 MHz, THF, 293 K): δ (ppm) = 119 (s);

^{13}C{^{1}H}-NMR (75.48 MHz, THF, 293 K): δ (ppm) = 217.1 (t, $^{1}J_{PC}$= 50.1 Hz, C=O), 158.5 (d, $^{1}J_{PBC}$ = 77.5 Hz, C$_{trityl}$), 158.2 (s, C$_{arom\text{-}p}$), 136.9 (d, $^{3}J_{PC}$= 2.5 Hz, C$_{arom\text{-}o}$), 135.2 (pseudo t, $^{2}J_{PC}$ = 3.7 Hz, $^{4}J_{PC}$ = 3.7 Hz, C$_{arom\text{-}ipso}$), 112.3 (s, C$_{arom\text{-}m}$), 54.4 (s, OCH_3);

^{1}H-NMR (300.13 MHz, THF-d8, 293 K): δ (ppm) = 7.47-6.77 (overlapping m, 24H, H$_{arom}$), 3.79 (s, 18H, CH_3);

IR (ATR): ν = 2831 (w, CH), 1635 (s, CO), 1604 cm^{-1} (s, (CC)$_{arom}$), 1579 (w), 1504 (vs, (CC)$_{arom}$), 1460 (s), 1441 (s), 1417 (w), 1308 (s), 1293 (vs), 1250 (vs, C$_{arom}$-O), 1175 (vs), 1117 (s), 1031 (vs), 837 (w), 820 (vs, CH_{arom}), 807 (vs, CH_{arom}), 783 (vs, CH_{arom}), 576 cm^{-1} (vs);

Elemental analysis (%) calculated for $C_{46} H_{42} O_8 P_2$: C 70.40, H 5.39. Found: C 69.77, H 5.39 .

9.3 Experimental procedures for Chapter 3

Generation of $^{i}Pr_3Si{-}O{-}C{\equiv}P$ (6)

A solution of $[Na(OCP)(dioxane)_{2.5}]$ (30 mg, 0.1 mmol) in THF (0.3 mL) was added dropwise at room temperature (25°C) to a solution of triisopropylsilyl-trifluoromethanesulfonate (37 mg, 0.12 mmol) in diethyl ether (0.3 mL). Beside **6** the solution contained **7** and **7'** (5%). An ^{17}O-NMR spectrum could not be obtained, presumably due to the low concentration of the sample.

$^{31}P\{^{1}H\}$-NMR (81.0 MHz, THF-d8/Et_2O, 25 °C): δ (ppm) = −307.2 (s);

$^{31}P\{^{1}H\}$-NMR (81.0 MHz, THF-d8/Et_2O, −40 °C): δ (ppm) = −308.5 (s);

$^{13}C\{^{1}H\}$-NMR (100.61 MHz, THF-d8/Et_2O, −40 °C): δ (ppm) = 145.5 (d, $^{1}J_{PC}$ = 9.8 Hz), 16.7 (s, 6C, C_{Me}), 11.7 (s, 3C, C_{CH});

^{1}H-NMR (400.1 MHz, THF-d8/Et_2O, −40 °C): δ (ppm) = 1.46-1.32 (overlapping m, CH, uncertain), 1.10-1.03 (overlapping m, CH_3 uncertain);

$^{29}Si\{^{1}H\}$-NMR (99.4 MHz, THF-d8/Et_2O, −50 °C): δ (ppm) = 30.2 (br s, $\nu_{½}$ = 40 Hz);

IR (THF/Et_2O): 1656 cm^{-1} (vs, ν_{asym}(PCO)).

Generation of $^{i}Pr_3Si{-}P{=}C{=}O$ (7)

A solution of $[Na(OCP)(dioxane)_{2.5}]$ (200 mg, 0.66 mmol) in THF (15 mL) was added dropwise, very slowly to a solution of triisopropylsilyl trifluoromethanesulfonate (255 mg, 0.79 mmol) in diisopropylether (2 mL) at 45°C. To minimize the amount of byproducts, a diluted solution of Na(OCP) was added to a concentrated solution of the silicon reagent. The reaction solution was stirred for 15 min at 45 °C. Then the solvent was removed under reduced pressure. The obtained yellow oily residue was suspended in 1 mL benzene-d6 and the suspension was filtered over celite. The yellow filtrate was investigated by NMR spectroscopy. In the ^{29}Si- and ^{17}O-NMR spectra the excess of triisopropylsilyl trifluoromethanesulfonate was observed (41.6, 167.5 ppm respectively).

^{31}P{^{1}H}-NMR (101.28 MHz, C_6D_6, 25 °C): δ (ppm) = −370.1 (s, $^{1}J_{PSi}$ = 48.3 Hz);

^{13}C{^{1}H}-NMR (125.8 MHz, C_6D_6, 25°C): δ (ppm) = 183.4 (d, $^{1}J_{PC}$ = 91.8 Hz), 18.8 (d, $^{2}J_{PC}$ = 3.5 Hz, 6C, C_{Me}), 14.6 (d, $^{3}J_{PC}$ = 8.7 Hz, 3C, CH);

^{1}H-NMR (500.3 MHz, C_6D_6, 25°C): δ (ppm) = 1.20-1.07 (overlapping m, CH_3), 0.99 (overlapping m, CH_3);

^{29}Si{^{1}H}-NMR (79.49 MHz, C_6D_6, 25 °C): δ (ppm) = 33.1 (d, $^{1}J_{PSi}$ = 48.3 Hz);

^{17}O-NMR (64.80 MHz, C_6D_6, 25 °C): δ (ppm) = 289.7 (s, $\nu_{1/2}$ = 60 Hz);

IR (THF/Et_2O): 1947 cm^{-1} (vs, ν_{asym}(PCO)).

Generation of $Ph_3Si-P=C=O$ (9)

A solution of [Na(OCP)(dioxane)$_{2.5}$] (30 mg, 0.1 mmol) in THF (0.5 mL) was added dropwise at room temperature to a solution of triphenylsilyl trifluoromethanesulfonate (50 mg, 0.12 mmol) in diethyl ether (0.5 mL). The reaction solution contained small amounts of an impurity, which was assigned to **10** (δ ^{31}P (ppm): 305.3 (d, $^{2}J_{PP}$ = 18 Hz), 105.7 (d, $^{2}J_{PP}$ = 18 Hz));

^{31}P{^{1}H}-NMR (101.28 MHz, THF/Et_2O, 25 °C): δ (ppm) = −343.6 (s, $^{1}J_{PSi}$ = 41.5 Hz);

^{31}P{^{1}H}-NMR (121.5 MHz, C_6D_6, 25 °C): δ (ppm) = −338.8 (s, $^{1}J_{PSi}$ = 41.6 Hz);

^{13}C{^{1}H}-NMR (75.5 MHz, C_6D_6, 25°C): δ (ppm) = 184.5 (d, $^{1}J_{PC}$ = 99.1Hz, C≡P), 135.8 (d, $^{3}J_{PC}$ = 2.7 Hz, C_{arom-o}), 133.9 (d, $^{2}J_{PC}$ = 9.7 Hz, C_{arom-i}), 130.4 (s, C_{arom-p}), 128.4 (s, C_{arom-m});

^{1}H-NMR (300.1 MHz, C_6D_6, 25°): δ (ppm) = 7.75-7.17 (m, 15H, H_{arom});

^{29}Si{^{1}H}-NMR (56.9 MHz, C_6D_6, 25°C): δ (ppm) = 1.6 (br s);

IR (THF/Et_2O): 1662 cm^{-1} (vs, ν_{asym}(PCO)).

Synthesis of $Ph_3Ge-P=C=O$ (11)

A solution of [Na(OCP)(dioxane)$_{2.5}$] (356 mg, 1.18 mmol) in THF (4 mL) was added dropwise at room temperature to a solution of triphenylgermanium chloride (400 mg, 1.18 mmol) in THF (4 mL). The reaction solution was concentrated to 3 mL under reduced pressure to facilitate the precipitation of sodium chloride. The solution was filtered and the solvent was removed under reduced pressure to obtain a yellow powder. The product was washed with *n*-hexane and dried *in vacuo* yielding 274 mg (64%) yellow solid. The compound was found to be well soluble in THF and slightly soluble in *n*-hexane.

$^{31}P\{^1H\}$-NMR (101.26 MHz, THF, 25 °C): δ (ppm) = −344 (s);

$^{13}C\{^1H\}$-NMR (176.07 MHz, THF, 25 °C): δ (ppm) = 182.5 (d, $^1J_{PC}$ = 105 Hz), 135-125 (m, C_{arom});

^1H-NMR (300.1 MHz, THF-d8, 25°C): δ (ppm) = 7.90-7.00 (m, H_{arom});

IR (*n*-hexane): 1954 cm^{-1} (vs, ν_{asym}(PCO));

Elemental analysis (%) calculated for $C_{19}H_{15}GeOP$: C, 62.88; H, 4.17; Found: C, 62.61; H, 4.26;

m.p.: 84 ± 2 °C.

Synthesis of $Ph_3Sn-P=C=O$ (12)

A solution of [Na(OCP)(dioxane)$_{2.5}$] (2.00 g, 6.6 mmol) in THF (15 mL) was added dropwise at room temperature to a solution of triphenyltin chloride (2.55 g, 6.6 mmol) in THF (10 mL). It is important to add the [Na(OCP)(dioxane)$_{2.5}$]-THF solution very slowly, since high local concentration of Na(OCP) in the reaction solution engenders a consecutive reaction. The reaction solution was concentrated to 5 mL under reduced pressure to facilitate the precipitation of sodium chloride. The solution was filtered and the solvent was removed under reduced pressure to obtain a yellow powder. The product was washed with *n*-hexane and dried *in vacuo*. Yield: 2.19 g (78 %).

^{31}P{^{1}H}-NMR (101.22 MHz, THF, 25 °C): δ (ppm) = −378 (s, $^{1}J_{SnP}$ = 678 Hz);
^{13}C{^{1}H}-NMR (75.47 MHz, THF-d8, 25 °C): δ (ppm) = 180.6 (d, $^{1}J_{PC}$ = 108 Hz, $^{2}J_{SnC}$ = 23.8 Hz), 140.8-127.2 (m, C_{arom} overlapping);
^{1}H-NMR (300.13 MHz, THF-d8, 25°): δ (ppm) = 8.60-6.85 (m, H_{arom});
^{119}Sn{^{1}H}-NMR (93.28 MHz, THF, 25 °C): δ (ppm) = −50.7 (d, $^{1}J_{SnP}$ = 678 Hz);
IR (*n*-hexane): 1946 cm^{-1} (vs, ν_{asym}(PCO));
IR (CCl$_4$): 1944 cm^{-1} (vs, ν_{asym}(PCO));
IR (solid, ATR): 1930 cm^{-1} (vs, ν_{asym}(PCO));
Elemental analysis (%) calculated for $C_{19}H_{15}SnOP$: C, 55.79; H, 3.70; O, 3.91; Found: C, 54.82; H, 3.86; O, 3.33.

The analogous reaction was repeated following the same synthetic procedure with different organotin chlorides. The ^{31}P-NMR spectra of these compounds R$_3$Sn−P=C=O were recorded from the reaction solutions:

R = Cyclohexyl:
^{31}P{^{1}H}-NMR (101.26 MHz, THF, 25 °C): δ (ppm) = −403.9 (s, $^{1}J_{SnP}$ = 720 Hz);
R= Isopropyl:
^{31}P{^{1}H}-NMR (101.26 MHz, THF, 25 °C): δ (ppm) = −404.7 (s, $^{1}J_{SnP}$ = 700 Hz);
R= Benzyl:
^{31}P{^{1}H}-NMR (101.26 MHz, THF, 25 °C): δ (ppm) = −383.8 (s, $^{1}J_{SnP}$ = 736 Hz);
R = Methyl
^{31}P{^{1}H}-NMR (202.5 MHz, THF, 25 °C): δ (ppm) = −378.6 (s).

Reaction of [Na(OCP)(dioxane)$_{2.5}$] with Ph_3PbCl (13)

A solution of [Na(OCP)(dioxane)$_{2.5}$] (0.663 g, 2.19 mmol) in THF (5 mL) was added dropwise at room temperature to a solution of triphenyllead chloride (1.04 g, 2.19 mmol) in THF (10 mL). The yellow orange solution was concentrated to 5 mL and was investigated by ^{31}P-, ^{13}C-, and ^{207}Pb-NMR spectroscopy. (The highly sensitive **13** decomposed partially during the attempts for isolation.)

$^{31}P\{^1H\}$-NMR (202.46 MHz, THF, 25 °C): δ (ppm) = −364.2 (s, $^1J_{PbP}$ = 1224 Hz);

$^{13}C\{^1H\}$-NMR (100.6 MHz, THF, 25 °C): δ (ppm) = 181.7 (d, $^1J_{PC}$ = 110 Hz), 159.8-128.1 (C_{arom} overlapping);

^{1}H-NMR (500.23 MHz, THF-d8, 25°): δ (ppm) = 8.1-7.0 (m, 15H, H_{arom});

$^{207}Pb\{^1H\}$-NMR (104.7 MHz, THF, 25 °C): δ (ppm) = −15.4 (d, $^1J_{PbP}$ = 1224 Hz);

IR (THF): 1923 cm^{-1} (vs, ν_{asym}(PCO)).

9.4 Experimental procedures for Chapter 4

Reaction of $Ph_3Sn{-}P{=}C{=}O$ (12) with dimethyl sulfoxide (DMSO)

$Ph_3Sn{-}P{=}C{=}O$ (30 mg, 0.07 mmol) was dissolved in DMSO (0.5 mL) in an NMR tube. The solution was sonicated for 1 hour at 23 °C. The color of the solution changed from yellow to orange and a slight gas evolution (carbon monoxide) was observed. The reaction solution was investigated by ^{31}P- and ^{119}Sn-NMR spectroscopy.

$^{31}P\{^1H\}$-NMR (101.25 MHz, DMSO, 25 °C): δ (ppm)= 124.5 (t, $^2J(P^AP^M)$= 20.9 Hz, $^3J(SnP^A)$ = 20.0 Hz, 1P, P^A), −68.3 (d, $^2J(P^AP^M)$= 20.9 Hz, $^1J(SnP^M)$ = −830.9 Hz, $^2J(SnP^M)$ = 115.6 Hz, $^1J(P^MP^{M'})$ = 220.0 Hz, 2P, P^M);

$^{119}Sn\{^1H\}$-NMR (111.9 MHz, DMSO, 25 °C): δ (ppm) = −129.3 (m, X of [AMN]X spin system, $^1J(SnP^M)$ = −830.9 Hz, $^2J(SnP^N)$ = 115.6 Hz, $^3J(SnP^A)$ = 20.0 Hz); −224.2 (s, $[Ph_3Sn(DMSO)_x]^+$), −235.0 (s, $[Ph_3Sn(DMSO)_x]^+$).

Synthesis of the sodium salt of 1,2-bis(triphenylstannyl)-1,2,4-triphospholane-3,5-dione (14a)

A solution of $[Na(OCP)(dioxane)_{2.5}]$ (74 mg, 0.24 mmol) in THF (3 mL) was added dropwise at room temperature to a solution of $Ph_3Sn{-}P{=}C{=}O$ (200 mg, 0.49 mmol) in THF (5 mL) and a color change from yellow to orange was observed. The solvent was removed under reduced pressure to obtain an orange powder, which was washed with *n*-hexane and dried *in vacuo*. Yield: 139 mg (52%) (Calculated for $[Na(THF)_3$**14a**$]$ M = 1088.29 g/mol). Single crystals suitable for X-ray diffraction were obtained by slowly cooling of a saturated DME solution of the compound down to −8°C (further cooling led to precipitation of the product). The crystals are stable at room temperature and can be handled on air. Note that the same compound can also be synthesized in a direct reaction of 2 equivalents Ph_3SnCl with 3 equivalents Na(OCP) (Yield calculated for $[Na(THF)_3$**14a**] M = 1088.29 g/mol: 68 %).

$^{31}P\{^1H\}$-NMR (101.25 MHz, THF, 25 °C): δ (ppm)= 132.2 (t, $^2J(P^AP^M)$= 20.2 Hz, $^3J(SnP^A)$ = 19.1 Hz, 1P, P^A), −70.4 (d, $^2J(P^AP^M)$= 20.2 Hz, $^1J(SnP^M)$ = −835.5 Hz, $^2J(SnP^M)$ = 124.7 Hz, $^1J(P^MP^{M'})$ = 202.5 Hz, 2P, P^M);

$^{13}C\{^1H\}$-NMR (125.8 MHz, THF, 25 °C): δ (ppm)= 249.3 (m, Y part of AMM'[Y] spin system, $^1J(P^AC)$ = 83.2 Hz, $\Sigma(^1J(P^MC) + {}^2J(P^NC))$ = 76.4 Hz, 142.7-126.9 (m, uncertain due to overlapping, C_{arom});

^1H-NMR (200.1 MHz, THF-d8, 25 °C): δ (ppm) = 7.7-6.6 (overlapping m, 30H, H_{arom});

$^{119}Sn\{^1H\}$-NMR (149.2 MHz, THF, −40 °C): δ (ppm) = −126.8 (m, X of AMM'[X] spin system, $^1J(SnP^M)$ = −835.5 Hz, $^2J(SnP^N)$ = 124.7 Hz, $^3J(SnP^A)$ = 19.1 Hz);

IR (ATR): ν = 1610 cm^{-1} (s, $\nu_{asym}CO$);

m.p.: 115 °C.

LT-NMR investigation on the formation mechanism of 14a

A solution of $Ph_3Sn{-}P{=}C{=}O$ (20 mg, 48.9 μmol) in THF-d8 (0.3 mL) was prepared in a J. Young NMR tube. A solution of $[Na(OCP)(dioxane)_{2.5}]$ (2.4 mg, 7.9 μmol) in THF-d8 (0.2 mL) was added slowly dropwise at −60°C. The reaction was followed for 20 hours by ^{31}P- and ^{119}Sn- spectroscopy at −40°C.

For the numbering of the phosphorous atoms see Figure 4.2.

Intermediate **A**

$^{31}P\{^1H\}$-NMR (162.0 MHz, THF-d8, −40 °C): δ (ppm) = 290.9 (d, $^2J_{PP}$ = 8.2 Hz, $^3J_{SnP}$ = 136.4 Hz, P2), 78.2 (d, $^2J_{PP}$ = 8.2 Hz, $^1J_{SnP}$ = 1189 Hz, P1);

$^{119}Sn\{^1H\}$-NMR (149.2 MHz, THF-d8, −40 °C): δ (ppm) = −142.0 (dd, $^1J_{SnP}$ = 1189 Hz, $^3J_{SnP}$ = 136.4 Hz).

Intermediate **B**

$^{31}P\{^1H\}$-NMR (162.0 MHz, THF-d8, −40 °C): δ (ppm) = 224.2 (dd, $^1J_{P7P6}$ = 401.7 Hz, $^2J_{P7P8}$ = 135.8 Hz, P7), 3.7 (d, $^1J_{P6P7}$ = 401.7 Hz, $^4J_{SnP}$ = 25.1 Hz, P6), −167.1 (d, $^2J_{P8P7}$ = 135.8 Hz, $^1J_{SnP}$ = 852.5 Hz, P8); Simulated as an AMQ[X] spin system, see appendix.

$^{119}Sn\{^1H\}$-NMR (149.2 MHz, THF-d8, −40 °C): δ (ppm) = −112.6 (ddd, $^1J_{SnP8}$ = 852.5 Hz, $^3J_{SnP7}$ = 136.5 Hz, $^4J_{SnP6}$ = 25.1 Hz, $^2J_{SnSn}$ not observed because of low intensity).

Intermediate **C**

$^{31}P\{^1H\}$-NMR (162.0 MHz, THF-d8, −40 °C): δ (ppm) = 118.8 (pseudo t, $^2J_{P5P4} \approx {}^3J_{P5P3} \approx$ 17 Hz, P5), 60.4 (dd, $^1J_{P4P3}$ = 319.4 Hz, $^2J_{P4P5}$ = 17.4 Hz, P4), −228.2 (dd, $^1J_{P3P4}$ = 319.4 Hz, $^3J_{P3P5}$ = 16.8 Hz, P3);

$^{119}Sn\{^1H\}$-NMR (149.2 MHz, THF-d8, −40 °C): δ (ppm) = −89.04 (dd, $^1J_{SnP4}$ = 899.8 Hz, $^2J_{SnP3}$ = 27.7 Hz, Sn at P4), −96.8 (ddd, $^1J_{SnP5}$ = 896.7 Hz, $^3J_{SnP4}$ = 106.6 Hz, $^4J_{SnP3}$ < 5 Hz).

Generation of the sodium salt of 1,2-bis(tricyclohexylstannyl)-1,2,4-triphospholane-3,5-dione (14b)

A solution of [Na(OCP)(dioxane)$_{2.5}$] (30 mg, 0.1 mmol) in THF-d8 (0.3 mL) was added dropwise at room temperature to a solution of tri(cyclohexyl)tin chloride (28.3 mg, 0.07 mmol) in THF-d8 (0.2 mL). The solution was refluxed for 10 min and investigated by NMR spectroscopy.

$^{31}P\{^1H\}$-NMR (101.3 MHz, THF-d8, 25 °C): δ (ppm) = 130.0 (t, $^2J(P^AP^M)$ = 24.2 Hz, −66.7 (d, $^2J(P^AP^M)$ = 24.2 Hz, $^1J(SnP^M)$ = −678.2 Hz, $^2J(SnP^M)$ = 57.2 Hz, $^1J(P^MP^{M'})$ = −126.4 Hz, 2P, P^M);

^1H-NMR (500.3 MHz, DMSO-d6, 25 °C): δ (ppm) = 2.08-1.0 (br m, CH_2);

^{119}Sn{^{1}H}-NMR (186.55 MHz, DMSO-d6, 25 °C): δ (ppm) = −70.4 (m) (m, X of [AMN]X spin system, $^{1}J(\mathrm{SnP^{M}}) = -678.2$ Hz, $^{2}J(\mathrm{SnP^{N}}) = 57.2$ Hz).
Due to the low solubility of the compound in common organic solvents, no ^{13}C data are available.

Reaction of Na(OCP) with triphenylgermanium chloride in the ratio 3:2

A solution of [Na(OCP)(dioxane)$_{2.5}$] (8.3 mg, 0.03 mmol) in THF (0.3 mL) was added dropwise at −70°C to a solution of $Ph_3Ge{-}P{=}C{=}O$ (20 mg, 0.06 mmol) in THF (0.2 mL). The reaction solution was investigated by low temperature ^{31}P-NMR spectroscopy.
^{31}P{^{1}H}-NMR (101.3 MHz, THF, 25 °C): δ (ppm) = 230.3 (d, $^{1}J_{PP} = 404.0$ Hz), −27.87 (d, $^{1}J_{PP} = 404.0$ Hz).

Synthesis of 3,5-bis(trimethylsiloxy)-1,2,4-triphospholide (15)

A solution of trimethylsilyl azide (0.317 g, 2.75 mmol) in THF (10 mL) was added dropwise at room temperature to a suspension of [Na(OCP)(dioxane)$_{2.5}$] (1.0 g, 3.3 mmol) in THF (10 mL). The suspension was stirred for 12 h at 50°C. Subsequently, sodium azide was removed from the dark red reaction solution by filtration. The solvent and the excess of trimethylsilyl azide were removed under reduced pressure and the resulting brown residue was washed with *n*-hexane to yield a brown powder. Yield: 97 mg (64%).
^{31}P{^{1}H}-NMR (81.01 MHz, THF-d8, 25 °C): δ (ppm) = 186.1 (t, $J(\mathrm{P^{A}P^{M}}) = 52.2$ Hz), 173.4 (d, $J(\mathrm{P^{A}P^{M}}) = 52.2$ Hz);
^{13}C{^{1}H}-NMR (100.6 MHz, DME, 25 °C): δ (ppm) = 209.5 (m, X of [AMN]X spin system, $^{1}J(\mathrm{P^{A}C}) = 46.4$ Hz, $\Sigma^{1}(J(\mathrm{P^{M}C}) + {}^{2}J(\mathrm{P^{N}C})) = 72.2$ Hz), 2.6 (s, CH_3);
^{1}H-NMR (300.1 MHz, THF-d8, 25 °C): δ (ppm) = 0.8-0.0 (br m, CH_3);

^{29}Si{^{1}H}-NMR (79.49 MHz, DME, 25°C): δ (ppm) = 5.4 (s);

IR (ATR): ν = 2961 (w, CH), 2898 (w, CH), 1538 (w br), 1447 (w), 1364 (w), 1250 (vs), 1144 (s), 1063 (vs), 1015 (vs, CO), 835 (vs, CO), 800 (vs), 750 cm^{-1} (s);

Elemental analysis (%) calculated for $C_8H_{18}O_2NaSi_2P_3$: C 30.19, H 5.70; found: C 27.26, H 5.67. The low carbon value is presumably due to trace amounts of non-combustible solid residues.

Synthesis of 1,1',2,2',4,4'-hexaphosphaferrocene (16)

The following synthesis was performed under the exclusion of light.

A solution of **15** (1.00 g, 3.21 mmol) in THF (30 mL) was added dropwise at room temperature to a suspension of [$FeBr_2(THF)_2$] (0.58 g, 1.62 mmol) in THF (4 mL). After 15 min stirring, the solvent was removed under reduced pressure yielding a brown residue. Extraction with *n*-hexane (30 mL) and subsequent removal of the solvent under reduced pressure gave the final product as a brown solid. Yield: 716 mg (70 %).

^{31}P{^{1}H}-NMR (81.01 MHz, THF, 25 °C): δ (ppm) = 5.0 (m, A part of $[A_2M]_2$ spin system, −8.8 (m, M of $[A_2M]_2$ spin system); Simulated coupling constants for $[A_2M]_2$ spin system (as a simplified [AA'M][A''A'''M']): $^{2}J_{AM}$ = 40.4 Hz, $^{2}J_{AA''}$ = ± 11.0 Hz, $^{2}J_{MA''}$ = −10.8 Hz, $^{2}J_{MM'}$ = ± 6.4 Hz;

^{1}H-NMR (500.26 MHz, THF-d8, 25 °C): δ (ppm) = 0.61-0.0 (br m, CH_3);

^{29}Si{^{1}H}-NMR (79.49 Hz, THF, 25 °C): δ (ppm) = 22.8 (s);

^{13}C{^{1}H}-NMR (100.6 MHz, THF-d8, 25 °C): δ (ppm) = 165.2 (m, X of [AA'M]X spin system, $^{1}J(P^{M}C)$ = 57.1 Hz, $\Sigma(^{1}J(P^{A}C) + ^{2}J(P^{A'}C))$ = 75.7 Hz), 3.6-0.5 (br m, CH_3);

Elemental analysis (%) calculated for $C_{16}H_{36}O_4Si_4P_6Fe$: C 29.73, H 5.61; found: C 29.89, H 5.73;

MS (MALDI) (m/z): 643.9507 (6.4 %), 645.9461 (100 %), 646.9445 (19.0 %), 647.9426 (12.0 %).

Generation of sodium 1,2,4-triphospholane-3,5-dionide (17)

Degassed water (50 µL, 2.8 mmol) was added at room temperature to a solution of **3** (35 mg, 0.05 mmol) in THF-d8 (0.5 mL). The reaction solution was investigated by NMR- and IR-spectroscopy. Compound **17** is stable in this solution for several days, however, in pure degassed water hydrolysis takes place to form $NaPH_2O_2$ among other decomposition products.

^{31}P-NMR (101.28 MHz, THF-d8, 25 °C): δ (ppm) = 116.0 (tt, A of AMM'XX', $^2J(P^A, P^M)$ = 16.3 Hz, $^3J(P^A, H^X)$ = 2.3 Hz), −66.2 (m, MM' of AMM'XX', $^1J(P^M, P^{M'})$ = 172.5 Hz, $^2J(P^A, P^M)$ = 16.3 Hz, $^1J(P^M, H^X)$ = 194.3 Hz, $^2J(P^M, H^{X'})$ = 23.8 Hz);

^{1}H-NMR (700.13 MHz, THF-d8, 25 °C): δ (ppm) = 3.9 (m, XX' of AMM'XX', $^1J(P^M, H^X)$ = 194.3 Hz, $^2J(P^{M'}, H^X)$ = 23.8 Hz, $^3J(P^A, H^X)$ = 2.3 Hz, $^3J(H^X, H^{X'})$ = 9.2 Hz).

The ^{13}C-NMR spectrum could not be measured due to low concentration.

IR (THF): 2237, 2082 (vs, ν_{asym}(PH)), calc.: 2251 (ν_{asym}(PH)), 2244 (ν_{sym}(PH)); 1647 (vs, ν_{asym}(CO)), calc.: 1583 cm^{-1} (ν_{asym}(CO)).

9.5 Experimental procedures for Chapter 5

Synthesis of the 1,2,4-oxadiphosphole 19

A solution of 2,4,6-trimethylbenzoyl chloride (1.35 g, 7.44 mmol) in THF (10 mL) was added slowly dropwise under vigorous stirring at -78°C to a solution of [Na(OCP)(dioxane)$_{2.5}$] (1.50 g, 4.96 mmol) in THF (20 mL). The reaction mixture was allowed to warm to room temperature within 60 min. During this, the reaction solution turned from colorless to yellow and a fine precipitate (sodium chloride) was formed. After stirring for another 60 minutes at room temperature, the solution was filtered. Then the solvent was removed under reduced pressure and the obtained yellow solid was washed with *n*-hexane to remove the excess of 2,4,6-trimethylbenzoyl chloride. The resulting fine yellow powder was dried *in vacuo*. Yield: 1.30 g (68%)

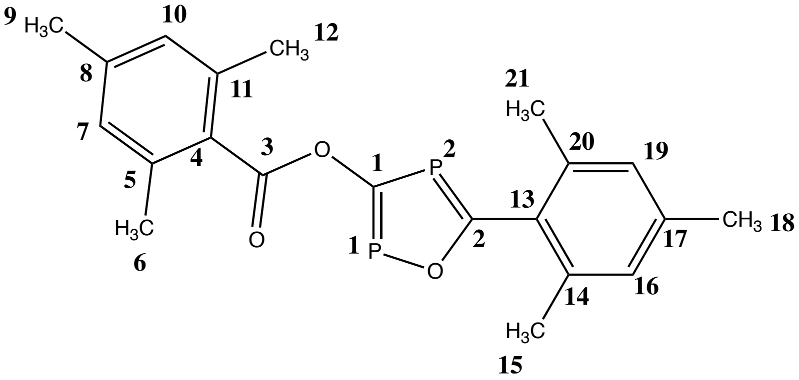

^{31}P{^{1}H}-NMR (CD$_2$Cl$_2$, 121.49 MHz, 298 K): δ (ppm) = 253.2 (d, $^{2}J_{PP}$ = 45.6 Hz, P1), 111.5 (d, $^{2}J_{PP}$ = 45.6 Hz, P2);

^{13}C{^{1}H}-NMR (CD$_2$Cl$_2$, 125.8 MHz, 298 K): δ (ppm) = 207.4 (dd $^{1}J_{PC}$ = 102.3 Hz, $^{1}J_{PC}$ = 55.1 Hz, C1), 203.5 (dd, $^{1}J_{PC}$ = 49.2 Hz, $^{2}J_{PC}$ = 4.3 Hz, C2), 169.4 (d, $^{4}J_{PC}$ = 6.4 Hz, C=O), 141.0 (s, 1C, C8), 138.8 (s, 2C, C5/C11), 137.6 (s, 1C, C17), 137.0 (d, J_{PC} = 5 Hz, 2C, C14/C20), 133.5 (dd, $^{2}J_{P2C}$ = 18.8 Hz, $^{3}J_{P1C}$ = 1.8 Hz, 1C, C13), 129.1 (s, 2C, C16/C19), 128.7 (s, 2 C, C7/C10), 126.5 (d, J_{PC} = 2.5 Hz, 1C, C4), 20.8-20.7 and

20.3-20.1 (6C, C_{methyl});

^{1}H-NMR (C_6D_6, 500.2 MHz, 298 K): δ (ppm) = 6.85 (s, 2H, $C^{16/19}H$), 6.68 (s, 2H, $C^{7/10}H$), 2.35 (s, 6H, $C^{6/12}H_3$), 2.30 (s, 6H, $C^{15/21}H_3$), 2.22 (s, 3H, $C^{18}H_3$), 2.10 (s, 3H, C^9H_3);

IR (ATR): 1788 (m), 1732 (m), 169 (m, C=O), 1607 (m), 1442 (br m), 1421 (br m), 1377 (m), 1246 (m), 1213 (s), 1177 (s, C2−O in ring), 1147 (s, C_1−O), 1059 (s), 970 (s), 946 (s), 849 (s), 698 cm^{-1} (s);

Elemental analysis (%) calculated for $C_{21}H_{22}O_3P_2$: C 65.63, H 5.77 %; found: C 63.19, H 5.90; The low carbon value is presumably due to trace amounts of non-combustible solid residues.

UV/VIS (*n*-hexane): λ_{max} = 247, 300 nm.

m.p.: 140 °C

^{31}P- NMR shifts of oxadiphospholes from Na(OCP) with further acid chlorides:

o-toluoyl chloride

$^{31}P\{^1H\}$-NMR (162.0 MHz, C_6D_6, 25°C) δ (ppm) = 248.8 (d, $^2J_{PP}$ = 45 Hz), 108.9 (d, $^2J_{PP}$ = 45 Hz);

2,6-difluorobenzoyl chloride (not isolated)

$^{31}P\{^1H\}$-NMR (121.5 MHz, THF, 25°C) δ (ppm) = 248.2 (d, $^2J_{PP}$ = 49 Hz), 122.8 (td, $^2J_{PP}$ = 49 Hz, $^4J_{PF}$ = 76 Hz);

Benzoyl chloride (not isolated)

$^{31}P\{^1H\}$-NMR (101.3 MHz, THF, 25°C) δ (ppm)= 260.1 (P1), 146.8 (P2);

Pivaloyl chloride (not isolated)

$^{31}P\{^1H\}$-NMR (162.0 MHz, THF, 25°C) isomer 1 (60%): δ (ppm) = 255.6 (d, $^2J_{PP}$ = 46 Hz), 90.3 (d, $^2J_{PP}$ = 46 Hz); isomer 2 (40%): δ (ppm) = 260.7 (d, $^2J_{PP}$ = 44 Hz), 91.5 (d, $^2J_{PP}$ = 44 Hz). Repetition of the reaction delivered different ratios of the two isomers.

Cyclohexanecarbonyl chloride (not isolated)

^{31}P{^{1}H}-NMR (162.0 MHz, THF, 25°C) isomer 1 (85%): δ (ppm) = 254.4 (d, $^{2}J_{PP}$ = 45 Hz), 91.3 (d, $^{2}J_{PP}$ = 45 Hz); isomer 2 (15%): δ (ppm) = 258.5 (d, $^{2}J_{PP}$ = 43 Hz), 92.4 (d, $^{2}J_{PP}$ = 43 Hz).

Low temperature-NMR kinetic investigation on the formation mechanism of 19

A solution of [Na(OCP)(dioxane)$_{2.5}$] (45 mg, 0.15 mmol) in THF (0.3 mL) was prepared in an NMR tube. To this solution 2,4,6-trimethylbenzoyl chloride (30 mg, 0.16 mmol) in THF (0.2 mL) was added slowly dropwise at −60°C under argon atmosphere. The reaction was followed for 117 h by ^{31}P-NMR spectroscopy at −35°C.

9.6 Experimental procedures for Chapter 6

Synthesis of [Na][25]

Dicyclohexylcarbodiimide (1.40 g, 6.8 mmol) and [Na(OCP)(dioxane)$_{2.5}$] (1.00 g, 3.3 mmol) were refluxed for 15 h in THF (20 mL). The solvent was removed under reduced pressure and the obtained yellow residue was washed with *n*-hexane yielding a bright-yellow powder, which was dried *in vacuo* yielding 991 mg (61 %) [Na][**25**] (M = 494.63 g/mol).

^{31}P{^{1}H}-NMR (75.47 MHz, THF-d8, 25 °C): δ (ppm) = −44.2 (s);

^{13}C{^{1}H}-NMR (62.9 MHz, THF-d8, 25 °C): δ (ppm) = 172.5 (d, $^1J_{PC}$ = 66.9 Hz, 2C; C=N), 157.6 (s, 1C; C=O), 57.7 (d, $^3J_{PC}$ = 37.6 Hz, 2C; CH), 57.1 (s, 2C; CH), 33.7 (s, 4C; CH$_2$), 30.7 (s, 4C; CH$_2$), 27.2 (s, 4C; CH$_2$), 26.8 (s, 2C; CH$_2$), 26.3 (s, 2C; CH$_2$), 24.9 (s, 4C; CH$_2$);

^{1}H-NMR (300.13 MHz, THF-d8, 25 °C): δ (ppm) = 4.61-4.41 (overlapping m, 2H; CH), 3.61-3.38 (overlapping m, 2H, CH), 1.93-0.87 (overlapping m, 40H; CH$_2$);

IR (ATR): ν = 2921 (vs, CH), 2850 (s, CH), 1667 (s, CO$_{str.}$), 1596 (s, CN$_{str.}$), 1446 (s), 1406 (s), 1359 (s), 1343 (s), 1324 (s), 1253 (w), 1235 (s), 1219 (s), 1179 (w), 1136 (w), 1068 (w), 1048 (s), 891 (s), 758 (w) cm^{-1};

Due to the uncertainty in the number of coordinated THF molecules the elemental analysis data were not reliable. The purity of the isolated compound was checked by ^{13}C-NMR spectroscopy.

UV/VIS in THF, λ = 383, 225 (shoulder) nm;

MALDI MS (positive mode): m/z = 473.3404 [$C_{27}H_{46}N_4PO$]$^+$ ([M +2H]$^+$);

m.p.: 133 °C.

Synthesis of the diisoproylanalogue of [Na][25]

The compound was synthesized based on the procedure for [Na][**25**], starting from diisopropylcarbodiimide (0.84 g, 6.7 mmol) and [Na(OCP)(dioxane)$_{2.5}$] (1.00 g, 3.3 mmol) yielding 850 mg (77 %) of the final product.

^{31}P{^{1}H}-NMR (161.98 MHz, THF-d8, 25 °C): δ (ppm) = −49.3 (s);

^{13}C{^{1}H}-NMR (100.61 MHz, THF-d8, 25 °C): δ (ppm) = 173.9 (d, $^{1}J_{PC}$ = 69.9 Hz, 2C, C=N), 158.8 (s, 1C, C=O), 51.5 (d, $^{3}J_{PC}$ = 39.0 Hz, 2C, CH), 49.0 (s, 2C, CH), 25.3 (s, 4C, CH_3), 22.6 (s, 4C, CH_3);

^{1}H-NMR (400.13 MHz, THF-d8, 25 °C): δ (ppm) = 5.03 (sept, $^{3}J_{HH}$ = 6.80 Hz, 2H, CH), 3.77 (2H, CH), 1.42 (d, $^{3}J_{HH}$ = 6.8 Hz, 12H, CH_3), 1.02 (d, 12H, $^{3}J_{HH}$ = 6.1 Hz, CH_3);

IR (ATR): ν = 2964 (w), 2923 (w), 2871 (w), 2361 (br w), 2174 (br w), 1655 (s), 1610 (s), 1561 (s), 1508 (w), 1450 (s), 1413 (s), 1376 (vs), 1357 (vs), 1241 (vs), 1085 (vs), 956 (s), 751 (vs) cm^{-1};

UV/VIS in THF, λ = 319 nm.

Due to the uncertain number of coordinated THF molecules the elemental analysis data were not reliable. The purity of the isolated compound was confirmed by ^{13}C-NMR spectroscopy.

m.p.: 170°C (decompos.)

Synthesis of the *p*-tolyl analogue of [Na][25]

1,3-Di-*p*-tolylcarbodiimide (300 mg, 1.31 mmol) in THF (3 mL) was added dropwise at room temperature to a solution of [Na(OCP)(dioxane)$_{2.5}$] (158 mg, 0.52 mmol). After two hours stirring at room temperature, the solvent was removed under reduced pressure. The obtained yellow residue was washed with *n*-hexane and the final product, a yellow solid, was dried *in vacuo*. Yield: 180 mg (66 %).

^{31}P{^{1}H}-NMR (81.01 MHz, THF-d8, 25 °C): δ (ppm) = −53.7 (s).

$^{13}C\{^1H\}$-NMR (50.32 MHz, THF-d8, 25 °C): δ (ppm) = 176.4 (d, $^1J_{PC}$ = 81.0 Hz, 2C, C=N), 157.4 (d, $^3J_{PC}$ = 3 Hz, 1C, C=O), 152.5 (d, $^3J_{PC}$ =11.3 Hz, 2C, C_{ipso}), 141.7 (d, $^3J_{PC}$ = 2.0 Hz, 2C, C_{ipso}), 136.3 (s, 2C, C_{para}), 131.1 (s, 4C, C_{arom}), 129.9 (s, 4C, C_{arom}), 129.6 (s, 4C, C_{arom}), 129.4 (s, 2C, C_{para}), 122.9 (s, 2C, C_{arom}), 122.8 (s, 2C, C_{arom}), 21.9 (s, 2C, CH_3), 21.6 (s, 2C, CH_3);

^1H-NMR (200.13 MHz, THF-d8, 25 °C): δ (ppm) = 7.16 (s, 8H, CH_{arom}), 6.65 (m, 8H, CH_{arom}), 2.36 (s, 6H, CH_3), 2.17 (s, 6H, CH_3);

IR (ATR): ν = 2964 (w), 2923 (w), 2871 (w), 2340 (w), 2124 (w), 1655 (s), 1610 (s), 1561 (s), 1450 (s), 1413 (s), 1376 (vs), 1357 (vs), 1242 (vs), 1085 (vs), 1070 (vs), 956 (s), 751 (vs), 658 (vs) cm^{-1};

UV/VIS in THF, λ = 344, 282 (shoulder), 226 nm.

Because of the uncertainty in the number of coordinated THF molecules the elemental analysis data were not reliable. The purity of the isolated compound was verified by ^{13}C-NMR spectroscopy.

m.p.: 160°C (decompos.)

Synthesis of [28][I_3]

I_2 (300 mg, 1.2 mmol) in diethyl ether (2 mL) was added dropwise at room temperature to a stirred solution of [Na][**25**] (200 mg, 0.4 mmol) in diethyl ether (5 mL). After stirring for 15 h at room temperature, the solvent and the excess of iodine were removed under reduced pressure and the product was extracted from the brown residue with dichloromethane (5 mL). The solvent from the filtrate was removed under reduced pressure and the final product - a brown powder - was dried *in vacuo*. Yield: 276 mg (77%).

$^{31}P\{^1H\}$-NMR (121.5 MHz, CD_2Cl_2, 25 °C): δ (ppm) = 196.3 (s);

$^{13}C\{^1H\}$-NMR (75.5 MHz, CD_2Cl_2, 25 °C): δ (ppm) = 153.1 (s, 1C; C=O), 125.5 (s, 2C; C=C), 60.9 (s, 2C; CH), 58.4 (s, 2C; CH), 36.0 (s, 2C; CH_2), 35.8 (s, 2C; CH_2), 30.6 (s, 4C; CH_2), 26.8 (s, 4C; CH_2), 25.8 (s, 4C; CH_2), 25.3 (s, 2C; CH_2), 25.2 (s, 2C; CH_2);

^{1}H-NMR (300.13 MHz, CD_2Cl_2, 25 °C): δ (ppm) = 4.87-4.20 (overlapping m, 2H; CH), 3.98-3.72 (overlapping m, 2H; CH), 2.60-0.95 (overlapping m, 40H; CH_2);

IR (ATR): ν = 2939 (s, CH), 2850 (s, CH), 1718 (vs, CO), 1671 (w), 1526 (s, aromatic ring breathing), 1520 (shoulder w), 1439 (s), 1365 (s), 1350 (s), 1254 (w), 1192 (w), 1166 (w), 1081 (w), 1042 (w), 987 (s), 908 (w), 891 (s), 770, (s), 753 (s), 740 (s), 708 (s), 688 (w) cm^{-1};

EA(%) calculated for $C_{27}H_{44}I_3N_4OP$: C 38.05, H 5.20 N 6.57; found: C 37.66, H 5.11, N 6.39;

UV/VIS in THF, λ = 360, 280 nm.

m.p.: 150°C (decomposition);

Reaction of [28][I_3] with elemental magnesium

A suspension of [**28**][I_3] (20 mg, 0.02 mmol) in THF (1 mL) was stirred at room temperature with magnesium turnings (100 mg, 4.1 mmol). After 1 hour the solution became yellow and a white precipitate was formed. The filtered solution was investigated by ^{31}P-NMR spectroscopy, which revealed the formation of a compound with a chemical shift of δ = 186.7 ppm (101.28 MHz, THF, 25 °C), assigned to [**28**][I] (for analytical data, see below). After stirring the solution with magnesium turnings for further 12 hours, the formation of anion [**25**]$^-$ was proven by spectroscopic methods.

^{31}P{^{1}H}-NMR (200.1 MHz, THF, 25 °C): δ (ppm) = −21.82 (s);

IR (ATR): ν = 2922 (vs, CH), 2851 (vs, CH), 1670 (s, CO str.), 1601 (CN str.), 1013 (s) cm^{-1}.

MALDI MS (positive mode): m/z = 473.3402 [$C_{27}H_{46}N_4PO$]$^+$ ([M +2H]$^+$).

Reaction of [Na][25] with $MgCl_2$

A solution of [Na][**25**] (20 mg, 0.04 mmol) in THF (1 mL) was stirred for one hour at room temperature with anhydrous $MgCl_2$ (100 mg, 1.05 mmol). The obtained yellow suspension was filtered and the filtrate was analyzed by spectroscopic methods.

$^{31}P\{^1H\}$-NMR (200.1 MHz, THF, 25 °C): δ (ppm)= −21.7 (s);

IR (ATR) ν = 2927 (w, CH), 2849 (w, CH), 1667 (s, CO str.), 1626 (s, 1626 CN str.), 1105 (vs), 1092 (vs) cm^{-1}.

MALDI MS (positive mode): m/z = 473.3403 $[C_{27}H_{46}N_4PO]^+$ ($[M+2H]^+$).

Reaction of [Na][25] with different amounts of elemental iodine

a) A solution of I_2 (7.6 mg, 0.03 mmol) in THF (0.2 mL) was added dropwise at room temperature to a stirred solution of [Na][**25**] (30.0 mg, 0.06 mmol) in THF (0.5 mL). The reaction solution, which contained the spectroscopically pure **26**, was analyzed by spectroscopic methods.

$^{31}P\{^1H\}$-NMR (202.51 MHz, THF, 25 °C): δ (ppm) = −84.8 (s);

$^{13}C\{^1H\}$-NMR (62.92 MHz, THF, 25 °C): δ (ppm) = 152.8 (d, $^3J_{PC}$ = 3.2 Hz, 2C; C=O), 151.9 (dd, $^1J_{PC}$ = 50.5 Hz, $^2J_{PC}$ = 0.7 Hz, 4C; C=N), 61.9 (d, $^3J_{PC}$ = 37.8 Hz, CH), 59.6 (d, $^3J_{PC}$ = 1 Hz, CH), 33.8 (s, CH_2), 29.9 (s, CH_2), 27.5 (s, CH_2), 26.7 (s, CH_2), 26.6 (s, CH_2), 24.7 (s, CH_2);

ESI MS (positive mode) m/z = 943.6578 $[C_{54}H_{89}N_8P_2O_2]^+$ ($[M+H]^+$).

b) A solution of I_2 (7.6 mg, 0.03 mmol) in THF (0.2 mL) was added dropwise at room temperature to a stirred solution of **26** (0.06 mmol) in THF (0.5 mL) (generated analogously to a), see above). The reaction solution, which contains **27** (and small amounts of unidentified impurities), was analyzed by spectroscopic methods.

$^{31}P\{^1H\}$-NMR (202.51 MHz, THF, 25 °C): δ (ppm) = −87.4 (s);

$^{13}C\{^1H\}$-NMR (62.92 MHz, THF, 25 °C): δ (ppm) = 152.5 (d, $^1J_{PC}$ = 25.2 Hz, CN), 150.6 (s, C=O), 62.5 (s, CH), 59.9 (s, CH), 34.1 (s, CH_2), 29.9 (s, CH_2), 27.4 (s, CH_2), 27.3 (s, CH_2), 25.4 (s, CH_2), 24.7 (s, CH_2).
ESI MS m/z = 599.2370 $[C_{27}H_{45}IN4PO]^+$ ($[M+H]^+$).

Reaction of [28][I$_3$] with elemental magnesium to generate [28][I]

A suspension of [**28**][I_3] (30 mg, 0.035 mmol) in THF-d8 (0.5 mL) was stirred with magnesium turnings (320 mg, 13 mmol) for 15 min at room temperature. The obtained yellow reaction solution was investigated by NMR spectroscopy.
$^{31}P\{^1H\}$-NMR (81.0, THF-d8, 25 °C): δ (ppm) = 186.7 (s);
$^{13}C\{^1H\}$-NMR (62.91 MHz, THF-d8, 25 °C): δ (ppm) = 155.0 (s, 1C; C=O), 125.6 (s, 2C; C=C), 60.4 (d, $^2J_{PC}$ = 6.5 Hz, 2C; CH), 59.0 (s, 2C; CH), 34.8 (s, 2C; CH_2), 34.6 (s, 2C; CH_2), 31.2 (s, 4C; CH_2), 27.8 (s, 4C; CH_2); remaining CH_2 carbon resonances overlap with solvent signals;
^1H-NMR (200.13 MHz, THF-d8, 25 °C): δ (ppm) = 4.49-4.15 (2H; CH), 4.07-3.74 (2H; CH), 2.65-0.90 (40 H; CH_2, overlapping);

Reaction of [28][I$_3$] with elemental sodium

A suspension of [**28**][I_3] (85 mg, 0.1 mmol) in THF (4 mL) was stirred with elemental sodium (125 mg, 5.4 mmol) at room temperature until the reaction solution turned colourless and a white precipitate was formed. After filtration, the solution was investigated by NMR spectroscopy and mass spectrometry.
$^{31}P\{^1H\}$-NMR (81.0, THF-d8, 25 °C): δ (ppm) = 122.7 (s);
$^{13}C\{^1H\}$-NMR (125.81 MHz, THF-d8, 25 °C): δ (ppm) = 152.8 (s, C=O), 129.5 (pseudo-t, $^{2/3}J_{PC}$ = 14 Hz, C=C), 62.1 (m, CH), 54.5 (s, CH), 36.5 (s, CH_2), 35.2 (s, CH_2), 32.2 (s, CH_2), 31.7 (s, CH_2), 31.6 (s, CH_2), 27.5 (br s, CH_2).
MALDI MS (positive mode): m/z = 471.3326 $[C_{27}H_{44}N_4PO]^+$ ($[M/2]^+$).

9.7 Experimental procedures for Chapter 7

Reaction of sodium phosphide with two equivalents of 2,6-diisopropylphenyl isocyanate

A solution of 2,6-diisopropylphenyl isocyanate (248 mg, 1.22 mmol) in DME (1 mL) was added dropwise at room temperature to a suspension of sodium phosphide $NaPH_2$ (50 mg, 0.61 mmol) in DME (1 mL). After refluxing for 5 min the reaction mixture was analyzed by ^{31}P-NMR spectroscopy.

^{31}P-NMR (101.27 MHz, DME, 25 °C): δ (ppm) = −150 ppm (t, $^{1}J_{PH}$ = 207 Hz, **I1**), −83 ppm (d, $^{1}J_{PH}$ = 240 Hz, **I2** isomer 1), −70 (d, $^{1}J_{PH}$ = 260 Hz, **I2** isomer 2), −388 (s, Na(OCP)).

Synthesis of the sodium salt of 1,4,2-diazaphospholidine-3,5-dione (33a)

A solution of 2,6-diisopropylphenyl isocyanate (1.25 g, 6.6 mmol) in THF (4 mL) was added dropwise at room temperature to a solution of [Na(OCP)(dioxane)$_{2.5}$] (1.00 g, 3.3 mmol) in THF (6 mL). The reaction mixture was stirred for 15 h at 50°C. The solvent was removed under reduced pressure and the obtained orange residue was washed with *n*-hexane to yield an orange-red powder, which was dried *in vacuo*. Yield: 0.89 g (44%) (calculated for **33a**(THF)$_2$ M = 604.74 g/mol). Yellow-orange crystals suitable for X-ray diffraction were obtained by slow concentration of a THF solution.

^{31}P{^{1}H}-NMR (101.28 MHz, D_3C-CN, 25 °C): δ (ppm) = 117.2 (s);

^{13}C{^{1}H}-NMR (125.79 MHz, D_3C-CN, 25 °C): δ (ppm) = 195.8 (br d, $^{1}J_{PC}$ = 50 Hz, C=O), 153.8 (br s, C=O), 148.3 (s, C_{ipso}), 148.2 (s, C_{ipso}), 128.2 (s, C_{para}), 127.4 (s, C_{para}), 123.4 (s, C_{meta}), 123.1 (s, C_{meta}), 28.8 (s, CH), 28.3 (s, CH), 23.6 (s, CH_3), 23.5 (s, CH_3), 23.5 (s, CH_3), 23.2 (s, CH_3);

^{1}H-NMR (250.20 MHz, D_3C-CN, 25 °C): δ (ppm) = 7.47-7.01 (m, 6H, H_{arom}), 3.74-2.95 (m, 4H, CH), 1.37-0.97 (m, 24H, CH_3);
IR (ATR): 1643 (vs, C=O), 1523 (vs, C=O), 1469 (s), 1446 (s), 1390 (s), 1060 (vs), 800 cm^{-1} (s).
Reliable data of an elemental analysis could not be obtained, presumably due to the non-stoichiometric amount of coordinated solvent molecules. The purity was checked by ^{13}C-NMR spectroscopy.

Applying [Na(OCP)(dioxane)$_{2.5}$] as catalyst for the trimerization of phenyl isocyanate

Phenyl isocyanate (3.90 g, 33 mmol) was added dropwise at room temperature under vigorous stirring to a solution of [Na(OCP)(dioxane)$_{2.5}$] (0.10 g, 0.33 mmol) in THF (4 mL). The reaction solution was stirred for 5 min at room temperature. Triphenylisocyanurate (**31b**) was allowed to crystalize at RT over 15 hours and subsequently washed with THF and dried *in vacuo*. Yield: 3.57 g (92%).
Elemental analysis (%) calculated for $C_{21}H_{15}N_3O_3$: C 70.58, H 4.23, N 11.76; found: C 70.47, H 4.15, N 11.66.

Reaction of sodium phosphide with phenyl isocyanate in the ratio 2:1

A solution of phenyl isocyanate (145 mg, 1.22 mmol) in DME (1 mL) was added dropwise at room temperature to a suspension of sodium phosphide (50 mg, 0.61 mmol) in DME (1 mL). After stirring for 5 min at room temperature the reaction mixture was analyzed by ^{31}P-NMR spectroscopy. The ^{31}P-NMR spectrum showed the formation of Na(OCP), **33b** (104.8 ppm), **34b** (−20.1 ppm) and **35b** (−67.2 ppm).

General procedure for the reaction of [Na(OCP)(dioxane)$_{2.5}$] with phenyl- (29b), cyclohexyl- (29c) and *n*-butyl- (29d) isocyanate in the ratio 1:8

A solution of isocyanate (8 eq., ca. 3.3 mmol) in THF (2 mL) was added dropwise at room temperature to a solution of [Na(OCP)(dioxane)$_{2.5}$] (0.10 g, 3.3 mmol) in THF (2 mL). The solutions were stirred for 1 hour at room temperature and a color change to yellow was observed. In the reaction with **29b** colorless crystals were formed, which were identified by single crystal X-ray diffraction analysis as **31b**. Investigation of the reaction solutions by ^{31}P- and ^{13}C-NMR spectroscopy revealed the formation of compounds **31**, **34** and **35** and the characteristic data for these compounds are summarized in Table 8.1. Colorless single crystals of **35c** and **35d** suitable for X-ray diffraction were obtained by slow evaporation of the solvent at room temperature.

Table 9.1 ^{31}P and ^{13}C (carbonyl carbons) chemical shifts for **31**, **34** and **35** in THF. Chemical shifts are given in ppm, coupling constants in Hz.

Reaction product	δ ^{31}P	δ ^{13}C
31b		-[a]
31c		146.7
31d		147.1
34b 15%	−16 (s)	-[a]
34c 35%	−20 (s)	192.8 (d, $^{1}J_{PC}$ = 50) 151.6 (d, $^{3}J_{PC}$ = 2)
34d 9%	−20 (s)	192.2 (d, $^{1}J_{PC}$ = 54) 151.8 (d, $^{3}J_{PC}$ = 3)
35b 85%	− 64 (s)	-[a]
35c 65%	− 86 (s	175.3 (d, $^{1}J_{PC}$ = 36) 152.8 (d, $^{3}J_{PC}$ = 6)
35d 91%	− 85 (s)	174.7 (d, $^{1}J_{PC}$ = 41) 153.5 (d, $^{3}J_{PC}$ = 7)

Due to the low solubility of the compounds **31b**, **34b** and **35b** no ^{13}C-NMR data is available for the carbonyl groups.

Generation of the sodium salt of 2,6-difluorophenyl substituted phosphoranide (35f)

A solution of cyclohexyl isocyanate (83 mg, 0.66 mmol) in THF (0.2 mL) was added dropwise at room temperature to a solution of [Na(OCP)(dioxane)$_{2.5}$] (25 mg, 0.08 mmol) in THF (0.3 mL). After 30 min stirring the reaction solution was transferred to an NMR tube and cooled to −80 °C. At this temperature slowly a solution of 2,6-difluorophenyl isocyanate (103 mg, 0.66 mmol) in THF (0.2 mL) was added dropwise.

^{31}P{^{1}H}-NMR (162.0 MHz, THF, −40 °C): δ (ppm)= −67.4 (t, J_{PF} = 126 Hz);

^{19}F{^{1}H}-NMR (376.5 MHz, THF, −40 °C): δ (ppm) = −116.53 (s, 2F), −118.65 (d, J_{PF} = 126 Hz, 2F^{A}), −117.39 (s, 2F), −118.95 (s, 2F); F^{B}, F^{C} and F^{D} cannot be assigned unambiguously.

^{31}P{^{1}H}-NMR (162.0 MHz, THF, 10 °C): δ (ppm) = −65.8 (q, J_{PF} = 61 Hz);

^{19}F{^{1}H}-NMR (376.5 MHz, THF, 10 °C): δ (ppm) = −118.12 (s, 2F), −118.88 (s, 2F), −119.53 (br s, 4F (2F^{A} + 2F^{B}); F^{C} and F^{D} cannot be assigned unambiguously.

Isocyanate exchange experiment: Substitution of cyclohexyl isocyanate units of 35c by phenyl isocyanates to generate 35b

A solution of cyclohexyl isocyanate (100 mg, 0.8 mmol) in THF (0.3 mL) was added at room temperature to a solution of [Na(OCP)(dioxane)$_{2.5}$] (30 mg, 0.1 mmol) in THF (0.3 mL). A ^{31}P-NMR spectrum of the reaction mixture was recorded to ensure that the sample contains no Na(OCP). Subsequently, an excess of phenyl isocyanate was added and a ^{31}P-NMR spectrum of the sample was recorded. A conversion of the cyclohexyl-substituted phosphoranide to the phenyl-substituted phosphoranide was observed. For ^{31}P-NMR chemical shifts see the table above.

Generation of a TDI/Cy-phosphoranide-mixture and subsequent generation of the corresponding polyurethane with 1,4-cyclohexandimethanol. Subsequent catalytic formation of triphenyl isocyanurate (31b)

A solution of cyclohexyl isocyanate (170 mg, 1.36 mmol) in THF (0.5 mL) was added dropwise at room temperature to a solution of [Na(OCP)(dioxane)$_{2.5}$] (50 mg, 0.17

mmol) in THF (0.5 mL). After 10 min stirring at room temperature, a ^{31}P-NMR spectrum of the reaction mixture was recorded to ensure that the sample contains no Na(OCP). Then a solution of toluene diisocyanate (TDI) (236 mg, 1.36 mmol) in THF (2 mL) was added drop wise at room temperature. After 5 min stirring a ^{31}P-NMR spectrum of the reaction mixture was recorded, showing a broad signal (δ ^{31}P (ppm): −60 to −75), which is assigned to a mixture of phosphoranides. To form a polyurethane, a solution of 1,4-cyclohexandimethanol (190 mg, 1.6 mmol) in THF (1.0 mL) was added dropwise at room temperature. Immediately after the addition no change in the ^{31}P-NMR spectrum was observed. After 12 h stirring at room temperature the ^{31}P-NMR spectrum showed – beside a hydrolysis product at 0 ppm – still the broad signal of the TDI/Cy-phosphoranides ((δ ^{31}P (ppm): −60 to −75). (Note: using smaller amounts of solvent throughout the entire experiment, a gel can be obtained.) Finally an excess (0.5 mL, 0.55 g, 4.6 mmol) of phenyl isocyanate was added to the reaction mixture. After 1 h standing at room temperature a colorless crystalline material was formed which was identified by X-ray diffraction analysis as **31b**.

IR investigation after the final reaction step:

IR (ATR): 3424 (vbr, NH), 2978 (w, CH_{arom}), 2933 (w, CH_{arom}), 2856 (w, CH_{arom}), 1708 (vs, C=O urethane, C=O phosphoranides), 1686 (vs, C=O isocyanurates), 1596 (w), 1576 (s), 1535 (w), 1506 (w), 1405 (vs), 1224 (br s, CN), 1535 (w), 1203 (s), 1060 (vs, C−O stretch), 1034 (s), 906 (s), 793 (vs), 753 (vs), 674 cm^{-1} (s).

10. Appendix

10.1 Measured and simulated NMR spectra of selected compounds

Sodium salt of 1,2-bis(triphenylstannyl)-1,2,4-triphospholane-3,5-dione (14a)

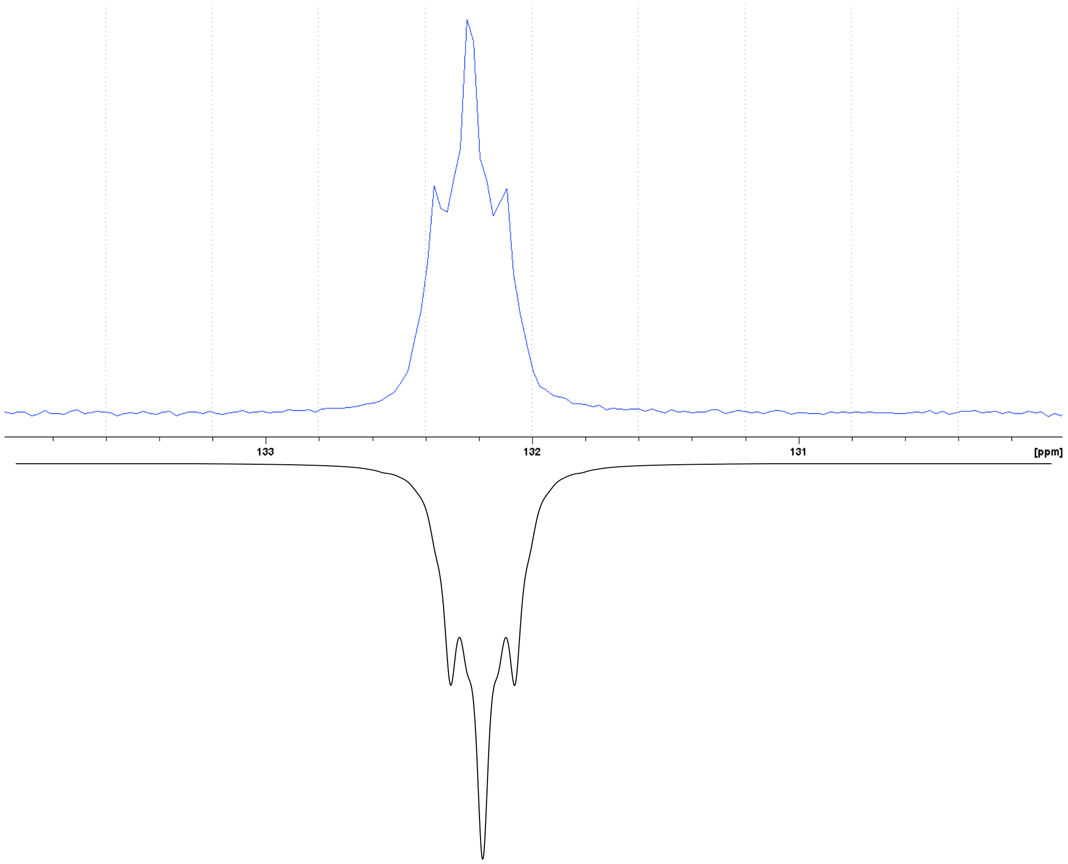

Figure 10.1 Detail at δ = 132.2 ppm (A part of the AMM'[X] spin system) of measured (blue) and simulated (black) 101.3 MHz $^{31}P\{^{1}H\}$-NMR spectra of **14a**. The line width allows no better resolution of the Sn satellites.

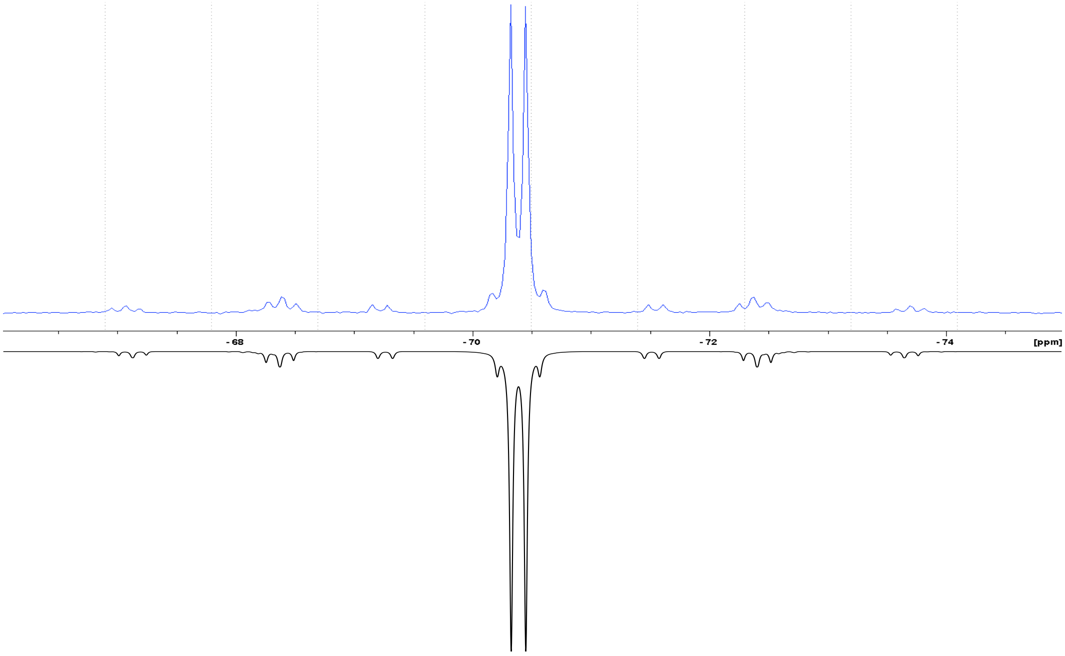

Figure 10.2 Detail at δ = –70.4 ppm (M part of the AMM'[X] spin system) of measured (blue) and simulated (black) 162.0 MHz $^{31}P\{^{1}H\}$-NMR spectra of **14a**.

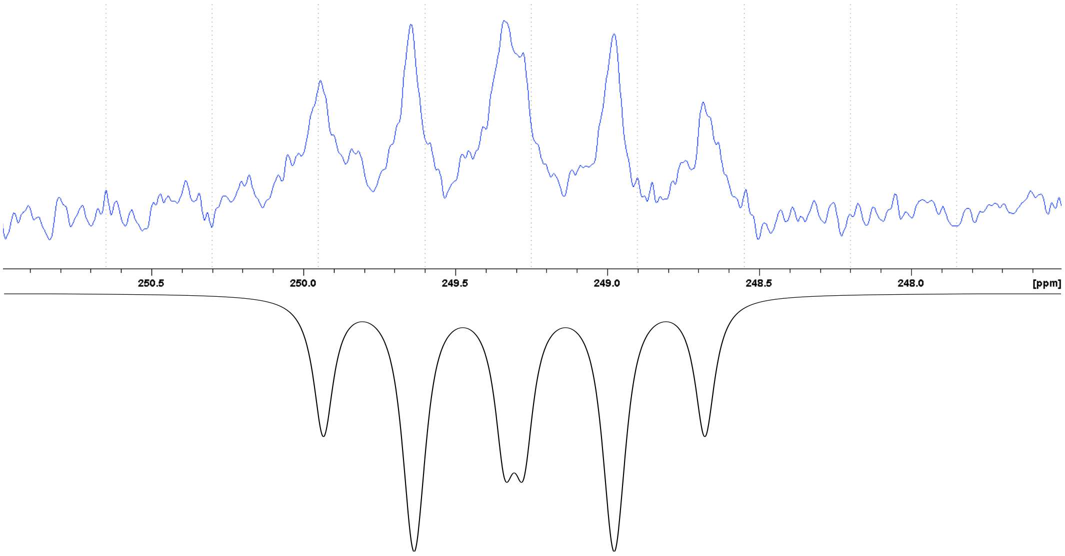

Figure 10.3 Detail at δ = 249.3 ppm (Y part of the AMM'[Y] spin system) of measured (blue) and simulated (black) 125.8 MHz $^{13}C\{^{1}H\}$-NMR spectra of **14a**.

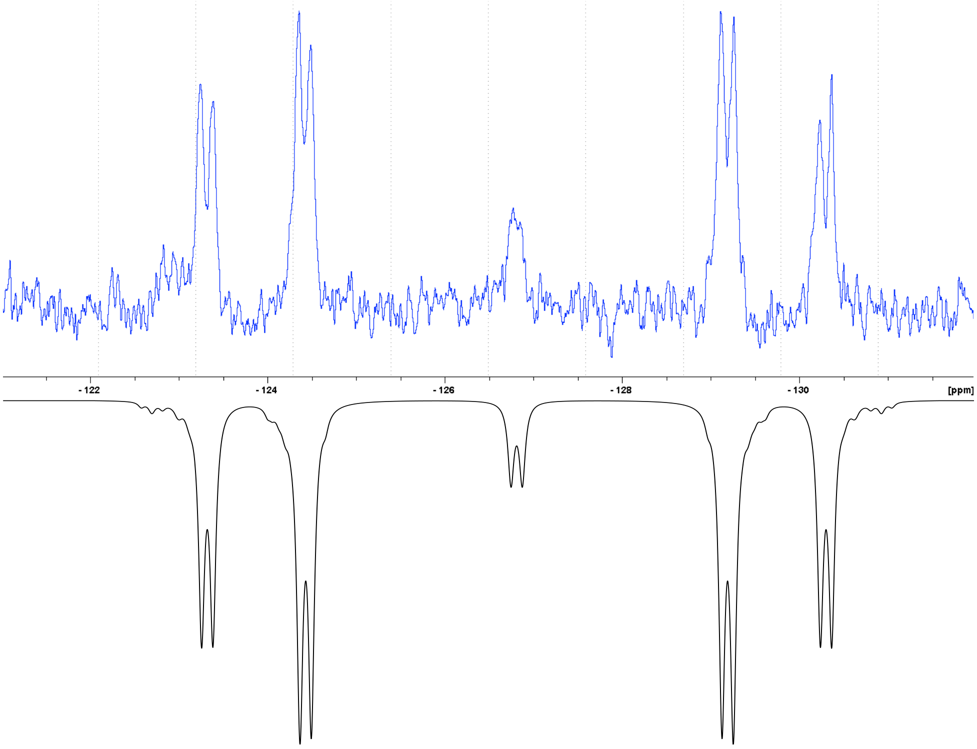

Figure 10.4 Detail at δ = -126.8 ppm (X part of the AMM'[X] spin system) of measured (blue) and simulated (black) 149.2 MHz ^{119}Sn{^{1}H}-NMR spectra of **14a**.

Intermediate B in chapter 4

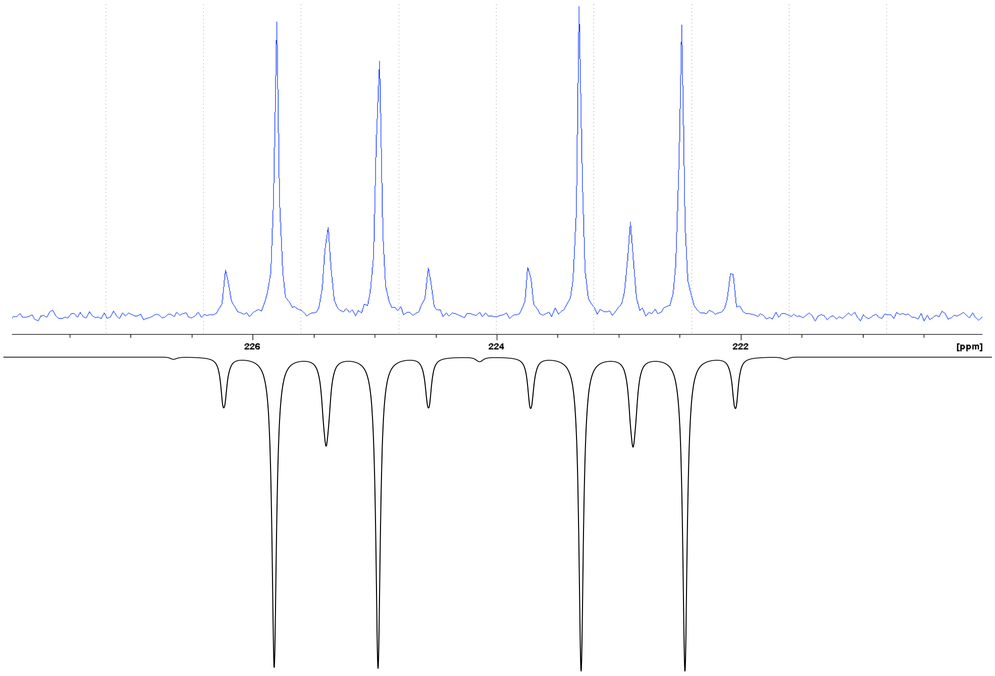

Figure 10.5 Detail at δ = 224.2 ppm (M part of the AMQ[X] spin system) of measured (−40 °C) (blue) and simulated (black) 162.0 MHz ^{31}P{^{1}H}-NMR spectra of intermediate **B**.

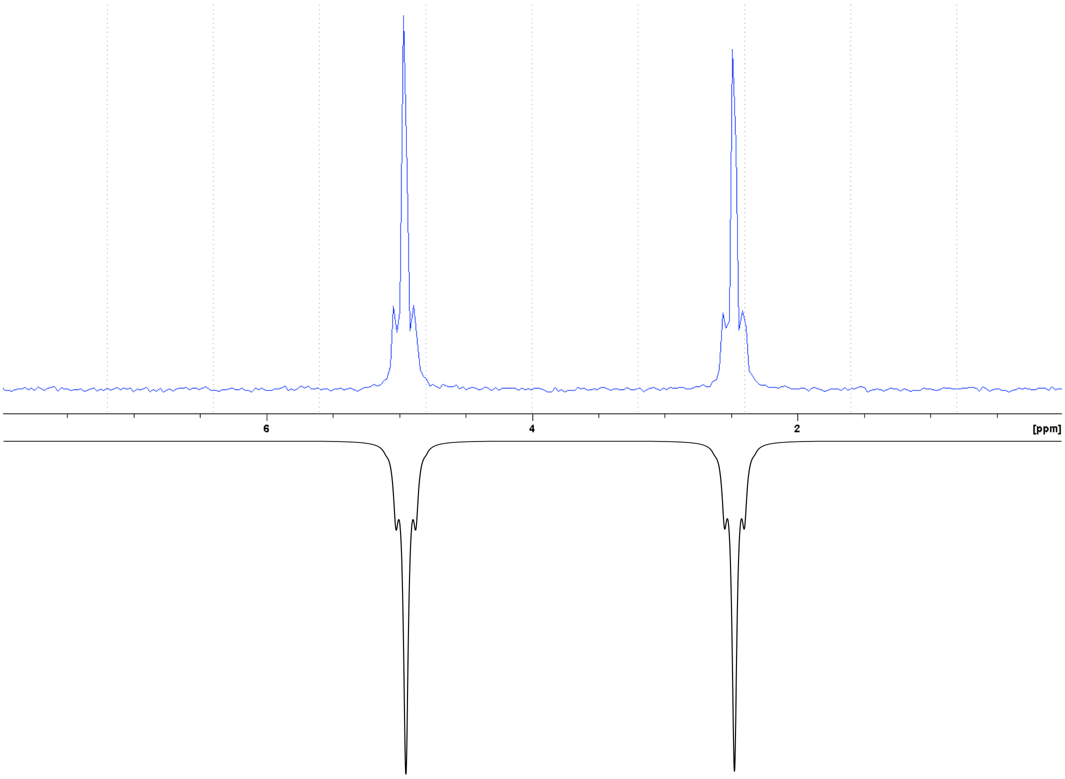

Figure 10.6 Detail at δ = 3.7 ppm (A part of the AMQ[X] spin system) of measured (blue) (–40 °C) and simulated (black) 162.0 MHz $^{31}P\{^{1}H\}$-NMR spectra of intermediate **B**.

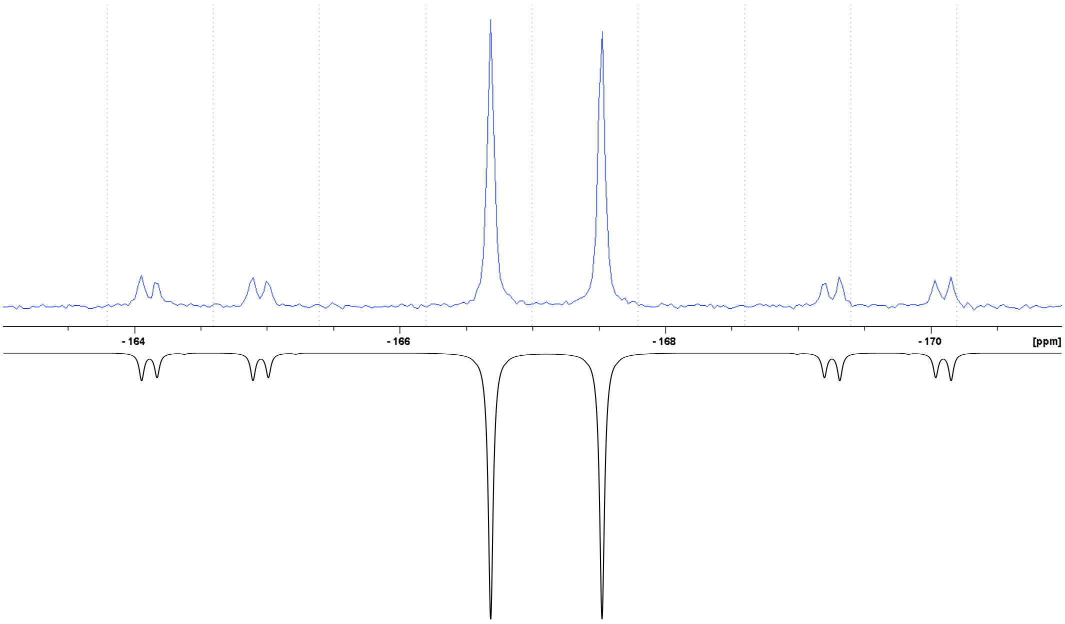

Figure 10.7 Detail at δ = –167.1 ppm (Q part of the AMQ[X] spin system) of measured (–40 °C) (blue) and simulated (black) 162.0 MHz $^{31}P\{^{1}H\}$-NMR spectra of intermediate **B**.

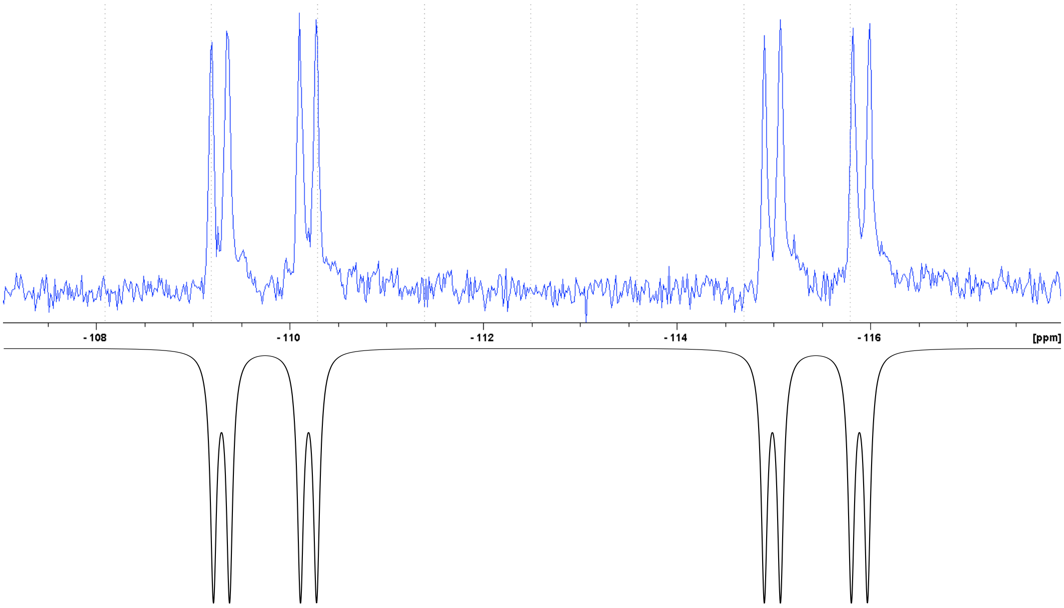

Figure 10.8 Detail at δ = –112.6 ppm (X part of the AM[X] spin system) of measured (–40 °C) (blue) and simulated (black) 149.2 MHz ^{119}Sn{^{1}H}-NMR spectra of intermediate **B**.

Sodium 1,2,4-triphospholane-3,5-dionide (17)

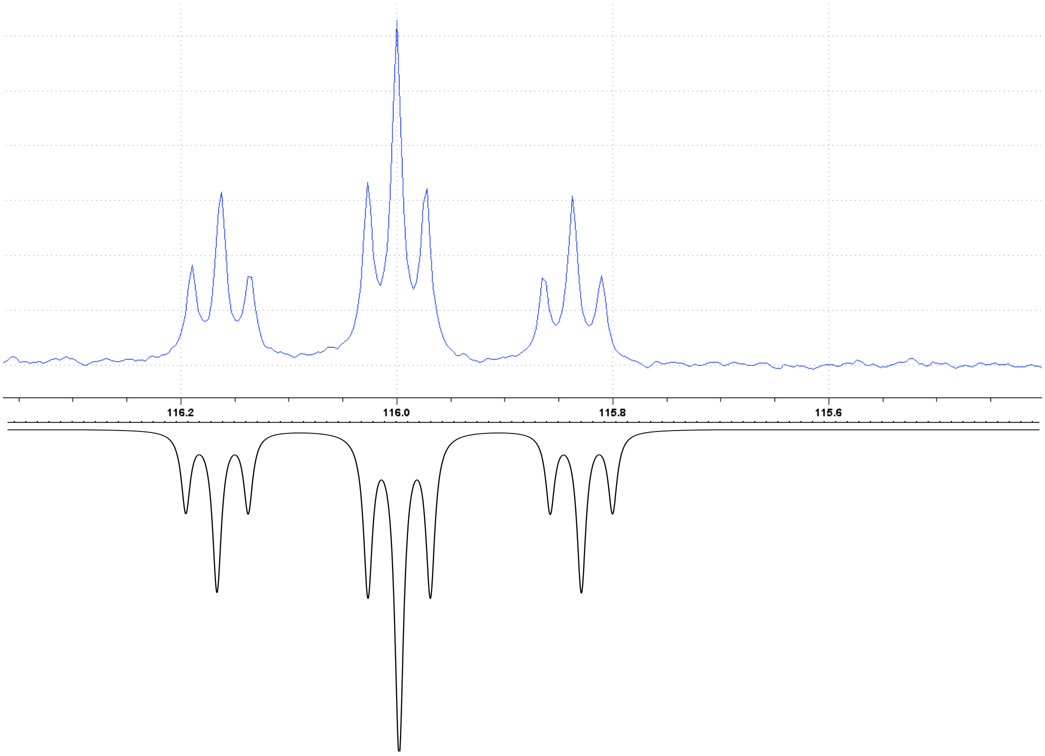

Figure 10.9 Detail at δ = 116.0 ppm (A part of the AMM’XX’ spin system) of measured (blue) and simulated (black) 101.3 MHz ^{31}P-NMR spectra of **17**.

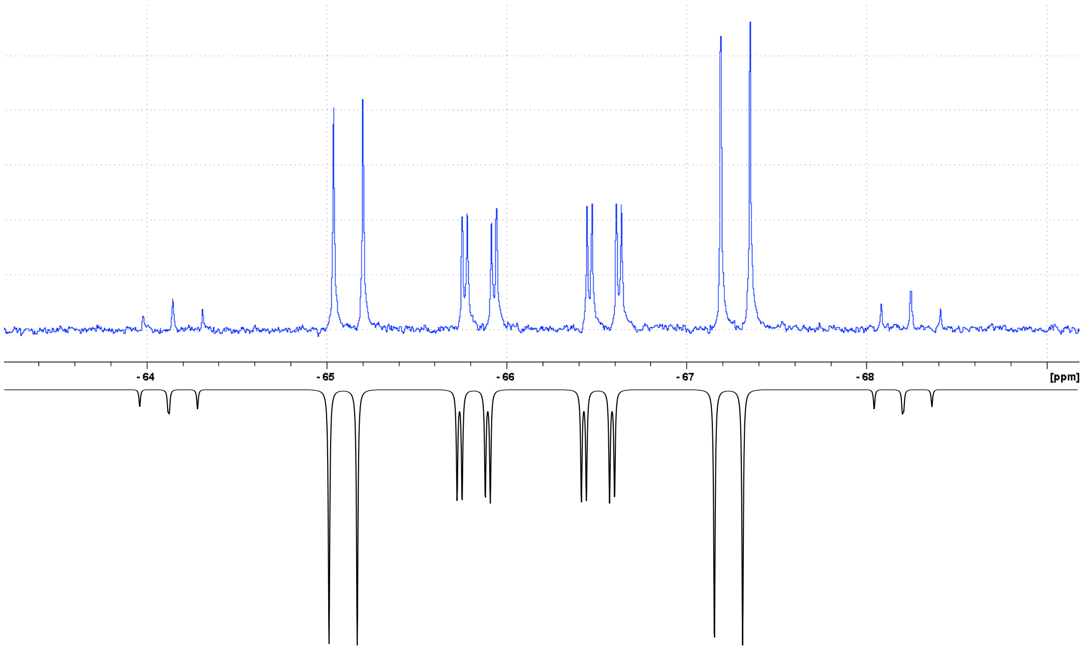

Figure 10.10 Detail at δ = -66.2 ppm (MM' part of the AMM'XX' spin system) of measured (blue) and simulated (black) 101.3 MHz ^{31}P-NMR spectra of **17**.

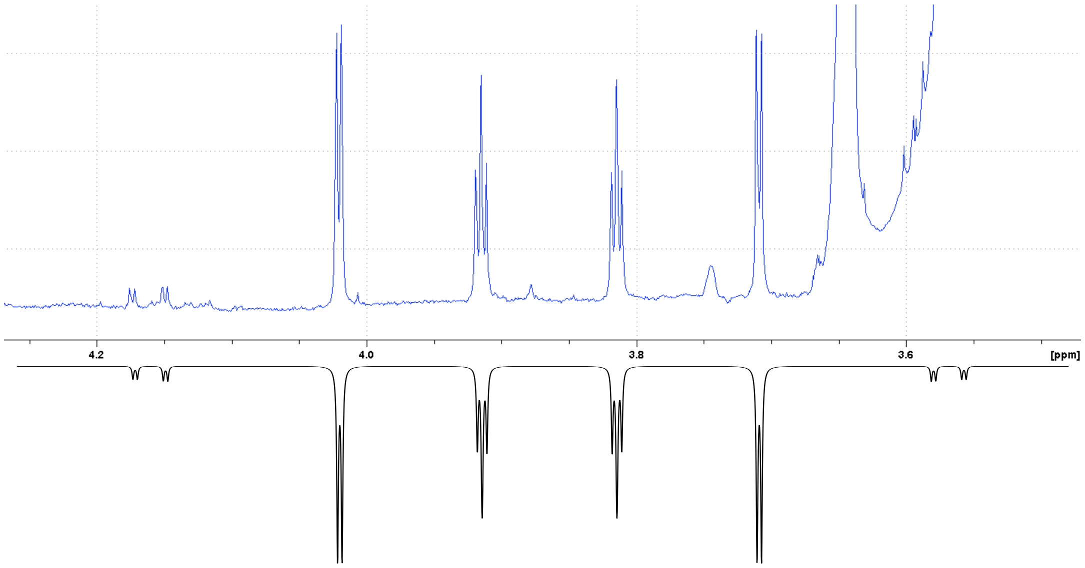

Figure 10.11 Detail at δ = 3.87 ppm (XX' part of the AMM'XX' spin system) of measured (blue) and simulated (black) 700.13 MHz ^{1}H-NMR spectra of **17**. A part of the measured spectrum is covered by the residue solvent signal of THF-d8.

1,1’,2,2’,4,4’-hexaphosphaferrocene (16)

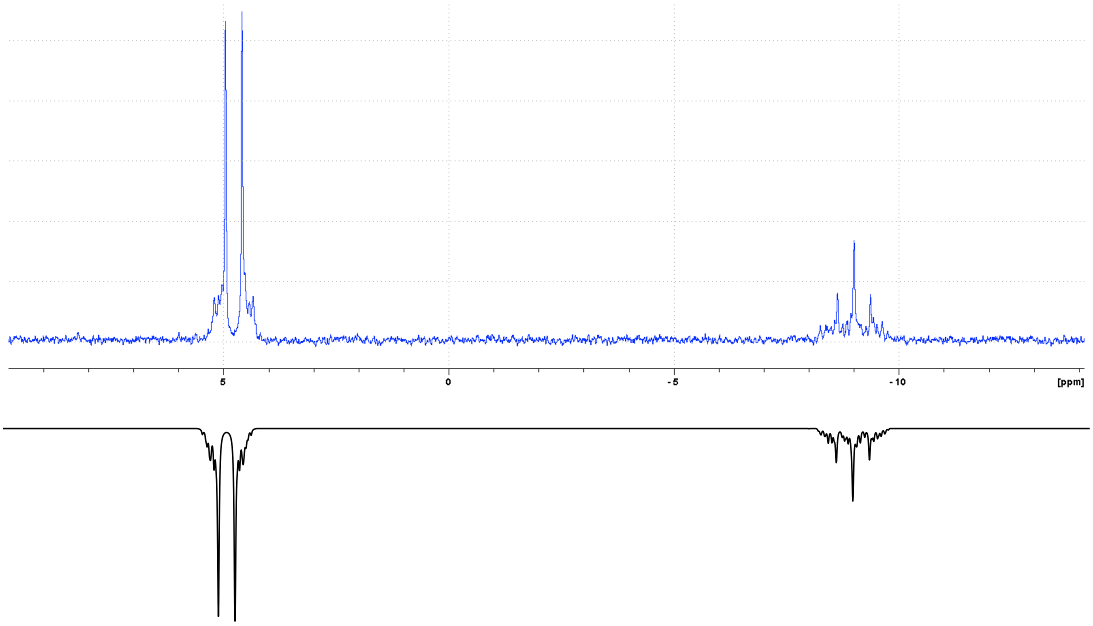

Figure 10.12 Detail at δ = 165.2 ppm (m, A part of the $[A_2M]_2$ spin system) of measured (blue) and simulated (black) 125.8 MHz $^{31}P\{^1H\}$-NMR spectra of **16**.

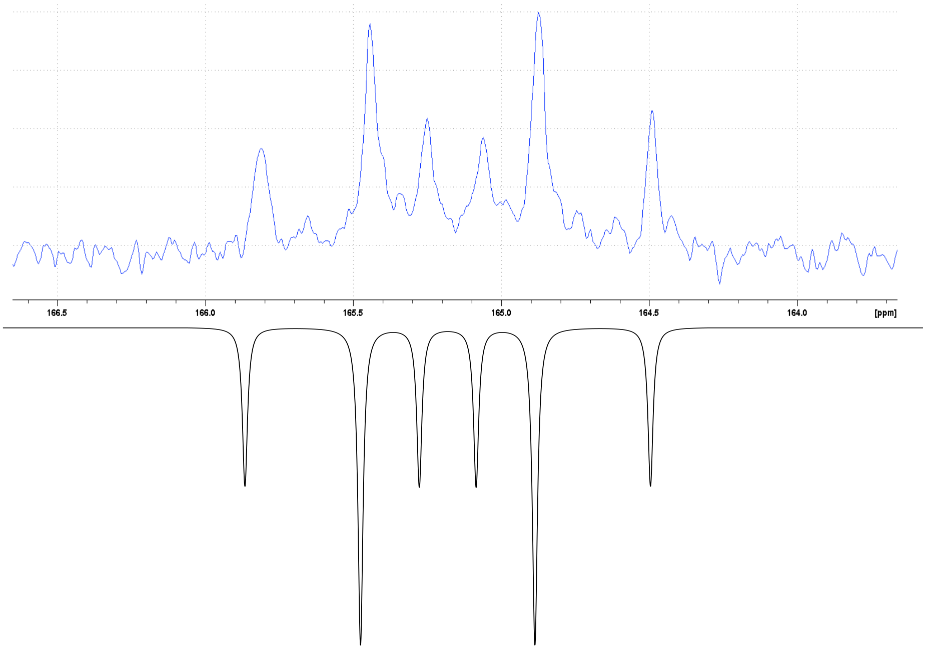

Figure 10.13 Detail at δ = 165.2 ppm (X part of the [AA’M]X spin system) of measured (blue) and simulated (black) 125.8 MHz $^{13}C\{^1H\}$-NMR spectra of **16**.

10.2 Crystallographic tables

Crystal data and structure refinement for $\mathbf{2}^{\mathbf{Tr*}}$

Empirical formula	$C_{54}H_{58}O_{10}P_2$
Formula weight / g mol^{-1}	929.00
Temperature / K	100(2)
Crystal system	triclinic
Space group	P-1
a / Å	11.2018(6)
b / Å	11.2296(6)
c / Å	11.4596(6)
α / °	118.377(6)
β / °	107.308(5)
γ / °	93.323(4)
Volume / Å^3	1176.28(11)
Z	1
ρ_{calc} / mg/mm^3	1.311
m / mm^{-1}	0.153
F(000)	492.0
Crystal size / mm^3	0.3 × 0.2 × 0.2
2Θ range for data collection	6.16 to 54.96°
Index ranges	$-14 \le h \le 14$, $-14 \le k \le 14$, $-14 \le l \le 14$
Reflections collected	12035
Independent reflections	5378[R(int) = 0.0253]
Data/restraints/parameters	5378/0/338
Goodness-of-fit on F^2	1.010
Final R indexes [I>=2σ (I)]	$R_1 = 0.0580$, $wR_2 = 0.1592$
Final R indexes [all data]	$R_1 = 0.0755$, $wR_2 = 0.1774$
Largest diff. peak/hole / e Å^{-3}	0.66/−0.64

Crystal data and structure refinement for the sodium salt of **14a**

Empirical formula	$C_{104}H_{130}Na_2O_{18}P_6Sn_4$
Formula weight / g mol^{-1}	2374.64
Temperature/K	100(2)
Crystal system	monoclinic
Space group	P2/c
a/Å	21.1479(5)
b/Å	11.4374(3)
c/Å	22.7441(5)
α/°	90.00
β/°	95.9850(10)
γ/°	90.00
Volume/Å^3	5471.3(2)
Z	2
ρ_{calc} / mg/mm^3	1.441
m/mm^{-1}	1.060
F(000)	2420.0
Crystal size/mm^3	0.2 × 0.15 × 0.03
2Θ range for data collection	1.94 to 52.74°
Index ranges	$-23 \leq h \leq 26$, $-14 \leq k \leq 13$, $-28 \leq l \leq 28$
Reflections collected	36790
Independent reflections	11192[R(int) = 0.0495]
Data/restraints/parameters	11192/0/607
Goodness-of-fit on F^2	0.953
Final R indexes [I>=2σ (I)]	$R_1 = 0.0326$, $wR_2 = 0.0583$
Final R indexes [all data]	$R_1 = 0.0596$, $wR_2 = 0.0738$
Largest diff. peak/hole / e Å^{-3}	1.06/−0.73

Crystal data and structure refinement for the sodium salt of **14b**

Empirical formula	$C_{50} H_{90} Na O_5 P_3 Sn_2$
Formula weight / g mol^{-1}	1124.49
Temperature/K	100(2)
Crystal system	monoclinic
Space group	$P2_1/n$
a/Å	13.3529(4)
b/Å	16.4933(4)
c/Å	24.5548(8)
α/°	90.00
β/°	92.7900(10)
γ/°	90.00
Volume/$Å^3$	5401.4(3)
Z	4
ρ_{calc} / mg/mm^3	1.383
m/mm^{-1}	1.063
F(000)	2344
Crystal size/mm^3	0.44 × 0.25 × 0.25
2Θ range for data collection	3.92 to 59.14°
Index ranges	$-18 \leq h \leq 18$, $-22 \leq k \leq 22$, $-34 \leq l \leq 34$
Reflections collected	72933
Independent reflections	15152[R(int) = 0.0284]
Data/restraints/parameters	15152/880/829
Goodness-of-fit on F^2	1.121
Final R indexes [I>=2σ (I)]	$R_1 = 0.0303$, $wR_2 = 0.0665$
Final R indexes [all data]	$R_1 = 0.0393$, $wR_2 = 0.0705$
Largest diff. peak/hole / e $Å^{-3}$	0.92/−1.24

Crystal data and structure refinement for **19**

Empirical formula	$C_{21}H_{22}O_3P_2$
Formula weight / g mol^{-1}	384.33
Temperature/K	120(2)
Crystal system	triclinic
Space group	P-1
a/Å	7.1039(5)
b/Å	8.2133(6)
c/Å	17.3480(12)
α/°	102.227(6)
β/°	90.177(6)
γ/°	90.407(6)
Volume/Å^3	989.20(12)
Z	2
ρ_{calc} / mg/mm^3	1.290
m/mm^{-1}	0.237
F(000)	404.0
Crystal size/mm^3	0.41 × 0.23 × 0.21
2Θ range for data collection	6.06 to 58.04°
Index ranges	$-9 \le h \le 9$, $-10 \le k \le 11$, $-23 \le l \le 23$
Reflections collected	19150
Independent reflections	4744[R(int) = 0.0561]
Data/restraints/parameters	4744/0/242
Goodness-of-fit on F^2	1.105
Final R indexes [I>=2σ (I)]	$R_1 = 0.0476$, $wR_2 = 0.1280$
Final R indexes [all data]	$R_1 = 0.0539$, $wR_2 = 0.1319$
Largest diff. peak/hole / e Å^{-3}	0.40/−0.45

Crystal data and structure refinement for [Na][**25**]

Empirical formula	$C_{43}H_{76}N_4NaO_5P$
Formula weight / g mol^{-1}	783.04
Temperature/K	100(2)
Crystal system	triclinic
Space group	P-1
a/Å	9.2375(7)
b/Å	11.0943(4)
c/Å	21.8510(12)
α/°	90.712(4)
β/°	94.256(6)
γ/°	90.814(5)
Volume/Å^3	2232.8(2)
Z	2
ρ_{calc} / mg/mm^3	1.165
m/mm^{-1}	0.117
F(000)	856.0
Crystal size/mm^3	0.4 × 0.18 × 0.11
2Θ range for data collection	5.7 to 51.36°
Index ranges	$-11 \leq h \leq 11$, $-13 \leq k \leq 13$, $-26 \leq l \leq 26$
Reflections collected	27047
Independent reflections	8367[R(int) = 0.0479]
Data/restraints/parameters	8367/0/621
Goodness-of-fit on F^2	1.060
Final R indexes [I>=2σ (I)]	R_1 = 0.0600, wR_2 = 0.1598
Final R indexes [all data]	R_1 = 0.0738, wR_2 = 0.1715
Largest diff. peak/hole / e Å^{-3}	0.87/−0.40

Crystal data and structure refinement for [**28**][I_3]

Empirical formula	$C_{27}H_{44}I_3N_4OP$
Formula weight / g mol^{-1}	852.33
Temperature/K	100(2)
Crystal system	orthorhombic
Space group	$P2_12_12_1$
a/Å	9.1672(9)
b/Å	18.0921(19)
c/Å	19.6810(16)
α/°	90.00
β/°	90.00
γ/°	90.00
Volume/Å^3	3264.2(5)
Z	4
ρ_{calc} / mg/mm^3	1.734
m/mm^{-1}	2.947
F(000)	1664.0
Crystal size/mm^3	0.1 × 0.1 × 0.04
2Θ range for data collection	3.06 to 54.2°
Index ranges	$-11 \leq h \leq 10$, $-15 \leq k \leq 23$, $-25 \leq l \leq 25$
Reflections collected	25925
Independent reflections	4037[R(int) = 0.0398]
Data/restraints/parameters	4037/0/382
Goodness-of-fit on F^2	1.022
Final R indexes [I>=2σ (I)]	$R_1 = 0.0199$, $wR_2 = 0.0389$
Final R indexes [all data]	$R_1 = 0.0255$, $wR_2 = 0.0407$
Largest diff. peak/hole / e Å^{-3}	0.58/−0.36
Flack parameter	0.449(18)

Crystal data and structure refinement for **33a**

Empirical formula	$C_{34}H_{50}N_2NaO_4P$
Formula weight / g mol^{-1}	604.75
Temperature/K	100(2)
Crystal system	monoclinic
Space group	$P2_1/n$
a/Å	10.6728(3)
b/Å	15.0865(4)
c/Å	21.8147(6)
α/°	90.00
β/°	93.643(3)
γ/°	90.00
Volume/Å^3	3505.40(17)
Z	4
ρ_{calc} / mg/mm^3	1.145
m/mm^{-1}	0.128
F(000)	1304.0
Crystal size/mm^3	0.26 × 0.21 × 0.15
2Θ range for data collection	5.72 to 54.2°
Index ranges	$-13 \leq h \leq 8$, $-18 \leq k \leq 19$, $-27 \leq l \leq 27$
Reflections collected	29868
Independent reflections	7720[R(int) = 0.0668]
Data/restraints/parameters	7720/0/388
Goodness-of-fit on F^2	1.095
Final R indexes [I>=2σ (I)]	$R_1 = 0.0772$, $wR_2 = 0.1252$
Final R indexes [all data]	$R_1 = 0.1159$, $wR_2 = 0.1396$
Largest diff. peak/hole / e Å^{-3}	0.84/−0.97

Crystal data and structure refinement for **35c**

Empirical formula	$C_{32}H_{54}N_4NaO_6P$
Formula weight / g mol^{-1}	644.75
Temperature/K	100(2)
Crystal system	orthorhombic
Space group	$P2_12_12_1$
a/Å	10.4709(3)
b/Å	17.4983(5)
c/Å	18.6976(5)
α/°	90.00
β/°	90.00
γ/°	90.00
Volume/Å^3	3425.83(17)
Z	4
ρ_{calc} / mg/mm^3	1.250
m/mm^{-1}	1.220
F(000)	1392.0
Crystal size/mm^3	0.08 × 0.05 × 0.03
2Θ range for data collection	6.92 to 77.6°
Index ranges	$-8 \le h \le 8$, $-14 \le k \le 14$, $-14 \le l \le 15$
Reflections collected	9948
Independent reflections	1889[R(int) = 0.0390]
Data/restraints/parameters	1889/0/189
Goodness-of-fit on F^2	1.173
Final R indexes [I>=2σ (I)]	$R_1 = 0.0409$, $wR_2 = 0.0926$
Final R indexes [all data]	$R_1 = 0.0460$, $wR_2 = 0.1001$
Largest diff. peak/hole / e Å^{-3}	0.18/−0.21
Flack parameter	0.08(6)

Crystal data and structure refinement for **35d**

Empirical formula	$C_{48}H_{88}N_8Na_2O_{10}P_2$
Formula weight / g mol^{-1}	1045.18
Temperature/K	100(2)
Crystal system	monoclinic
Space group	$P2_1/n$
a/Å	19.3693(13)
b/Å	14.6742(10)
c/Å	21.9183(17)
α/°	90.00
β/°	111.339(2)
γ/°	90.00
Volume/Å^3	5802.7(7)
Z	4
ρ_{calc} / mg/mm^3	1.196
m/mm^{-1}	0.148
F(000)	2256.0
Crystal size/mm^3	0.16 × 0.16 × 0.08
2Θ range for data collection	4.52 to 46.5°
Index ranges	$-21 \leq h \leq 21$, $-16 \leq k \leq 16$, $-24 \leq l \leq 24$
Reflections collected	81997
Independent reflections	8325[R(int) = 0.0740]
Data/restraints/parameters	8325/0/782
Goodness-of-fit on F^2	1.027
Final R indexes [I>=2σ (I)]	$R_1 = 0.0503$, $wR_2 = 0.1097$
Final R indexes [all data]	$R_1 = 0.0783$, $wR_2 = 0.1234$
Largest diff. peak/hole / e Å^{-3}	0.49/−0.34

10.3 Abbreviations

Ad	adamantyl
AIM	atoms in molecules
a.u.	arbitrary units
ATR	attenuated total reflectance
calc.	calculated
CCD	charge-coupled device
COE	cyclooctene
Cy	cyclohexyl
d	doublet
dd	doublet of doublets
DCC	N,N'-dicyclohexylcarbodiimide
DFT	density functional theory
Dipp	2,6-diisopropylphenyl
DME	1,2-dimethoxyethane
DMF	dimethylformamide
DMSO	dimethyl sulfoxide
EA	elemental analysis
EPR	electron paramagnetic resonance
EN	electronegativity
ESI	electrospray ionization
Et	ethyl

eV	electron volt
eq.	equivalent
GIAO	gauge-independent atomic orbital
HMPTA	hexamethylphosphoramide
HOMO	highest occupied molecular orbital
HSAB	hard and soft acids and bases
IM	intermediate
^{i}Pr	isopropyl
IR	infra-red
LUMO	lowest occupied molecular orbital
MDI	methylenediphenyl diisocyanate
Me	methyl
MERP	minimum energy reaction pathway
Mes	mesityl (2,4,6-trimethylphenyl)
Mes*	2,4,6-tri-*tert*-butylphenyl
MS	mass spectrum
m.p.	melting point
NICS	nuclear independent chemical shift
NMR	nuclear magnetic resonance
NBO	natural bonding orbital
NPA	natural population analysis
ORTEP	oak ridge thermal ellipsoid plot

Ph	phenyl
ppm	parts per million
Pr	propyl
Py	pyridine
q	quartet
RT	room temperature
t	triplet
^{t}Bu	tertiary butyl
TBP	trigonalbipyramidal
TDI	toluene diisocyanate
TfO	trifluoromethanesulfonate
Tr	trityl, triphenylmethyl
Tr*	4,4',4"-trimethoxytriphenylmethyl
triphos	1,1,1-tris(diphenylphosphinomethyl)ethane
THF	tetrahydrofuran
TMS	trimethylsilyl
TS	transition state
UV	ultra violet
VIS	visible
VSEPD	valence shell electron pair domain
VT	variable temperature
WBI	Wiberg bond index

11. Literature

1. F. Mathey, *Angew. Chem. Int. Ed.*, 2003, **42**, 1578-1604.
2. K. S. Pitzer, *J. Am. Chem. Soc.*, 1948, **70**, 2140-2145.
3. M. Regitz, *Chem. Rev.*, 1990, **90**, 191-213.
4. M. Regitz and P. Binger, *Angew. Chem. Int. Ed.*, 1988, **27**, 1484-1508.
5. K. Dimroth and P. Hoffmann, *Angew. Chem. Int. Ed.*, 1964, **3**, 384-385.
6. G. Märkl, *Angew. Chem. Int. Ed.*, 1966, **5**, 846-847.
7. T. E. Gier, *J. Am. Chem. Soc.*, 1961, **83**, 1769-1770.
8. D. P. Gates, C. W. Tsang, V. A. Wright and M. Yam, *Macromol. Symp.*, 2003, **196**, 271-278.
9. H. Oberhammer, G. Becker and G. Gresser, *J. Mol. Struct.*, 1981, **75**, 283-289.
10. A. Chirila, R. Wolf, J. Chris Slootweg and K. Lammertsma, *Coord. Chem. Rev.*, 2013 http://dx.doi.org/10.1016/j.ccr.2013.10.005.
11. R. Bartsch and J. F. Nixon, *Polyhedron*, 1989, **8**, 2407-2407.
12. R. Bartsch, P. B. Hitchcock and J. F. Nixon, *J. Organomet. Chem.*, 1988, **340**, C37-C39.
13. R. Bartsch, P. B. Hitchcock and J. F. Nixon, *J. Chem. Soc. Chem. Comm.*, 1987, 1146-1148.
14. S. M. Mansell, M. Green, R. J. Kilby, M. Murray and C. A. Russell, *C. R. Chim.*, 2010, **13**, 1073-1081.
15. G. Becker, W. Schwarz, N. Seidler and M. Westerhausen, *Z. anorg. allg. Chem.*, 1992, **612**, 72-82.
16. M. Westerhausen, S. Schneiderbauer, H. Piotrowski, M. Suter and H. Nöth, *J. Organomet. Chem.*, 2002, **643–644**, 189-193.
17. F. F. Puschmann, D. Stein, D. Heift, C. Hendriksen, Z. A. Gál, H.-F. Grützmacher and H. Grützmacher, *Angew. Chem. Int. Ed.*, 2011, **50**, 8420-8423.
18. A. R. Jupp and J. M. Goicoechea, *Angew. Chem. Int. Ed.*, 2013, **52**, 10064-10067.
19. G. Becker, G. Heckmann, K. Hübler and W. Schwarz, *Z. anorg. allg. Chem.*, 1995, **621**, 34-46.
20. U. Ray, D. Banerjee, B. G. Chand, J. Cheng, T. H. Lu and C. Sinha, *J. Coord. Chem.*, 2005, **58**, 1105-1113.
21. J. L. Zuffa and W. L. Gladfelter, *J. Am. Chem. Soc.*, 1986, **108**, 4669-4671.
22. W. Beck, W. P. Fehlhamm, P. Pöllmann and H. Schachl, *Chem. Ber.*, 1969, **102**, 1976-1987.
23. W. Beck, *J. Organomet. Chem.*, 1990, **383**, 143-160.
24. S. Alidori, D. Heift, G. Santiso-Quinones, Z. Benkő, H. Grützmacher, M. Caporali, L. Gonsalvi, A. Rossin and M. Peruzzini, *Chem. Eur. J.*, 2012, **18**, 14805-14811.
25. R. Appel and W. Paulen, *Angew. Chem. Int. Ed.*, 1983, **22**, 785-786.
26. P. Fölling, Ph. D. Thesis, Rheinische Friedrich-Wilhelms Unversität zu Bonn, 1988.
27. R. Appel and W. Paulen, *Tetrahedron Lett.*, 1983, **24**, 2639-2642.
28. V. Plack, J. R. Görlich, A. Fischer and R. Schmutzler, *Z. anorg. allg. Chem.*, 1999, **625**, 1979-1984.
29. L. Weber, B. Torwiehe, G. Bassmann, H.-G. Stammler and B. Neumann, *Organometallics*, 1996, **15**, 128-132.
30. U. Salzner and S. M. Bachrach, *J. Am. Chem. Soc.*, 1994, **116**, 6850-6855.
31. Y. Mao, Z. Wang, R. Ganguly and F. Mathey, *Organometallics*, 2012, **31**, 4786-4790.
32. G. Becker, G. Heckmann, K. Hübler and W. Schwarz, *Z. anorg. allg. Chem.*, 1995, **621**, 34-46.

33. R. Hagen and J. D. Roberts, *J. Am. Chem. Soc.*, 1969, **91**, 4504-4506.
34. K. Diemert, T. Hahn and W. Kuchen, *Phosphorus Sulfur*, 1991, **60**, 287-294.
35. G. Ménard and D. W. Stephan, *J. Am. Chem. Soc.*, 2010, **132**, 1796-1797.
36. C. M. Mömming, E. Otten, G. Kehr, R. Frohlich, S. Grimme, D. W. Stephan and G. Erker, *Angew. Chem. Int. Ed.*, 2009, **48**, 6643-6646.
37. G. L. Gutsev, R. J. Bartlett and R. N. Compton, *J. Chem. Phys.*, 1998, **108**, 6756-6762.
38. G. Becker and K. Hübler, *Z. anorg. allg. Chem.*, 1994, **620**, 405-417.
39. P. v. R. Schleyer and D. Kost, *J. Am. Chem. Soc.*, 1988, **110**, 2105-2109.
40. C. Palomo, M. Oiarbide and J. M. Garcia, *Chem. Soc. Rev.*, 2004, **33**, 65-75.
41. J. D. White and R. G. Carter, in *Science of Synthesis*, ed. I. Fleming, Thieme Publishing, Stuttgart, 2002, pp. 371-412.
42. G. Becker, *Z. anorg. allg. Chem.*, 1976, **423**, 242-254.
43. G. Becker, *Z. anorg. allg. Chem.*, 1977, **430**, 66-76.
44. G. Becker, G. Ditten, K. Hübler, U. Hübler, K. Merz, M. Niemeyer, N. Seidler, M. Westerhausen and Z. Zheng, *Organosilicon Chemistry II, Wiley-VCH Weinheim, N. Auner and J. Weis (eds.)*, 1996, 161-186.
45. G. Heckmann, G. Becker and H. Kraft, *Magn. Reson. Chem.*, 1999, **37**, 667-671.
46. G. Becker, G. Ditten, S. T. Horner, A. H. Maulitz and E.-U. Würthwein, *Organosilicon Chemistry V, Wiley-VCH Weinheim*, 2003.
47. R. Appel and M. Poppe, *Angew. Chem. Int. Ed.*, 1989, **28**, 53-54.
48. K. Hübler and P. Schwerdtfeger, *Inorg. Chem.*, 1998, **38**, 157-164.
49. G. Heckmann, G. Becker, S. Horner, H. Richard, H. Kraft and P. Dvortsak, *Z. Naturforsch. Section B Chem. Sci.*, 2001, **56**, 146-151.
50. M. I. Povolotskii, A. S. Tarasevich and I. E. Boldeskul, *Zh. Obshch. Khimii*, 1989, **59**, 805-808.
51. G. Cerioni, A. Plumitallo, J. Frey and Z. Rappoport, *Magn. Reson. Chem.*, 1995, **33**, 669-673.
52. A. D. Allen, I. Egle, R. Janoschek, H. W. Liu, J. H. Ma, R. M. Marra and T. T. Tidwell, *Chem. Lett.*, 1996, 45-46.
53. L. C. Allen, *J. Am. Chem. Soc.*, 1989, **111**, 9003-9014.
54. W. T. Brady and T. C. Cheng, *J. Org. Chem.*, 1977, **42**, 732-734.
55. T. A. K. Al-Allaf, *J. Organomet. Chem.*, 1986, **306**, 337-346.
56. W. W. Schoeller, *J. Mol. Struct.: THEOCHEM*, 1995, **332**, 225-229.
57. X. Chen, S. Alidori, F. F. Pushmann, G. Santiso-Quinones, Z. Benkő, Z. Li, G. Becker, H.-F. Grützmacher and H. Grützmacher, *Angew. Chem. Int. Ed.*, 2014, **53**, 1641-1645.
58. G. Becker, W. Becker, R. Knebl, H. Schmidt, U. Weeber and M. Westerhausen, *Nova Acta Leopoldina*, 1985, **59**, 55-67.
59. A. H. Cowley and S. W. Hall, *Polyhedron*, 1989, **8**, 849-850.
60. A. Modak, A. Deb, T. Patra, S. Rana, S. Maity and D. Maiti, *Chem. Commun.*, 2012, **48**, 4253-4255.
61. M. A. Garralda, *Dalton Trans.*, 2009, 3635-3645.
62. T. T. Tidwell, *Ketenes*, 2nd edn., Wiley, Hoboken, NJ, 2006.
63. J. Escudie, H. Ranaivonjatovo and L. Rigon, *Chem. Rev.*, 2000, **100**, 3639-3696.
64. M. T. Nguyen, A. F. Hegarty, M. A. McGinn and P. Ruelle, *J. Chem. Soc., Perkin Trans. 2*, 1985, 1991-1997.
65. D. H. Champion and A. H. Cowley, *Polyhedron*, 1985, **4**, 1791-1792.
66. M. A. David, D. K. Wicht, D. S. Glueck, G. P. A. Yap, L. M. Liable-Sands and A. L. Rheingold, *Organometallics*, 1997, **16**, 4768-4770.

67. M. A. David, S. N. Paisner and D. S. Glueck, *Organometallics*, 1995, **14**, 17-19.
68. M. A. David, D. S. Glueck, G. P. A. Yap and A. L. Rheingold, *Organometallics*, 1995, **14**, 4040-4042.
69. A. M. Tondreau, Z. Benkő, J. Harmer and H. Grützmacher, *Chem. Sci.*, 2014, DOI: 10.1039/c1033sc53140f.
70. S. Weidner, J. Renner, U. Bergstrasser, M. Regitz and H. Heydt, *Synthesis*, 2004, 241-248.
71. A. Mack, U. Bergstrasser, G. J. Reiss and M. Regitz, *Eur. J. Org. Chem.*, 1999, 587-595.
72. A. S. Ionkin, W. J. Marshall, B. M. Fish, M. F. Schiffhauer, F. Davidson and C. N. McEwen, *Organometallics*, 2009, **28**, 2410-2416.
73. S. J. Collier, *Science of synthesis*, 2004, 659-687.
74. H. D. Hausen and G. Weckler, *Z. anorg. allg. Chem.*, 1985, **520**, 107-112.
75. K. H. Dotz, A. Tiriliomis and K. Harms, *J. Chem. Soc. Chem. Comm.*, 1989, 788-790.
76. K. H. Dotz, A. Tiriliomis and K. Harms, *Tetrahedron*, 1993, **49**, 5577-5597.
77. N. H. Martin and J. D. Robinson, *J. Mol. Graphics Modell.*, 2012, **38**, 26-30.
78. M. K. Cyranski, P. v. R. Schleyer, T. M. Krygowski, H. J. Jiao and G. Hohlneicher, *Tetrahedron*, 2003, **59**, 1657-1665.
79. M. K. Cyranski, T. M. Krygowski, A. R. Katritzky and P. v. R. Schleyer, *J. Org. Chem.*, 2002, **67**, 1333-1338.
80. F. G. N. Cloke, P. B. Hitchcock, J. F. Nixon, D. J. Wilson, F. Tabellion, U. Fischbeck, F. Preuss, M. Regitz and L. Nyulaszi, *Chem. Commun.*, 1999, 2363-2364.
81. P. v. R. Schleyer, C. Maerker, A. Dransfeld, H. J. Jiao and N. J. R. V. Hommes, *J. Am. Chem. Soc.*, 1996, **118**, 6317-6318.
82. M. Mantina, A. C. Chamberlin, R. Valero, C. J. Cramer and D. G. Truhlar, *J. Phys. Chem. A*, 2009, **113**, 5806-5812.
83. A. Bondi, *J. Phys. Chem.*, 1964, **68**, 441-451.
84. R. F. W. Bader, *Atoms in molecules a quantum theory*, Clarendon Press, Oxford 1990.
85. G. Becker, W. Becker, M. Schmidt, W. Schwarz and M. Westerhausen, *Z. anorg. allg. Chem.*, 1991, **605**, 7-23.
86. R. Suter and H. Grützmacher, unpublished results.
87. S. E. d'Arbeloff-Wilson, P. B. Hitchcock, S. Krill, J. F. Nixon, L. Nyulaszi and M. Regitz, *J. Am. Chem. Soc.*, 2000, **122**, 4557-4562.
88. S. E. d'Arbeloff-Wilson, P. B. Hitchcock, J. F. Nixon and L. Nyulaszi, *J. Organomet. Chem.*, 2002, **655**, 7-15.
89. R. Appel and R. Moors, *Angew. Chem. Int. Ed. Eng.*, 1986, **25**, 567-567.
90. R. Herges, *Angew. Chem. Int. Ed. Eng.*, 1994, **33**, 255-276.
91. R. Herges, *J. Chem. Inf. Comput. Sci.*, 1994, **34**, 91-102.
92. B. S. Young, R. Herges and M. M. Haley, *Chem. Commun.*, 2012, **48**, 9441-9455.
93. D. Geuenich, K. Hess, F. Kohler and R. Herges, *Chem. Rev.*, 2005, **105**, 3758-3772.
94. A. Pena-Gallego, J. Rodriguez-Otero and E. M. Cabaleiro-Lago, *Eur. J. Org. Chem.*, 2005, 3228-3232.
95. D. Förster, H. Dilger, F. Ehret, M. Nieger and D. Gudat, *Eur. J. Inorg. Chem.*, 2012, 3989-3994.
96. S. L. Hinchley, C. A. Morrison, D. W. H. Rankin, C. L. B. Macdonald, R. J. Wiacek, A. H. Cowley, M. F. Lappert, G. Gundersen, J. A. C. Clyburne and P. P. Power, *Chem. Commun.*, 2000, 2045-2046.
97. S. L. Hinchley, C. A. Morrison, D. W. H. Rankin, C. L. B. Macdonald, R. J. Wiacek, A. Voigt, A. H. Cowley, M. F. Lappert, G. Gundersen, J. A. C. Clyburne and P. P. Power, *J. Am. Chem. Soc.*, 2001, **123**, 9045-9053.

98. J. P. Bezombes, K. B. Borisenko, P. B. Hitchcock, M. F. Lappert, J. E. Nycz, D. W. H. Rankin and H. E. Robertson, *Dalton Trans.*, 2004, 1980-1988.
99. J. P. Bezombes, P. B. Hitchcock, M. F. Lappert and J. E. Nycz, *Dalton Trans.*, 2004, 499-501.
100. R. Edge, R. J. Less, E. J. L. McInnes, K. Muther, V. Naseri, J. M. Rawson and D. S. Wright, *Chem. Commun.*, 2009, 1691-1693.
101. K. Issleib and W. Seidel, *Chem. Ber.*, 1959, **92**, 2681-2694.
102. G. Reeske and A. H. Cowley, *Inorg. Chem.*, 2007, **46**, 1426-1430.
103. Z. F. Chen, C. S. Wannere, C. Corminboeuf, R. Puchta and P. v. R. Schleyer, *Chem. Rev.*, 2005, **105**, 3842-3888.
104. D. Gudat, *Acc. Chem. Res.*, 2010, **43**, 1307-1316.
105. Z. Wirpsza, *Polyurethanes chemistry, technology and applications*, Ellis Horwood, New York, 1993.
106. Y. Nambu and T. Endo, *J. Org. Chem.*, 1993, **58**, 1932-1934.
107. H. A. Duong, M. J. Cross and J. Louie, *Organic Letters*, 2004, **6**, 4679-4681.
108. A. W. Hofmann, *Chem. Ber.*, 1870, **3**, 761-772.
109. Z. Pusztai, G. Vlad, A. Bodor, I. T. Horvath, H. J. Laas, R. Halpaap and F. U. Richter, *Angew. Chem. Int. Ed.*, 2006, **45**, 107-110.
110. S. M. Raders and J. G. Verkade, *J. Org. Chem.*, 2010, **75**, 5308-5311.
111. F. U. Richter, *Chem. Eur. J.*, 2009, **15**, 5200-5202.
112. F. U. Richter, 1,4,2-Diazaphospholidine derivatives, Bayer Materialscience AG, 2010, WO 2010/037499A1.
113. W. Y. Yi, J. Zhang, L. C. Hong, Z. X. Chen and X. G. Zhou, *Organometallics*, 2011, **30**, 5809-5814.
114. A. J. Roering, S. E. Leshinski, S. M. Chan, T. Shalumova, S. N. MacMillan, J. M. Tanski and R. Waterman, *Organometallics*, 2010, **29**, 2557-2565.
115. U. Segerer, J. Sieler and E. Hey-Hawkins, *Organometallics*, 2000, **19**, 2445-2449.
116. G. Becker, K. Hübler, M. Niemeyer, N. Seidler and B. Thinus, *Z. anorg. allg. Chem.*, 1996, **622**, 197-211.
117. G. Becker, M. Bader, U. Hübler and W. Schwarz, in *XVIIIth International Conference on Organometallic Chemistry (XVIIIth ICOMC)*, Munich, Germany, 1998.
118. J. N. Gibb and J. M. Goodman, *Org. Biomol. Chem.*, 2013, **11**, 90-97.
119. J. S. Tang and J. G. Verkade, *Angew. Chem. Int. Ed. Eng.*, 1993, **32**, 896-898.
120. M. Roman, B. Andrioletti, M. Lemaire, J. M. Bernard, J. Schwartz and P. Barbeau, *Tetrahedron*, 2011, **67**, 1506-1510.
121. D. Schomburg, W. Storzer, R. Bohlen, W. Kuhn and G. V. Röschenthaler, *Chem. Ber.*, 1983, **116**, 3301-3308.
122. K. B. Dillon, *Chem. Rev.*, 1994, **94**, 1441-1456.
123. D. Schomburg, U. Wermuth and R. Schmutzler, *Chem. Ber.*, 1987, **120**, 1713-1718.
124. M. Lattman, M. M. Olmstead, P. P. Power, D. W. H. Rankin and H. E. Robertson, *Inorg. Chem.*, 1988, **27**, 3012-3018.
125. G. W. T. M. J. Frisch, H. B. Schlegel, G. E. Scuseria, M. A. Robb, J. R. Cheeseman, G. Scalmani, V. Barone, B. Mennucci, G. A. Petersson, H. Nakatsuji, M. Caricato, X. Li, H. P. Hratchian, A. F. Izmaylov, J. Bloino, G. Zheng, J. L. Sonnenberg, M. Hada, M. Ehara, K. Toyota, R. Fukuda, J. Hasegawa, M. Ishida, T. Nakajima, Y. Honda, O. Kitao, H. Nakai, T. Vreven, J. A. Montgomery, Jr., J. E. Peralta, F. Ogliaro, M. Bearpark, J. J. Heyd, E. Brothers, K. N. Kudin, V. N. Staroverov, R. Kobayashi, J. Normand, K. Raghavachari, A. Rendell, J. C. Burant, S. S. Iyengar, J. Tomasi, M. Cossi, N. Rega, J. M. Millam, M. Klene, J. E. Knox,

J. B. Cross, V. Bakken, C. Adamo, J. Jaramillo, R. Gomperts, R. E. Stratmann, O. Yazyev, A. J. Austin, R. Cammi, C. Pomelli, J. W. Ochterski, R. L. Martin, K. Morokuma, V. G. Zakrzewski, G. A. Voth, P. Salvador, J. J. Dannenberg, S. Dapprich, A. D. Daniels, Ö. Farkas, J. B. Foresman, J. V. Ortiz, J. Cioslowski and D. J. Fox, Gaussian 09, Revision A.02, *Gaussian Inc. , Wallingford CT*, 2009.

126. C. van Wüllen, *Phys. Chem. Chem. Phys.*, 2000, **2**, 2137-2144.
127. E. D. Glendening, A. E. Reed, J. E. Carpenter, J. A. Bohmann, C. M. Morales and F. Weinhold, in *NBO 5.0.*, Theoretical Chemistry Institute, University of Wisconsin, Madison, 2001.
128. G. Schaftenaar and J. H. Noordik, *J. Comput.-Aided Mol. Des.*, 2000, **14**, 123-134.
129. S. Jansburli and P. S. Pregosin, *Magn. Reson. Chem.*, 1985, **23**, 198-201.
130. C. Blanco, C. Godard, E. Zangrando, A. Ruiz and C. Claver, *Dalton Trans.*, 2012, **41**, 6980-6991.
131. SDOC, Spectral Database for Organic Compounds: http://sdbs.riodb.aist.go.jp.